Spectrum-aware and Reliable Distributed Sensing in Cognitive Radio Networks

by

Ahmet Ozan Biçen

A Thesis Submitted to the
Graduate School of Engineering
in Partial Fulfillment of the Requirements for
the Degree of

Master of Science
in
Electrical and Electronics Engineering

Koç University

July 2012

Koç University

Graduate School of Sciences and Engineering

This is to certify that I have examined this copy of a master's thesis by

Ahmet Ozan Biçen

and have found that it is complete and satisfactory in all respects,
and that any and all revisions required by the final
examining committee have been made.

Committee Members:

_____

Özgür B. Akan, Ph. D. (Advisor)

_____

A. Murat Tekalp, Ph. D.

_____

Öznur Özkasap, Ph. D.

Date: _____

Anneme ve Babama,

Ayşe ve Halil Biçen.

ABSTRACT

The ever increasing demand for wireless communication technologies causes spectrum scarcity and inspires researchers to envision the dynamic spectrum access techniques, i.e., cognitive radio, for efficient utilization of spectrum. Wireless sensor networks (WSN) have been considered as operating at unlicensed bands, however, sensor nodes can access licensed spectrum opportunistically with incorporation of cognitive radio capability. Sensor nodes equipped with cognitive radio emerges a new distributed sensing paradigm, i.e., Cognitive Radio Sensor Networks (CRSN). CRSN alleviates spectrum scarcity via enabling access to and distributed sensing operation over licensed bands. The unique characteristics and research challenges posed by CRSN call for novel networking solutions tailored to realize reliable and energy-efficient distributed sensing. The objective of this research is to design, develop and analyze new advanced communication schemes for reliable and energy-efficient distributed sensing in CRSN. More specifically, a comprehensive performance evaluation of existing transport protocols is performed for reliability and congestion control in CRSN. Delay-sensitive and multimedia communication in CRSN is investigated for various smart grid environments. Furthermore, the spectrum-aware and energy-adaptive reliable transport (SERT) protocol for event delivery is first proposed for CRSN. Next, a new spectrum hole assignment for reliable estimation (SHARE) scheme is proposed to achieve reliable local estimation at actor and reach global consensus among actor nodes. The analysis of dedicated radio utilization for spectrum handoff and efficiency is presented for the cognitive radio networks. Moreover, spectrum-aware and cognitive sensor networks (SCSN) are introduced to address the unique challenges of the smart grid environments for distributed sensing. Finally, Spectrum-aware Underwater Networks are investigated to increase achievable capacity under the limited availability and harsh conditions of the underwater acoustic spectrum.

ÖZET

Kablosuz iletişim teknolojileri için artan talep spektrum kıtlığına neden olmakta ve spektrumun etkin kullanımı için dinamik spektrum erişim tekniklerine, bir diğer değişle bilişsel radyoya ihtiyaç duymaktadır. Kablosuz algılayıcı ağları (KAA) haberleşme için lisanssız bantları kullanmaktadır, fakat bilişsel radyo yeteneğiyle algılayıcı düğümler lisanslı tayfa fırsatçı bir şekilde erişebilirler. Bilişsel radyo ile donatılmış algılayıcı düğümler yeni bir dağıtık algılama paradigmasını, Bilişsel Radyo Algılayıcı Ağlarını (BRAA) ortaya çıkarmaktadır. BRAA lisanslı bantlara erişimi ve bu bantlar üzerinden dağıtık algılamayı mümkün kılarak tayf kıtlığını azaltmaktadır. BRAA'nın eşsiz karakteristikleri ve zorlukları güvenilir ve enerji verimli dağıtık algılamanın gerçekleştirilebilmesi için yenilikçi ağ çözümlerini gerektirmektedir. Bu araştırmanın amacı BRAA'da güvenilir ve enerji verimli dağıtık algılama için yeni gelişmiş haberleşme algoritmalarının tasarımı, geliştirilmesi ve analizidir. Detaylı olarak, BRAA'da güvenilirlik ve tıkanıklık kontrolü için literatürdeki taşıma katmanı protokollerinin detaylı performans degerlendirmesi yapılmıştır. Çeşitli akıllı şebeke çevrelerinde gecikme-duyarlı ve çoklu-ortam haberleşmesi incelenmiştir. BRAA'da olay aktarımı için ilk defa tay-bilinçli ve enerji-uyumlu güvenilir taşıma protokolü önerilmiştir. Sonrasında, aktörde güvenilir yerel kestirim sağlanması ve globalde aktörler arasında konsensüs ulaşılması için yeni bir güvenilir kestirim için tayf boşluğu ataması algoritması önerilmiştir. Tayf bırakma ve verimlilik için ayrı radyo kullanımı analiz edilmiştir. Akıllı şebeke ortamlarının dağıtık algılama için zorluklarının üstesinden gelmek için tayf-bilinçli ve bilişsel algılayıcı ağları tanıtılmıştır. Son olarak, limitli ve zorlu su altı akustik tayf koşullarında ulaşılabilir kapasiteyi arttırmak için tayf-bilinçli su altı ağları incelenmiştir.

ACKNOWLEDGMENTS

I would like to express my gratitude and sincere thanks to my advisor, Dr. Ozgur B. Akan, who led me into this exciting area of wireless communications. I am indebted to Dr. Akan for his invaluable and seamless support, guidance, and friendship throughout my master study. What I have learned from him is not just how to conduct research, but his insights, inspiration, his way of living.

My cordial thanks also extend to Dr. Murat Tekalp and Dr. Oznur Ozkasap for being on my master of science thesis jury.

I would like to acknowledge the members of the Next-generation and Wireless Communications Laboratory (NWCL) due to the excellent atmosphere they created.

Finally, I thank my parents, and my brothers for their constant support, love, encouragement, and sacrifices.

TABLE OF CONTENTS

DEDICATION iii

ABSTRACT iv

ÖZET v

ACKNOWLEDGMENTS vi

TABLE OF CONTENTS vii

LIST OF TABLES xiv

LIST OF FIGURES xv

ABBREVIATIONS xix

CHAPTERS

1 INTRODUCTION 1

1.1 Cognitive Radio Networks 1

1.2 Cognitive Radio Sensor Networks 2

1.3 Research Objectives and Solutions 3

1.3.1 Reliability and Congestion Control in Cognitive Radio Sensor Networks 4

1.3.2 Delay-sensitive and Multimedia Communication in Cognitive Radio Sensor Networks 4

1.3.3 Spectrum-aware and Energy-adaptive Reliable Event Transport in Cognitive Radio Sensor Networks 5

1.3.4 Adaptive Spectrum Sharing in Distributed Sensing with Cognitive Radio Sensor and Actor Nodes 5

1.3.5 Dedicated Radio Utilization for Spectrum Handoff and Efficiency in Cognitive Radio Networks 6

1.3.6 Cognitive Radio Sensor Networks in Smart Grid Applications 7

1.3.7 Spectrum-aware Underwater Networks: Cognitive Acoustic Communications . . . 7

1.4 Thesis Outline . . . 8

2 RELIABILITY AND CONGESTION CONTROL IN COGNITIVE RADIO SENSOR NETWORKS . . . 9

2.1 Motivation . . . 9

2.2 Transport Layer in Cognitive Radio Sensor Networks . . . 10

2.2.1 CRSN Challenges . . . 11

2.2.1.1 Intermittent Communication due to Spectrum Sensing . . . 11

2.2.1.2 Connection Blackout due to Spectrum Handoff 11

2.2.1.3 Spiky End-to-end RTT due to Dynamic Spectrum Availability . . . 11

2.2.1.4 Packet Losses due to Spectrum Mobility . . . 12

2.2.1.5 Varying Network Capacity . . . 12

2.2.1.6 Need for Synchronization of Transmission Periods . . . 13

2.2.2 Overview of Existing Transport Protocols . . . 13

2.3 Performance Evaluation . . . 14

2.3.1 Spectrum Sensing in CRSN . . . 15

2.3.2 Spectrum Mobility with Primary User Arrival in CRSN . . 17

2.3.2.1 Licensed User Activity Pattern . . . 18

2.3.2.2 Number of Available Channels (Opportunistic Reliability) . . . 19

2.3.2.3 Transient Effects of Licensed User Arrival . . 20

2.3.2.4 Spatially Varying Licensed User Arrival . . . 21

2.3.3 Spectrum Coordination in CRSN . . . 22

2.4 Shortcomings and Future Directions . . . 24

2.4.1 Overview of Simulation Results . . . 24

2.4.2 Open Research Issues . . . 25

3 DELAY-SENSITIVE AND MULTIMEDIA COMMUNICATION IN COGNITIVE RADIO SENSOR NETWORKS . . . 28

3.1 Motivation . . . 28

3.2 Real-Time Transport in Cognitive Radio Sensor Networks 30
3.2.1 CRSN Challenges for Real-Time Transport 31
3.2.1.1 Intermittent Connectivity 31
3.2.1.2 Licensed User Interference 32
3.2.1.3 Spectrum Sensing 32
3.2.1.4 Opportunistic Spectrum Access 33
3.2.1.5 Spectrum Mobility 33
3.2.1.6 Spectrum Coordination 33
3.2.2 Overview of Existing Approaches for Real-Time Transport in Sensor Networks 34
3.3 Multimedia and Delay-Sensitive Data Delivery of Cognitive Radio Sensor Networks in Smart Grids : A Case Study 36
3.3.1 Delay-Sensitive Transport in CRSN 38
3.3.1.1 Throughput 39
3.3.1.2 Packet Delivery 43
3.3.1.3 Average Packet Receiving Interval 44
3.3.1.4 Packet Delivery Ratio 45
3.3.2 Real-time Video Streaming in CRSN 46
3.3.2.1 Throughput, Packet Delivery and Energy Efficiency 46
3.3.2.2 Frame End-to-end Delay and Jitter 48
3.3.2.3 Peak Signal to Noise Ratio (PSNR) 50
3.4 Observations and Future Research Directions 51
3.4.1 Overview of Simulation Results 51
3.4.2 Open Research Issues 53
4 SPECTRUM-AWARE AND ENERGY-ADAPTIVE RELIABLE TRANSPORT IN COGNITIVE RADIO SENSOR NETWORKS 55
4.1 Motivation 55
4.2 Related Work 58
4.3 CRSN Architecture 59
4.3.1 Spectrum Management Model 59
4.3.2 Event-to-sensor Dispersion and Distributed Sensing Model 60

4.4 SERT Design Principles 61
4.4.1 Impact of OSA and Spectrum Heterogeneity on Reliable Event Transport 61
4.4.2 Impact of Spectrum Opportunity Loss and Source Node Selection on Reliable Event Transport 64
4.5 Spectrum-aware and Energy-adaptive Reliable Transport 66
4.5.1 Instant Start 66
4.5.2 Spectrum-aware Rate Control 66
4.5.3 Energy-adaptive Source Node Selection for Collaboration 67
4.5.4 Proactive Local Congestion Detection 68
4.6 Performance Evaluation 69
4.6.1 Spectrum Mobility 69
4.6.1.1 Reliability Performance After Spectrum Handoff 69
4.6.1.2 Transient Reliability Performance 70
4.6.2 Spectrum Opportunity Loss 73
5 ADAPTIVE SPECTRUM SHARING IN DISTRIBUTED SENSING WITH COGNITIVE RADIO SENSOR AND ACTOR NODES 75
5.1 Motivation 75
5.2 Related Work 77
5.3 Network Setup 78
5.4 Impact of Spectrum Mobility 80
5.4.1 Instantaneous Throughput 80
5.4.2 Packet Error Rate 83
5.5 Distortion-aware Minimized Spectrum Access 87
5.5.1 Reliable Local Distributed Sensing 87
5.5.2 Minimized Spectrum Access 89
5.5.3 Spectrum Access Duration and Sensor Scheduling Order . 92
5.6 Opportunistic Consensus 93
5.6.1 Overview of Consensus Model 94
5.6.2 Algebraic Connectivity and Consensus Convergence . . . 95
5.7 SHARE: Spectrum Hole Assignment for Reliable Estimation 97

5.7.1 Distributed Online Spectrum Assessment 97
5.7.2 Estimation Interval Partitioning For Consensus 99
5.8 Performance Evaluation 100
5.8.1 Spectrum Opportunity Tracking 100
5.8.2 Adaptive Spectrum Sharing for Consensus 101
6 DEDICATED RADIO UTILIZATION FOR SPECTRUM HANDOFF AND EFFICIENCY IN COGNITIVE RADIO NETWORKS 103
6.1 Motivation 103
6.2 Related Work 105
6.3 Successful Frame Transmission Duration Analysis 106
6.3.1 System Model 106
6.3.2 SFT Duration without CCI 108
6.3.3 SFT Duration with CCI 110
6.4 Spectrum Efficiency Analysis 112
6.5 Energy Efficiency Analysis 112
6.6 Distributed Event Sensing Distortion Analysis 113
6.7 Performance Evaluation 114
6.7.1 Network Setup 114
6.7.1.1 The Nearest-neighbor Model 114
6.7.1.2 Wireless Channel Model 115
6.7.2 SFT Duration 115
6.7.2.1 Validation of Delay Analyses 115
6.7.2.2 SFT Duration with and without CCI 116
6.7.3 Spectrum Efficiency 117
6.7.4 Energy Efficiency 118
6.7.5 Distributed Event Sensing Performance 119
7 SPECTRUM-AWARE AND COGNITIVE SENSOR NETWORKS FOR SMART GRID APPLICATIONS 121
7.1 Motivation 121
7.2 Potential Applications of SCSN in Smart Grid 124
7.2.1 Remote Monitoring for Electric Power Generation Systems 125

7.2.2 Remote Monitoring for Electricity T&D Network 125
7.2.3 Remote Monitoring for Consumer Facilities 126
7.3 Spectrum Management Requirements and Challenges of SCSN . . . 126
7.3.1 Spectrum Sensing 127
7.3.2 Spectrum Decision 127
7.3.3 Spectrum Sharing 128
7.3.4 Spectrum Mobility 129
7.4 SCSN Communication Protocol Suite 129
7.4.1 Physical Layer 129
7.4.2 Data Link Layer 130
7.4.2.1 Medium Access Control 130
7.4.2.2 Error Control 131
7.4.3 Routing Layer 132
7.4.4 Transport Layer 133
7.4.5 A Case Study of Reliable Transport in Different Smart Grid Environments 133
7.5 Energy Harvesting in SCSN 134
8 SPECTRUM-AWARE UNDERWATER NETWORKS: COGNITIVE ACOUSTIC COMMUNICATIONS 137
8.1 Motivation 137
8.2 Underwater Acoustic Communication Channel Model 140
8.3 Spectrum Scarcity in Underwater Acoustic Communications 141
8.4 Dynamic Spectrum Access for Underwater Acoustic Networks . . . 143
8.4.1 Deep Water 144
8.4.2 Shallow Water 145
8.5 Opportunistic Spectrum Access For Underwater Acoustic Networks . 146
8.5.1 Deep Water 147
8.5.2 Shallow Water 147
9 CONCLUSIONS AND FUTURE RESEARCH DIRECTIONS 149
9.1 Research Contributions 150

9.1.1 Reliability and Congestion Control in Cognitive Radio Sensor Networks . . . 150
9.1.2 Delay-sensitive and Multimedia Communication in Cognitive Radio Sensor Networks . . . 150
9.1.3 Spectrum-aware and Energy-adaptive Reliable Event Transport in Cognitive Radio Sensor Networks . . . 151
9.1.4 Adaptive Spectrum Sharing in Distributed Sensing with Cognitive Radio Sensor and Actor Nodes . . . 151
9.1.5 Dedicated Radio Utilization for Spectrum Handoff and Efficiency in Cognitive Radio Networks . . . 151
9.1.6 Spectrum-aware and Cognitive Sensor Networks for Smart Grid Applications . . . 152
9.1.7 Spectrum-aware Underwater Networks: Cognitive Acoustic Communications . . . 152
9.2 Future Research Directions . . . 153
9.2.1 Adaptive spectrum sharing for heterogeneous multi-event sensing in CRSN . . . 153
9.2.2 Co-existence and Integration of CRSN with the Internet . . . 153
9.2.3 Passive communications in CRSN . . . 154
9.2.4 Topology control and power adaptation in CRSN . . . 154
REFERENCES . . . 155
CURRICULUM VITAE . . . 163

LIST OF TABLES

Table 3.1 Summary of Existing Transport Protocols 34

Table 3.2 Log-normal shadowing path loss model parameters for different smart grid environments 37

Table 4.1 Lengths of τ_s^c and τ_t^c, and Spectrum Handoff Instants (t_c) Used in Experimental Analysis for Each Channel c 62

Table 6.1 Illustration of Spectrum Access Delay for a Channel List Composed of 3 Channels 107

Table 7.1 Summary of SCSN Applications for Smart Grid vs. Power Grid Segment . . 124

Table 7.2 Summary of Existing Energy Harvesting Techniques for SCSN 135

LIST OF FIGURES

Figure 1.1 A typical CRSN topology with heterogenous available spectrum opportunities. 2

Figure 2.1 Variation of throughput while τ_S^s is varying from 0 to 0.3 sec for $\tau_S^d = 3$ and 2 sec and $\tau_L^{on} = 0$, in (a) and (b), respectively. 15

Figure 2.2 Variation of throughput, in (a) and (b), and delay, in (c) and (d), with varying τ_L^{on} from 0 to 6 sec, for constant $\tau_L^{off} = 6$ and 3 sec, respectively. 16

Figure 2.3 Throughput for varying number of available channels with $\tau_L^{on} = 2$ and $\tau_L^{off} = 3$ sec. 19

Figure 2.4 Variation of goodput (a) and delay (b) with respect to time for increasing licensed user activity. 20

Figure 2.5 Event region and intermediate nodes in CRSN. 21

Figure 2.6 Transmitted packets to received packets ratio (a) and energy efficiency under high licensed user activity (b). 22

Figure 2.7 Variation of goodput with respect to percentage of network employing the same spectrum afterwards of spectrum handoff (in parenthesis number of coordinated event region nodes are given). 23

Figure 3.1 Two-state Markov chain for licensed user activity model. 35

Figure 3.2 Variation of throughput(a), packet delivery(b), packet receiving frequency(c) and packet delivery ratio(d) with respect to increasing P_{ON} for τ_S^d of 1.5 sec and τ_S^s of 0.5 sec. 38

Figure 3.3 Variation of throughput(a), packet delivery(b), packet receiving frequency(c) and packet delivery ratio(d) with respect to increasing P_{ON} for τ_S^d of 1.5 sec and τ_S^s of 0.2 sec. 40

Figure 3.4 Variation of throughput(a), packet delivery(b), packet receiving frequency(c) and packet delivery ratio(d) with respect to decreasing τ_S^s/τ_S^d ratio, for $\beta = 7$ and $\alpha = 3$. 41

Figure 3.5 Variation of throughput(a), packet delivery(b), packet receiving frequency(c) and packet delivery ratio(d) with respect to decreasing τ_S^s/τ_S^d ratio, for $\beta = 3$ and $\alpha = 7$. 42

Figure 3.6 Throughput (a), packet delivery(b) and energy efficiency(c) for video streaming in CRSN. 47

Figure 3.7 End-to-end packet packet delay(a), pdf of end-to-end packet delay(b), interframe gap of received frames(c) and cumulative jitter(d) for video streaming in CRSN. 48

Figure 3.8 Frame PSNR values of received video in different power grid environments. 50

Figure 4.1 CRSN node activity pattern with time. 60

Figure 4.2 Reliability performance at sink for $\tau_d = 0.5$ sec with OSA and $\tau_d = 1$ sec with OSA and without OSA. 63

Figure 4.3 Report rate updates after spectrum handoff for various τ_d values. 64

Figure 4.4 Number of source nodes with respect to distortion constraint (D_0). 65

Figure 4.5 Reliability performance of SERT after spectrum handoff for various τ_d values. 71

Figure 4.6 Transient reliability performance of SERT for τ_d values of 0.5 and 1 sec, in (a) and (b), respectively. 72

Figure 4.7 Total energy consumption of source nodes in CRSN for different sensor node energy constraint levels. 73

Figure 4.8 Number of selected source nodes for different number of spectrum opportunity lost nodes. 74

Figure 5.1 Comparision of calculated and achieved instantaneous throughput due to opportunistic spectrum access for $\tau_t = 0.1, \tau_t = 0.08, \tau_t = 0.06, \tau_t = 0.03$ sec. . . . 82

Figure 5.2 Licensed user interference patterns when mis-detection occurs, no state change in (a) and state transition occurs in (b). 84

Figure 5.3 Licensed user interference patterns when licensed user is initially OFF while *spectrum sensing*, no state change in (a) and state transition occurs in (b). . 84

Figure 5.4 Comparison of analytically calculated packet error rate and simulation results with respect to licensed user arrival rate β for SNR values under licensed user interference of P_l = 5 and 15 dB. 86

Figure 5.5 Required number of channels with respect to instantaneous throughput T_k for τ_e = 1 sec and distortion constraint D_o of −50 dB. 91

Figure 5.6 Consensus .duration with respect to algebraic connectivity for various P_l and β values. 96

Figure 5.7 Performance of DOSA compared to local tracking for different mean licensed user arrival with respect to learning rate. 101

Figure 5.8 Consensus reaching rate of actor nodes. 101

Figure 5.9 Consensus disagreement of actor nodes. 102

Figure 6.1 Illustration of spectrum access delay τ_{sft}. 107

Figure 6.2 Validation of successful frame transmission duration with and without CCI. $\text{E}\{\tau_s\}$ and $\text{E}\{\tau_{cyc}\}$ are uniformly distributed between 2.5 ms to 7.5 ms and 100 ms to 110 ms, respectively. 116

Figure 6.3 Variation of SFT duration by employing CCI, for different PU arrival rates and varying $\frac{\tau_f}{\text{E}\{\tau_s\}}$ ratios. Both AWGN and flat fading channels are considered. . . 117

Figure 6.4 Variation of SFT duration, with increasing SU node density, for both with CCI and without CCI cases. E_b/N_0 is assumed to be 15 dB for lowest SU density. 118

Figure 6.5 Variation of goodput, with increasing rate R for both with and without CCI cases, under different PU arrival rates. 119

Figure 6.6 Energy efficiency gain via CCI, for Υ_{s_1} = 180 mW, Υ_{f_1} = 320 mW (pair 1) and Υ_{s_2} = 240 mW, Υ_{f_2} = 200 mW (pair 2) 119

Figure 6.7 Distributed sensing distortion performance with and without CCI, under different PU arrival rates. 120

Figure 7.1 An illustrative architecture of smart grid using sensor networks. Smart grid can be defined as a modernized electric power T&D network using robust two-way communications, advanced sensors, and distributed computing technologies to improve efficiency, reliability and safety of power delivery and use. 123

Figure 7.2 Variation of (a) packet delivery and (b) packet receiving interval with respect to licensed user ON probability (P_{ON}). 132

Figure 8.1 Example UAC system consisting of sonar ships, AUVs, submarines, UASN, and a mobile sink. 138

Figure 8.2 Variation of absorption coefficient with respect to frequency. 140

Figure 8.3 Variation of capacity with respect to center frequency for d = 5 km, s = 1, and w = 10 m/s. 142

Figure 8.4 Capacity of DSA-enabled SUN with respect to number of channels in deep water (1 km). 143

Figure 8.5 Capacity of DSA-enabled SUN with respect to number of channels in shallow water (0.01 km). 144

Figure 8.6 Capacity of OSA-enabled SUN with respect to bandwidth in deep water (1 km). 145

Figure 8.7 Capacity of OSA-enabled SUN with respect to bandwidth in shallow water (0.01 km). 146

ABBREVIATIONS

CAC	Cognitive Acoustic Communications
CCI	Common Control Interface
COW	Congestion on the Way
CR	Cognitive Radio
CRN	Cognitive Radio Networks
CRSN	Cognitive Radio Sensor Networks
DOSA	Distributed Online Spectrum Assessment
DSA	Dynamic Spectrum Access
MAC	Medium Access Control
MSE	Mean Square Error
OSA	Opportunistic Spectrum Access
SCSN	Spectrum-aware and Cognitive Sensor Networks
SERT	Spectrum-aware and Energy-adaptive Reliable Transport
SHARE	Spectrum Hole Assignment for Reliable Estimation
SU	Secondary User
SUN	Spectrum-aware Underwater Networks
PU	Primary User

CHAPTER 1

INTRODUCTION

The ever growing demand for wireless communication technologies gives rise to cognitive radio for enabling co-existence of wide range of heterogeneous wireless systems from cellular wireless networks to ad hoc networks. This technological evolution is further inspiring the researchers to envision the utilization of cognitive radio for distributed sensing networks, i.e., Cognitive Radio Sensor Networks (CRSN). CRSN is a distinct communication paradigm and has challenges imposed by their unique characteristics and the objectives involved in their design and deployment.

1.1 Cognitive Radio Networks

Inefficient spectrum utilization has envisioned dynamic spectrum access (DSA) techniques for wireless communications. Cognitive radio is the fundamental progress towards realization of DSA in wireless communication networks [54, 10]. Cognitive radio capable nodes can tune their communication parameters autonomously to adapt and communicate over unoccupied frequency bands in the spectrum.

In licensed bands, wireless users with a specific license to communicate over the allocated band, i.e., the licensed user, has the priority to access the channel. Upon these natural habitants of a specific frequency band start communication; the cognitive radio users must detect the potentially vacant bands, through *spectrum sensing*. Then, they decide on which channels to move, i.e., perform *spectrum decision*. Finally, they adapt their transceiver so that the active communications are continued over the new channel as a result of *spectrum handoff*. This operation sequence is called cognitive cycle [10], and it can also be applied for an access to an unlicensed band by cognitive radios, i.e., unlicensed users, which have the same priority to

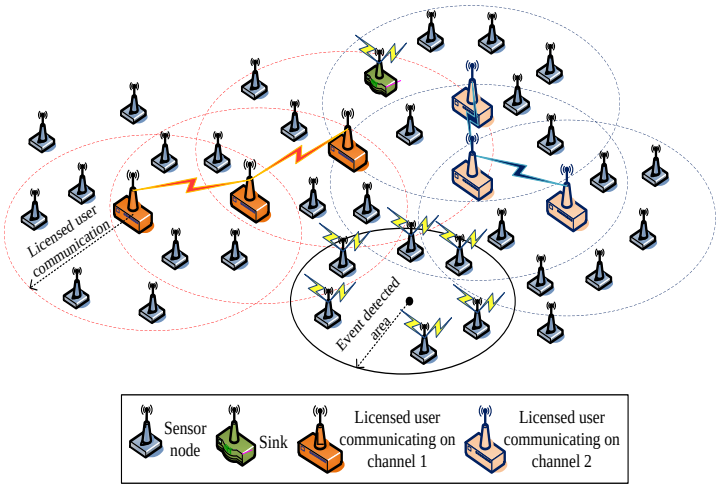

Figure 1.1: A typical CRSN topology with heterogenous available spectrum opportunities.

use the unlicensed channel.

Apart from salient improved spectrum efficiency and communication capacity promises, cognitive radio inherently brings burden of intermittent communication to wireless networks. Since spectrum access is paused during spectrum handoff functionality, communication is interrupted instantly with licensed user arrival. Even when sufficient spectrum opportunity for communication exists, i.e., there is always a vacant channel in which cognitive radio nodes can switch to, and communication can be resumed when a licensed user is detected, communication is still interrupted by periodic spectrum sensing functionality for licensed user detection.

1.2 Cognitive Radio Sensor Networks

The capabilities of cognitive radio may provide many of the current wireless systems with adaptability to existing spectrum allocation in the deployment field, and hence, improve overall spectrum utilization. Furthermore, these capabilities may provide efficient utilization of limited resources of sensor nodes in terms of communication and processing in wireless sensor networks (WSN). In fact, a WSN comprised of sensor nodes equipped with cognitive radio may benefit from the potential advantages of the salient features of dynamic spectrum access

(DSA), and therefore, this defines a new sensor network paradigm, i.e., cognitive radio sensor networks (CRSN) [8]. CRSN provides dynamic spectrum access in contrast to common fixed spectrum utilization of WSN.

CRSN nodes forming a network topology is shown in Fig. 1.1. The main duty of the sensor nodes is to perform sensing on the environment. In CRSN, depending on the spectrum availability, sensed data is transmitted to the sink in a multi-hop manner. Other than the event readings, sensor nodes may also require to exchange control data for licensed user activity detection, spectrum allocation, spectrum sensing, and spectrum coordination.

While the potential advantages of CRSN stand as a significant enhancement over traditional sensor networks, the realization of CRSN depends on addressing many difficult challenges, posed by the unique characteristics of both cognitive radio and sensor networks, and further amplified by their union.

1.3 Research Objectives and Solutions

To realize CRSN, the communication challenges posed by union of DSA and sensor networks must be effectively addressed. In this thesis, reliability and congestion control, and delay-sensitive and multimedia communications in CRSN are investigated. A new advanced transport protocol, and an adaptive spectrum sharing scheme are developed for reliable distributed event sensing in CRSN. Furthermore, impact of dedicated radio utilization for spectrum handoff on distributed event sensing efficiency is analyzed, and applications of CRSN for smart grid are investigated. Lastly, spectrum-aware underwater networks are proposed to mitigate harsh spectrum characteristics of underwater acoustic channels and achieve higher capacity with cognitive acoustic communications. The following seven areas are investigated under this research and each of them is described in the following subsections:

1. Reliability and Congestion Control in CRSN
2. Delay-sensitive and Multimedia Communication in CRSN
3. Spectrum-aware and Energy-adaptive Reliable Transport
4. Adaptive Spectrum Sharing

5. Dedicated Radio Utilization for Spectrum Handoff

6. Applications of CRSN in Smart Grid

7. Spectrum-aware Underwater Networks

1.3.1 Reliability and Congestion Control in Cognitive Radio Sensor Networks

Communication requirements for cognitive radio sensor networks (CRSN) necessitate addressing the problems posed by dynamic spectrum access (DSA) in an inherently resource-constrained sensor networks regime.

In this thesis, arising challenges for reliability and congestion control due to incorporation of cognitive radio capability into sensor network are investigated along with the open research issues. Impact of DSA, i.e., activity of licensed users, intermittent spectrum sensing and spectrum handoff functionalities based on spectrum availability, on the performance of the existing transport protocols are inspected. The objective of this paper is to point out the urgent need for a novel reliability and congestion control mechanism for CRSN. To this end, CRSN challenges for transport layer are revealed and simulation experiments are performed to demonstrate the performance of the existing transport protocols in CRSN.

1.3.2 Delay-sensitive and Multimedia Communication in Cognitive Radio Sensor Networks

Multimedia and delay-sensitive data applications in cognitive radio sensor networks (CRSN) require efficient real-time communication and dynamic spectrum access (DSA) capabilities. This requirement poses emerging problems to be addressed in inherently resource-constrained sensor networks, and needs investigation of CRSN challenges with real-time communication requirements.

In this thesis, the main design challenges and principles for multimedia and delay-sensitive data transport in CRSN are introduced. The existing transport protocols and algorithms devised for cognitive radio ad hoc networks and wireless sensor networks (WSN) are explored from the perspective of CRSN paradigm. Specifically, the challenges for real-time transport in CRSN are investigated in different spectrum environments of smart grid, e.g., 500kV substa-

tion, main power room and underground network transformer vaults. Open research issues for the realization of energy-efficient and real-time transport in CRSN are also presented. Overall, the performance evaluations provide valuable insights about real-time transport in CRSN and guide design decisions and trade-offs for CRSN applications in smart electric power grid.

1.3.3 Spectrum-aware and Energy-adaptive Reliable Event Transport in Cognitive Radio Sensor Networks

Sensor nodes equipped with a cognitive radio, i.e., cognitive radio sensor networks (CRSN), can access the spectrum in an opportunistic manner and co-exist with licensed users to mitigate the crowded spectrum problem and provide ubiquitous remote event monitoring and tracking. While opportunistic spectrum access (OSA) empowers communication in a dynamic and crowded spectrum environment, it further amplifies inherited reliable and energy-efficient event transport challenges in CRSN. Therefore, incorporating the intermittent communication and spectrum heterogeneity introduced by OSA into transport protocol design is imperative.

In this thesis, spectrum-aware and energy-adaptive reliable transport (SERT) protocol is presented for collaborative event sensing. To the best of our knowledge, this is the first attempt to specifically devise an event transport scheme for CRSN. SERT adapts the reporting rate of sensors based on spectrum opportunities to achieve adequate reliability in event sensing. It is intended to avoid oscillations in reliability due to interruptions in communication caused by spectrum sensing and handoff functions while preserving network life-time. Based on a distributed sensing distortion model, the desired number of sources, i.e., event reporting, nodes are determined via estimation theory. Extensive simulation experiments reveal that SERT achieves reliable energy-efficient distributed sensing in CRSN.

1.3.4 Adaptive Spectrum Sharing in Distributed Sensing with Cognitive Radio Sensor and Actor Nodes

Adaptive spectrum access is studied for multiple cognitive radio sensor networks observing the same event and reporting to actors, where actors cooperate to reach a global estimate, i.e., consensus, in an estimation interval. Reaching consensus among actor nodes in an estimation interval is an important concern as well as reliable local estimation of event features. There-

fore, local sample collection from sensors must be scheduled and completed accordingly to allow actors reaching consensus in an estimation interval.

In this thesis, first, spectrum access minimization during local estimation of actors is studied, where actors decide on accessed channels and schedule spectrum access of sensors to achieve desired reliability requirement. Required spectrum opportunity to achieve desired reliability is characterized in terms of number of channels and access duration. Then, reaching consensus under interruptions due to licensed user interference is studied and prolongation in convergence duration is investigated. Our analyses are also generic such that they can be applied to inhomogeneous licensed user activity and interference on channels. Spectrum hole assignment for reliable estimation (SHARE) scheme is proposed, in which spectrum access of sensor nodes is adapted to provide sufficient duration for reaching consensus while achieving desired reliability in local estimation. A simulation study is presented to demonstrate performance of SHARE in achieving consensus and mitigating disagreement among actor nodes.

1.3.5 Dedicated Radio Utilization for Spectrum Handoff and Efficiency in Cognitive Radio Networks

In cognitive radio networks (CRN), frame transmissions are interrupted by periodic spectrum sensing and instant spectrum handoff functionalities. To perform spectrum handoff, pairs within a given CRN need to communicate licensed user detection information over a common control channel. The spectrum coordination requirement for spectrum handoff can be fulfilled via either existing cognitive radio interface with time division or a separate dedicated radio, i.e., a common control interface (CCI), continuously. CRN nodes having CCI can instantly coordinate licensed detection information and cease frame transmission, while spectrum coordination can only be performed after frame transmission without CCI. Nevertheless, the benefits of CCI need to be thoroughly assessed due to its cost, prior to design decisions.

In this thesis, an analytical framework is presented to assess successful frame transmission duration, spectrum and energy efficiency, and distributed event sensing distortion with and without incorporation of CCI into CRN nodes. The developed framework provides opportunity to analyze trade-off between cost of a cognitive radio node equipped with CCI and achievable delay, spectrum utilization, energy consumption, and distributed event estimation

performance gains. Extensive performance evaluations are presented to illustrate impact of CCI on frame transmission delay, spectrum and energy efficiency, and distributed event sensing performance in CRN. The regimes that would yield having CCI favourable for CRN nodes are characterized in terms of spectrum conditions and cognitive radio parameters.

1.3.6 Cognitive Radio Sensor Networks in Smart Grid Applications

Recently, wireless sensor networks (WSN) have been considered as an opportunity to realize reliable and low-cost remote monitoring systems for smart grid. However, interference due to nonlinear electric power equipment and fading as a result of obstacles in various smart grid environments from generation to end-user sides make realization of reliable and energy-efficient communication a challenging task for WSN in smart grid.

In this thesis, spectrum-aware and cognitive sensor networks (SCSN) are proposed to overcome spatio-temporally varying spectrum characteristics and harsh environmental conditions for WSN-based smart grid applications. Specifically, potential advantages, application areas, and protocol design principles of SCSN are introduced. The existing communication protocols and algorithms devised for dynamic spectrum management networks and WSN are discussed along with the open research issues for the fulfilment of SCSN. A case study is also presented to reveal the reliable transport performance in SCSN for different smart grid environments. Lastly, different energy harvesting techniques for SCSN-based smart grid applications are reviewed. Here, our goal is to envision potentials of SCSN for reliable and low-cost remote monitoring solutions for smart grid.

1.3.7 Spectrum-aware Underwater Networks: Cognitive Acoustic Communications

Communication capacity in underwater acoustic networks is severely limited by the uniquely challenging characteristics of underwater acoustic communications (UAC). Path loss and noise in UAC vary spatiotemporally and depend highly on frequency.

In this thesis, dynamic spectrum sharing inspired from cognitive radio is applied to UAC networks, and spectrum-aware underwater networks (SUN), i.e., cognitive acoustic communications (CAC), is proposed. Firstly, the problem of spectrum scarcity in SUN is elaborated by investigating variation in acoustic channel capacity with respect to communication frequency

and bandwidth. Then, analysis of capacity gain via spectrum sharing in SUN is presented. To uncover the capacity gain via CAC, simulation experiments are performed considering effects of depth, distance, shipping, waves, spectrum management delay, and spectrum accessibility. Results of simulation experiments are elaborated to reveal the trade-off between capacity gain and spectrum management delay. Furthermore, the trade-off for capacity gain and spectrum accessibility period is also discussed. Here, our goal is to envision potentials of CAC for mitigating spectrum scarcity in UAC.

1.4 Thesis Outline

This thesis is organized as follows. Chapter 2 investigates the reliability and congestion control performance in CRSN. Chapter 3 studies delay-sensitive and multimedia communication performance in CRSN for various smart grid environments. Chapter 4 presents the spectrum-aware and energy-adaptive reliable transport (SERT) protocol developed for reliable event transport with minimum energy expenditure and congestion avoidance in CRSN. Chapter 5 introduces a new adaptive spectrum sharing scheme (SHARE) to reach consensus among actor nodes on a sensed event while spectrum access of sensor nodes is minimized. Chapter 6 presents the impact of dedicated radio utilization for communication of spectrum handoff information from transmission delay, spectrum efficiency, distributed event sensing performance, and energy efficiency perspectives. Chapter 7 introduces potentials and benefits of CRSN for smart grid applications. Chapter 8 investigates achievable capacity gains via cognitive acoustic communications in spectrum-aware underwater networks. Finally, Chapter 9 summarizes the research results and suggests a number of problems for future investigation.

CHAPTER 2

RELIABILITY AND CONGESTION CONTROL IN COGNITIVE RADIO SENSOR NETWORKS

In this chapter, reliability and congestion control in CRSN are investigated. The objective of this work is to reveal challenges and requirements of CRSN for reliable and energy-efficient event transport. This work is first presented in [20]. The transport layer issues in CRSN, challenges and overview of existing protocols are given in Section 2.2. In Section 2.3, results of simulation experiments and the effects of cognitive cycle on reliable data delivery with congestion control in CRSN are presented. Performance evaluation results are discussed, and the open research challenges for design of CRSN transport protocols are explored in Section 2.4.

2.1 Motivation

Reliable event detection and tracking with congestion control, which is, in general, responsibility of transport layer require addressing many difficult challenges, posed by the unique characteristics of CRSN. To conserve limited network and energy resources of sensor nodes and provide reliable event delivery, sufficient amount of information must be delivered to the sink while preventing congestion. However, the existing work on the reliable delivery of event features and congestion control in sensor networks do not consider challenges posed by the dynamic spectrum access. Furthermore, there is no specific solution for CRSN to this date. Hence, as the first step for the design of new transport layer solutions, it is imperative to understand the challenges and observe the shortcomings of these existing solutions through a comprehensive set of simulation experiments. Recently, there has been some ef-

forts to reveal challenges of cognitive radio networks for transmission control protocol (TCP) [90, 58, 64, 38]. To the best of our knowledge, there exists no such study for sensor networks in the current literature.

In this chapter, we introduce the main design challenges and principles for reliability and congestion control in CRSN. The existing communication protocols and algorithms devised for cognitive radio ad hoc networks as well as WSN are explored from the perspective of CRSN. Our objective is to acquaint CRSN challenges for transport layer, evaluate and reveal the performance and shortcomings of the existing transport protocols in CRSN communication scenarios. Additionally, the open research avenues for the realization of energy-efficient and reliable data communication in CRSN are highlighted.

2.2 Transport Layer in Cognitive Radio Sensor Networks

Transport protocols in wireless sensor networks (WSN) are primarily responsible for reliable and energy-efficient delivery of sensed event from source to sink. As well as considering quality of service (QoS) requirements of applications, congestion avoidance must be provided to preserve limited resources of sensor nodes in terms of processing, memory, communication, and more importantly, energy. CRSN is proposed to overcome spectrum scarcity and congestion problem caused by dense deployment of sensor nodes with opportunistic communication over licensed (and unlicensed) bands in WSN [8]. In addition to application-based reliability and energy-efficient communication notion in WSN, opportunistic spectrum access challenge emerges in CRSN. Intrinsically, transport protocols designed for traditional WSN do not take DSA into consideration. However, additional link delays and packet losses as a result of varying spectrum availability, spectrum mobility and spectrum sensing are the key issues for reliability and congestion control in CRSN.

In this section, we investigate the specific CRSN challenges for reliable and energy-efficient data delivery and explore the existing transport solutions developed for WSN and cognitive radio ad hoc networks together.

2.2.1 CRSN Challenges

To provide successful event detection and tracking in CRSN, sensed phenomena by sensor nodes must be delivered to the sink in accordance with the application-specific requirements such as number of delivered packets, delay bound, jitter, end-to-end delivery, etc. Additionally, this must be accomplished without interfering with licensed users and providing congestion avoidance for effective usage of limited resources of sensor nodes.

Clearly, in addition to inherent WSN demands, CRSN imposes unique challenges due to DSA functionalities, which are outlined as follows.

2.2.1.1 Intermittent Communication due to Spectrum Sensing

Silent periods of spectrum sensing prevents sensor nodes to deliver detected event to the sink. During spectrum sensing periods, sensor nodes do not transmit their collected information, since existing radio frequency modules cannot provide sensing and transmission functionalities at the same time. Thus, event transport is periodically disrupted in CRSN. Moreover, spectrum sensing duration brings a trade-off between false alarm and throughput. While a shorter sensing duration may result in an increase in the number of transmitted packets, inaccurate detection of licensed user activity may severely affect the transport layer.

2.2.1.2 Connection Blackout due to Spectrum Handoff

Upon licensed user activity detection, unlicensed users are required to vacate the channel. Until a vacant channel is found and spectrum handoff is performed by all sensor nodes participating in the event delivery, sink connection is disrupted due to spectrum unavailability. Connection blackout lasts depending on the licensed user activity, and event information cannot be delivered to the sink during blackouts.

2.2.1.3 Spiky End-to-end RTT due to Dynamic Spectrum Availability

Together with the extra delay introduced by cognitive cycle functionalities, limited spectrum availability and increasing licensed user activity may amplify round trip time (RTT). Due

to dynamically varying nature of licensed user activity, there may be large variations on the spectrum availability. Sudden decrease in spectrum availability, i.e., sharp increase in licensed user arrival rate or duration, is an expected situation in CRSN. Therefore, abrupt variation on the link level and end-to-end RTT estimates may be observed in CRSN. Additionally, based on varying interference limitations with licensed users at different channels, spectrum sensing duration may vary [66, 11] and further complicate estimation of RTT. Moreover, spectrum handoff mechanism also imposes additional delay on communication due to change of operating frequency. These various effects complicate the estimation of RTT. Thus, incorrect estimation of RTT may prevent the delay-based congestion control and rate adjustment mechanisms operate correctly, and hamper the performance of transport layer. In addition, achieving real-time communication in CRSN is quite challenging due to spiky end-to-end RTT imposed by DSA.

2.2.1.4 Packet Losses due to Spectrum Mobility

Spectrum mobility may cause packet drops due to link layer buffer overflows based on spectrum availability and connectivity. Due to intermittent link availability, link layer buffer fills up with the packets generated and coming from other nodes. Link layer queue overflows with the generation of new packets containing event readings and causes loss of event information, which is undesirable in WSN. On the other hand, spectrum mobility evokes congestion due to varying channel conditions and the need for coordination while connection establishment at the new operating channel. Due to bursty nature of sensor network, this connection establishment phase may result in excessive packet losses.

2.2.1.5 Varying Network Capacity

Event delivery performance is dependent on the capacity of network, which is varying due to DSA in CRSN. Depending on the network capacity, number of event reporting nodes and their reporting rates may need to be adjusted to avoid congestion. Moreover, network capacity may limit reliability in event detection and tracking, i.e., achievable maximum number of delivered packets and minimum delay bound may not satisfy QoS requirements of applications.

2.2.1.6 Need for Synchronization of Transmission Periods

Due to spatially varying licensed user activity, different sensing durations may be required at different regions of the network. While event information is being delivered to the sink, event-to-sink path may traverse along the regions with different spectrum sensing durations. Therefore, to deliver packets to the next node, sending node should be aware of sensing periods of the next node. Otherwise, while spectrum sensing, next node will not receive sent packets.

2.2.2 Overview of Existing Transport Protocols

Considerable amount of research efforts have yielded many transport protocols addressing challenges posed by WSN paradigm. Main properties of the existing protocols are classified in Table 3.1. In spite of providing congestion detection mechanisms and reliable transport functionalities, none considers both challenges of DSA and requirements of WSN.

Congestion Detection and Avoidance (CODA) protocol [104] presents an energy-efficient congestion control algorithm in order to prevent possible congestion on source-to-sink path by regulating source sending rate. Event-to-Sink Reliable Transport (ESRT) [6] and Real-Time and Reliable Transport ($(RT)^2$) [47] protocols are rate-based mechanisms which provide congestion avoidance and event-to-sink reliability. Additionally, $(RT)^2$ has real-time support. On the other hand, Pump Slowly Fetch Quickly (PSFQ) [103] provides reliability on downstream path and uses hop-by-hop recovery to retrieve missing packets. Reliable Multi-Segment Transport (RMST) protocol [93] provides negative acknowledgement (NACK) based guaranteed delivery like PSFQ, and both of them point out the importance of hop-by-hop recovery[1].

Recently, a window-based transport layer protocol addressing challenges of DSA in cognitive radio ad hoc networks, Transport Protocol for Cognitive Radio Ad-Hoc Networks (TP-CRAHN), is proposed in [33]. A cross-layer solution jointly considering the DSA functionalities, physical-layer modulation and coding scheme, and data-link layer frame size is presented in [76] to maximize TCP throughput. A set of protocols are derived from TCP in

[1] RMST [93] is not included in the performance evaluation as it aims to provide 100% reliability on a per packet basis, which is shown to be unsuitable for WSN [6].

[86] via tunning for DSA compatibility to serve delay-tolerant applications. Although those recently proposed algorithms incorporate cognitive radio functionalities, they are designed based on TCP congestion control mechanism, which has clearly been shown to have very poor performance in sensor networks [105].

Additionally, there has recently been active research on spectrum utilization efficiency and optimal spectrum sharing policies in cognitive radio networks [31, 87, 88, 57]. In [31], a new approach for spectrum sensing is developed with an analytical model to estimate the power in a given channel and location due to nearby communication, and then, these are used to formulate optimal channel assignment problem within the mesh network. In [87], per-node based power control for multi-hop cognitive radio networks is proposed, and a mathematical framework is developed to jointly optimize power control, scheduling, and routing. In order to increase data rates of secondary user communication sessions in a multi-hop cognitive radio network, joint optimization problem of power control, scheduling, and routing is studied in [88]. For video multicast in an infrastructure-based cognitive radio network coexisting with different licensed user networks, a cross-layer optimization approach is developed in [57] to optimize the overall received video quality, and provide proportional fairness among multicast users, while keeping the interference to licensed users below predefined constraints. Since these approaches are developed to increase end-to-end performance and spectrum efficiency in multi-hop cognitive radio networks, they do not consider neither many-to-one communication nature nor correlated data gathering of sensor networks.

Clearly, the existing transport protocols and spectrum sharing schemes are not specifically designed to achieve reliability in CRSN. To assess the performance of the existing transport protocols in CRSN, next, a wide range of simulations are performed and results are provided.

2.3 Performance Evaluation

Simulations are performed by extending NS-2 [3] with multichannel extensions to enable dynamic spectrum access and cognitive radio in sensor networks. 200 nodes and a sink are placed randomly in a 200m x 200m field. 25 source nodes are randomly selected within an event area of radius 20m. Packet size is 30 bytes and nodes are equipped with a single transmitter/receiver, which has a radio range of 40m. DSR [59] is used as routing protocol

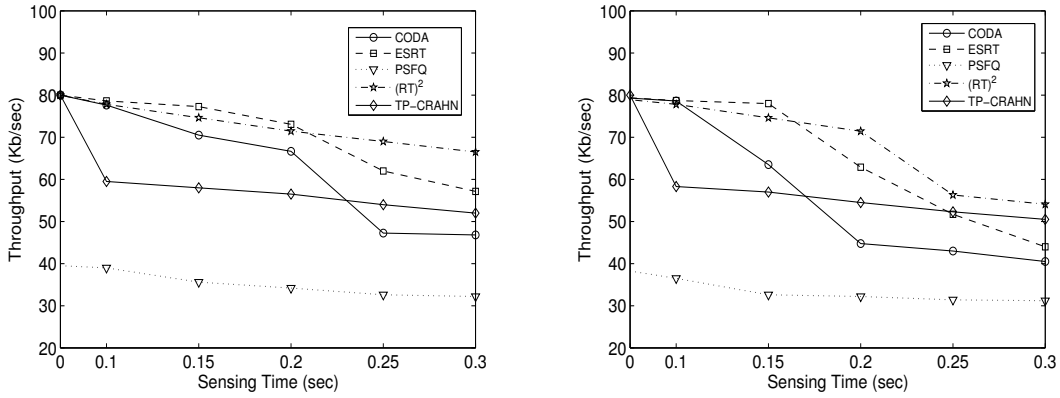

Figure 2.1: Variation of throughput while τ_S^s is varying from 0 to 0.3 sec for $\tau_S^d = 3$ and 2 sec and $\tau_L^{on} = 0$, in (a) and (b), respectively.

and each node has a simple CSMA/CA based medium access control layer with a queue size of 65.

Licensed user activity is modeled with active (τ_L^{on}) and inactive (τ_L^{off}) periods, and sensor node behavior is modelled with data transmission (τ_S^d), spectrum sensing (τ_S^s) and spectrum handoff (τ_S^h) periods. CODA [104], ESRT [6], PSFQ[2] [103], (RT)^2 [47] and TP-CRAHN [33] are included in the simulation experiments. Lastly, each simulation configuration is run 10 times and results are averaged.

2.3.1 Spectrum Sensing in CRSN

Effect of spectrum sensing period, i.e., transient lack of ability to transmit packets, on throughput is observed for varying τ_S^s from 0 to 0.3 sec in the absence of licensed user arrival. Fig. 2.1(a) and 2.1(b) show the throughput for τ_S^d= 3 and 2 sec, respectively.

Generally, all of the transport protocols exhibit a degradation in their throughput performance due to not considering silent sensing period. As spectrum sensing period increases, CODA, which uses feedback messages from intermediate nodes, sustains extra delays introduced by DSA. These delays cause highly variable RTT, and therefore, selective acknowledgement (SACK) packets are not received timely. This is interpreted as congestion and

[2] PSFQ is tested on reverse direction from sink to source, different than other protocols.

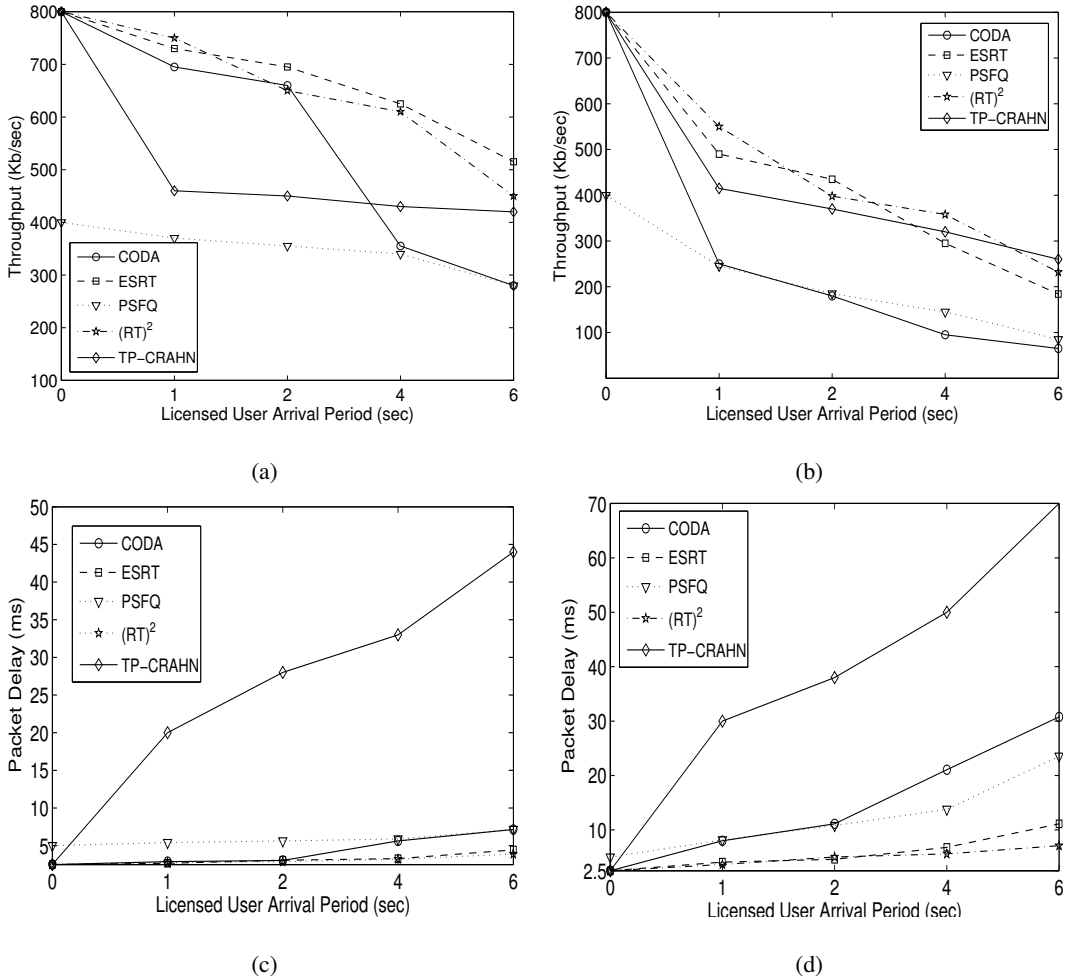

Figure 2.2: Variation of throughput, in (a) and (b), and delay, in (c) and (d), with varying τ_L^{on} from 0 to 6 sec, for constant τ_L^{off} = 6 and 3 sec, respectively.

CODA decreases its rate to one half. It can be seen in Fig. 2.1(b) that throughput decreases about 40% with the decreasing data transmission period. ESRT and (RT)^2 increase their reporting rate to obtain required reliability. They adjust transmission rate to compensate delay sustained in previous interval. However, due to misinterpretation of deficiency in reliability, inappropriate increase of transmission rate leads to congestion. On the other hand, PSFQ does not regulate its transmission rate, and hence, throughput performance degrades because of extra delay introduced by spectrum sensing, and there exists no mechanism considering this delay.

On the other hand, although initial drop, TP-CRAHN relatively maintains its performance as the sensing period increases. Especially, for higher spectrum sensing periods with lower data transmission period TP-CRAHN performs close to current WSN transport layer proto-

cols. Since current WSN transport protocols are not aware of cognitive cycle, they attribute delays, retransmission timeouts and packet losses caused by DSA functionalities to bad channel condition or congestion, and perform inappropriate rate control operations according to their algorithm, which result in up to 50% performance loss.

In Fig. 2.1(a) and Fig. 2.1(b), it is observed that decreasing data transmission period and increasing spectrum sensing period have adverse effect on throughput, however, this effect should be minimized to satisfy reliability requirements while retaining energy-efficient operation.

Spectrum sensing, which is a part of cognitive cycle, has a great importance to detect licensed user activities. Sensor nodes, which are secondary users, also need to sense the channel other than sensing the environment, and this sensing duration should be arranged accordingly to minimize false alarm probability. On the other hand, nodes need to transmit to deliver their collected information on the event. Hence, this constitutes a trade-off between sensing and event transport reliability. Moreover, real-time and delay-aware reliability requirements of some applications such as surveillance and target tracking may also introduce additional challenges on spectrum sensing. The effect of heterogeneous sensing duration on packet delivery ratio are also discussed in Section III-B.

2.3.2 Spectrum Mobility with Primary User Arrival in CRSN

When a licensed user arrival is detected, sensor nodes are required to stop transmitting data, vacate the channel and communicate over another free channel. To analyze the effects of licensed user arrival on throughput and packet delay, simulations are performed with different licensed user activity patterns. A licensed user is placed on each channel and transmits packets according to its activity pattern, so that its effect is clearly demonstrated. When the active period of licensed user is higher, finding an empty channel takes longer, i.e., τ_S^h increases. This delay has a direct effect on the network performance. Thus, to illustrate this, throughput and delay performances are given in Fig. 2.2 for varying τ_L^{on} from 0 to 6 sec with $\tau_L^{off} = 6$ and 3 sec, respectively.

2.3.2.1 Licensed User Activity Pattern

It can be seen in Fig. 2.2(a) and 2.2(b), especially, with the increasing licensed user active period throughput drastically decays. Since increasing link delay due to spectrum handoffs, increases the RTT and do not allow SACK packets to reach nodes on time, the highest, i.e., 60%, throughput degradation is experienced by CODA. On the other hand, ESRT and $(RT)^2$ inaccurately calculate their new reporting rates and fail to satisfy their reliability objectives. On the other hand, PSFQ experiences drop in the throughput above 50%, in Fig. 2.2(b). Intrinsically, traditional WSN transport protocols do not consider spectrum mobility and spectrum sensing functionalities, and do not adapt to the licensed user activity and spectrum sensing periods to achieve reliability and congestion control. Furthermore, they regulate sending rate assuming all the nodes are exposed to the same channel condition and licensed user activity. However, in CRSN, it may not be always possible for all sensor nodes to have the same channel conditions, i.e., this may not be the case in heterogeneous CRSN [8].

While the licensed user active period increases and probability of finding a vacant channel decreases, i.e., τ_S^h increases, TP-CRAHN performs slightly better than WSN transport protocols due to its DSA-aware functionalities. It assumes presence of a predefined common control channel (CCC) for coordination of channel information. This approach cannot handle cases, where a large number of nodes attempt to transmit in a short amount of time. Since a single channel is used, it gets congested very quickly. In fact, this is highly likely in CRSN due to its bursty traffic nature and dense deployment. Furthermore, this approach causes high end-to-end latency due to contention delay. Since CRSN generally operates in a multi-hop manner, this delay may exceed tolerable delay bound for some time-critical applications. Moreover, most of the time, it may not be possible to find such a CCC available throughout the entire network.

The results in Fig. 2.2(c) and 2.2(d) indicate that the lack of ability to coordinate with DSA functionalities causes existing transport layer protocols for WSN to amplify end-to-end delay. Because of extra time spent while retrieving the lost packets and its transmission rate regulation, observed delay for PSFQ is generally higher than others in Fig. 2.2(c). CODA experiences sharp increase in packet delay with the increase of licensed user active period (τ_L^{on}) from 2 to 4 sec in Fig. 2.2(d), since delays caused by DSA functionalities are attributed to congestion and evoke multiplicative decrease congestion avoidance, i.e., reducing rate to

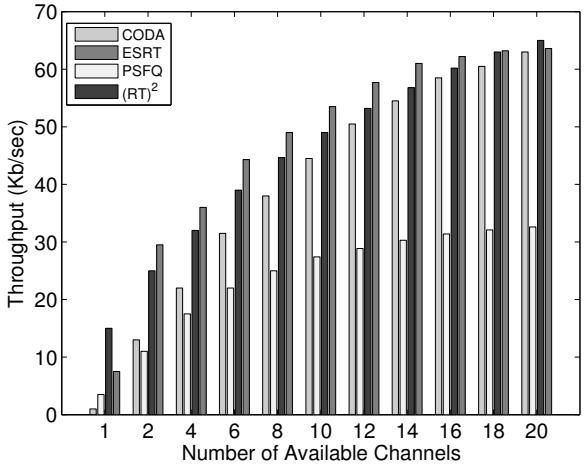

Figure 2.3: Throughput for varying number of available channels with $\tau_L^{on} = 2$ and $\tau_L^{off} = 3$ sec.

one half. Due to its real-time support, $(RT)^2$ performs relatively better than other protocols. Its performance can be improved by including spectrum sensing and mobility functionalities in the rate control algorithm.

2.3.2.2 Number of Available Channels (Opportunistic Reliability)

In Fig. 2.3, simulations are performed for varying number of available channels from 0 to 20, with $\tau_L^{on} = 2$ sec and $\tau_L^{off} = 3$ sec. RTT is highly variable in CRSN because spectrum handoff period vary with the number of available channels. Therefore, protocol-specific communication requirements cannot be met. In Fig. 2.3, CODA has the sharpest throughput increase with the number of available channels. As the number of available channels increases, initially estimated waiting period for SACK packets is approached. Furthermore, it can be observed for ESRT in Fig. 2.3 that, throughput improvement for increasing number of available channels from 4 to 6 is greater than the one achieved while increasing from 16 to 18. This result reveals that the throughput gain saturates as the number of available channels reaches to a certain level, which points out an important design trade-off to be further investigated.

In fact, higher number of available channels provides sensor nodes a flexible spectrum handoff operation, however, the impact of increasing available channels in throughput decreases as the throughput value without DSA is approached, i.e., gain obtained from increas-

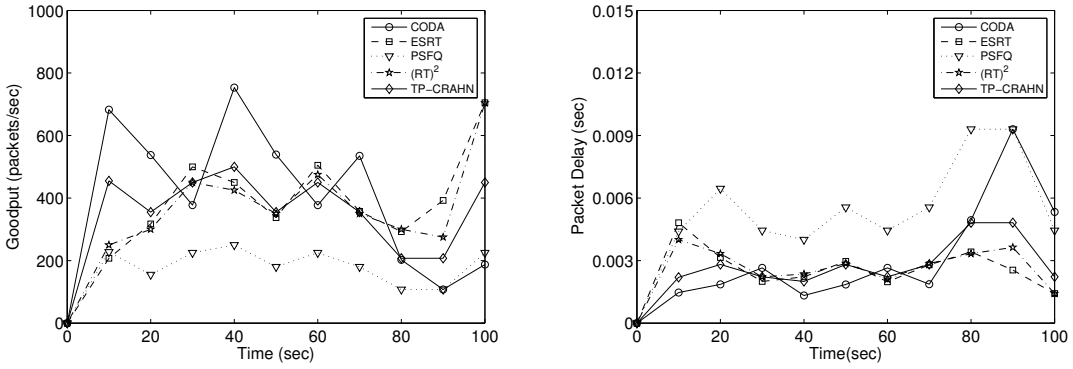

(a) (b)

Figure 2.4: Variation of goodput (a) and delay (b) with respect to time for increasing licensed user activity.

ing number of channel gets smaller. Therefore, access to sufficient number of channels, which is an important open issue to be determined, is essential for reliable and energy-efficient communication together with the efficient utilization of available spectrum in CRSN.

2.3.2.3 Transient Effects of Licensed User Arrival

Number of delivered packets at sink are examined to observe effects of varying licensed user activity with time. In these simulations, licensed user activity is increased gradually with time. Licensed user arrivals are scheduled at 15, 45, 55, 75, 80 and 85 sec, while the number of available channels are 20, 15, 10, 5, 2, 1, respectively.

CODA shows the highest oscillatory behavior as seen in Fig. 2.4(a). Consecutive licensed user activities result in drastic decrease in the number of delivered packets by CODA, e.g., delivered packets reduces to one half after licensed user activities between 80 and 90 sec. At the end of consecutive licensed user arrivals, CODA decreases its rate due to non-arriving SACK packets, i.e., time-outs and attributing them as congestion. After licensed user activity is removed between 90 and 100 sec, CODA lacks a fast increase in the rate, hence, the number of delivered packets stays below 30% of its initial value. In 2.4(a), it can be seen that oscillatory behavior in the number of delivered packets is decreased with respect to CODA, however, it still changes between 350 and 550 packets/sec for ESRT, $(RT)^2$ and TP-CRAHN. After consecutive licensed user arrivals, ESRT and $(RT)^2$ show a sharp increase in the num-

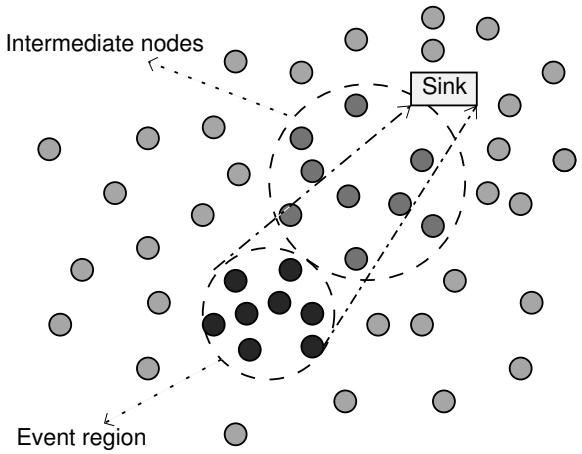

Figure 2.5: Event region and intermediate nodes in CRSN.

ber of delivered packets, e.g., from 90 to 100 sec, goodput increases about 230% after three consecutive licensed user arrivals in 70 and 90 sec. On the other hand, due to its adaptation to cognitive radio environment, TP-CRAHN returns around its initial value (at 10 sec) at 100 sec.

In Fig. 2.4(b), average measured packet delay varies between 1 and 10 ms for each protocol. $(RT)^2$ and ESRT outperform other protocols by their multiplicative rate increase property. CODA, which has an additive-increase multiplicative decrease (AIMD) rate control scheme, lacks fast recovery capability in case of connection disruptions due to spectrum handoffs. While licensed user activity increases in 70 and 90 sec, packet delay increases 5 times for CODA. Since PSFQ does not address for real-time event delivery, it is exposed to a greater delay than others. TP-CRAHN, which also employs an AIMD rate control, relatively performs better than CODA and close to ESRT and $(RT)^2$.

2.3.2.4 Spatially Varying Licensed User Arrival

It is possible to have different licensed user activity characteristics at different regions of a cognitive radio network. Therefore, sensing duration required to detect licensed user activity may change. To illustrate this in CRSN, we obtain results of having different spectrum sensing durations at event region and by intermediate nodes as in Fig. 2.5.

In Fig. 2.6(a), it is shown that how packet delivery ratio changes in percentage, while

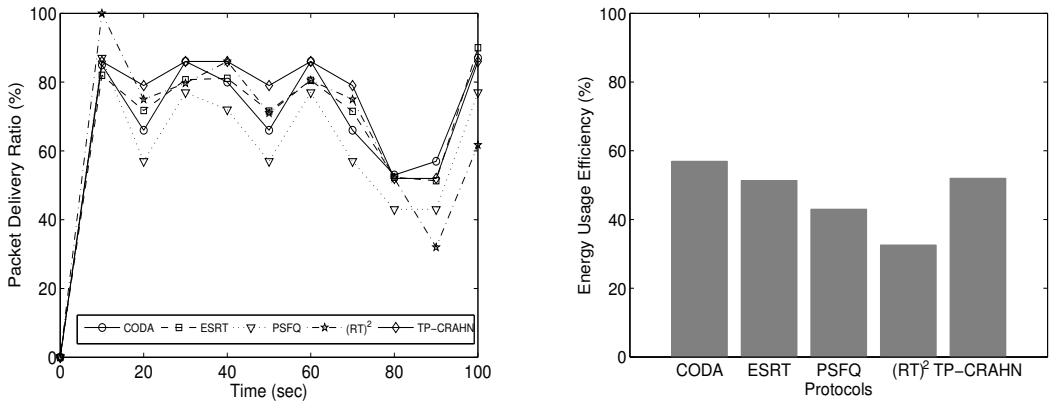

(a) (b)

Figure 2.6: Transmitted packets to received packets ratio (a) and energy efficiency under high licensed user activity (b).

different licensed user activities are observed in the network. Especially, between 80 and 90 sec with increasing licensed user activity, packet delivery ratio reaches about half of the value measured without licensed user activity. Since TP-CRAHN is designed for cognitive radio ad hoc networks, nodes adjust their transmission periods as not to overlap with the spectrum sensing period of the next node on the path. Hence, it performs slightly better than traditional WSN transport protocols in general. On the other hand, PSFQ performs below the others with excessive packet drops.

In Fig. 2.6(b), it is shown that under heavy licensed user activity all of the protocols show an efficiency under 50%. CODA, although exposed to degradation in packet delivery ratio up to 40% in Fig. 2.6(a), provides most efficient results due to its sharp congestion avoidance mechanism. On the other hand, $(RT)^2$ aiming to provide real-time support, updates its reporting rate sharply with respect to previous decision interval's packet delay. As a result of this, if no licensed user activity is observed in current interval, it causes transmission of more than required packets and these packets cause congestion, hence, energy is wasted.

2.3.3 Spectrum Coordination in CRSN

Spectrum coordination is an important topic in cognitive radio networks especially in CRSN, since to be able to communicate with each other, sensor nodes should be operating on the same channel. Sensor networks need special interest on this issue due to limited resources

and capabilities of sensor nodes, and reports of every node are important in event detection and tracking. To demonstrate the interaction of reliability and spectrum coordination, some parts of network left uncoordinated with the rest after spectrum handoff. These uncoordinated sensor nodes are selected in a random fashion, and their amount is given as percentage of the entire network.

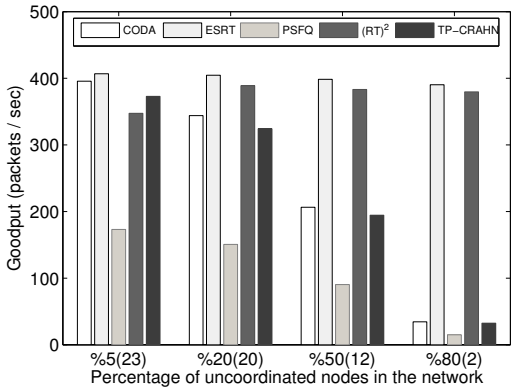

Figure 2.7: Variation of goodput with respect to percentage of network employing the same spectrum afterwards of spectrum handoff (in parenthesis number of coordinated event region nodes are given).

In Fig. 2.7, event-based protocols, i.e., ESRT and $(RT)^2$ are shown to maintain goodput although unreachable nodes. However, since number of connected sources are decreased, to preserve reliability, reporting rates are re-adjusted to compensate for lost nodes. Therefore, coordinated nodes' resources are overused to satisfy reliability condition. This result shows that network lifetime is highly dependent on spectrum coordination between sensor nodes. On the other hand, for packet-based reliability considering protocols, goodput decreases below one quarter of its initial value (from 400 packets to about 50 packets per-second), while the percentage of uncoordinated nodes are increased. This is due to that fact that, independent from event detection and tracking requirements of sink, every node sends its own measurements and regulate its own transmission rate with respect to feedback packets coming from intermediate nodes. Therefore, when the available source node count decreases, reliability observed at sink decreases. Strong interaction between reliability, network resources and spectrum coordination can be inferred from the results obtained with the existing transport protocols as shown in Fig. 2.7.

2.4 Shortcomings and Future Directions

There is a delicate balance between reliability and energy-efficiency, which has been the main focus of transport layer solutions proposed for sensor networks thus far [105]. While the same balance is also inherited by CRSN, dynamic spectrum management brings additional factors into this trade-off. Hence, all of the challenges introduced in Section II and clarified with simulation results in Section III, along with the ones inherited from WSN and amplified by cognitive radio, must be addressed through the design of novel dynamic spectrum-aware CRSN transport protocols.

In this section, main results of the simulations are analyzed and elaborated, afterwards, open research directions for reliability and congestion control in CRSN are pointed out.

2.4.1 Overview of Simulation Results

Comprehensive simulations clearly point out the shortcomings of the currently proposed transport protocols, and show that WSN protocols suffer from cognitive cycle introduced with DSA.

First, CODA infers high licensed user activity as congestion, and regulates its transmission rate accordingly. Thus, CODA necessitates incorporation of DSA functionalities. Despite its relatively higher energy-efficiency, reliability stays far behind the requirements in CRSN. Additionally, CODA lacks a fast increase in the rate control afterwards of a high licensed user activity.

On the other hand, ESRT and $(RT)^2$ provide application-based reliability. However, since inherent rate regulation simply does not take DSA challenges into account, extra delays and packet losses caused by cognitive cycle result in undesired behaviors such as transmission of redundant packets along with packet drops, i.e., depletion of confined resources. Although $(RT)^2$ considers real-time communication requirements, it encounters increase in the packet delay in the order of 5, especially, while the number of available channels is extremely low and licensed user activity is high.

PSFQ aims to provide guaranteed packet delivery on the reverse path, i.e., from sink to sources. When available spectrum is bounded and high licensed user activity is exposed, it

causes excessive losses while recovering missing packets from neighbor nodes. Especially, in heterogeneous licensed user activity case PSFQ underperforms.

TP-CRAHN provides adaptive sensing duration adjustment and congestion window scaling to handle DSA challenges. Nonetheless, it does not take inherent constraints and requirements of sensor networks into account, i.e., it does not consider energy-efficiency and many-to-one (source-to-sink) event delivery requirements. Additionally, end-to-end reliability notion does not suite very well in WSN, due to its bursty and many-to-one traffic nature.

Due to unawareness of cognitive cycle, and hence, misinterpretation of its functionalities, traditional WSN transport protocols do not function properly and achieve required energy-efficient reliable operation. New solutions are needed to overcome challenges introduced by cognitive radio. In simulation results, effects of generated extra delays and packet losses imposed by cognitive radio are explored. These results show the need for DSA-aware transport protocols for CRSN. TP-CRAHN is designed to operate on cognitive radio ad hoc networks and has features such as sensing duration minimization and adaptation to bandwidth variations. However, it does not consider inherent requirements of sensor networks and employs TCP congestion control algorithm, which is unsuitable for bursty many-to-one flow in CRSN.

2.4.2 Open Research Issues

In addition to energy-efficient and reliable communication requirements in WSN, emerging challenges of CRSN must be addressed through the design of novel, adaptive and spectrum-aware CRSN transport protocols. Clearly, none of the existing approaches devised for WSN can be directly employed in CRSN. Together with the extra delays and losses introduced by DSA functionalities in sensor nodes, reliability and congestion control in CRSN becomes an extremely challenging task. To this end, the open research issues for transport layer in CRSN are outlined as follows:

- Collaboration of transport layer protocols and DSA functionalities may provide efficient usage of available spectrum. Thus, cros-layer interaction of spectrum management and rate control mechanisms should be studied.

- There is a trade-off between required reporting rate and interference with licensed users.

New metric definitions combining reliability and congestion with licensed user interference and spectrum characteristics are required.

- Varying spectrum availability and channel conditions require novel congestion avoidance algorithms. Higher licensed user activity may augment probability of congestion due to intermittent spectrum availability. On the other hand, congestion control mechanism should also take spectrum sensing duration into consideration together with varying licensed user activity, since sharp increases in number of packets injected into the network due to increasing transmission period may result in congestion. There may be bottlenecks, due to spatially varying spectrum sensing duration, i.e., licensed user activity, in the network. Therefore, congestion control mechanisms should consider sensing durations of the nodes on the event delivery path.

- For delay-bounded applications, real-time DSA-aware transport layer solutions should be developed. Based on acquired transmission behavior of licensed users, probabilistic rate control models may be developed. Probabilistic and predictive frameworks can be derived to reduce increasing delay with increasing licensed user activity. To this end, analytical models including licensed user activity with congestion and wireless loss probability could be developed.

- Spectrum coordination must be incorporated in energy-efficient protocol stack in CRSN to provide reliable data delivery and congestion avoidance. Common control channel (CCC) is an alternative for spectrum coordination. However, since it requires high cost to lease a channel, it would amplify the cost of the sensor network [8]. Research on finding such a suitable CCC in unlicensed spectrum channels or coordination without CCC is required.

- Transport protocols should interact with sensing mechanism since it has a direct effect on throughput as it can be seen in Fig. 2.1 and utilize it to minimize licensed user interference and false detection probability while maximizing reliability. Hence, a cross-layer spectrum sensing and congestion control mechanism must be designed.

- Congestion control algorithms should also be adaptive to dynamically changing licensed user activity. Moreover, varying network capacity should be taken into consideration, since transmission more packets than network can tolerate will result in inefficient usage of limited resources of sensor nodes. Development of new congestion

avoidance mechanisms incorporating licensed user activity and network capacity are essential. In addition, in order to utilize opportunistic spectrum availabilities and satisfy reliability requirements, DSA-aware fast rate increase algorithms are also required.

CHAPTER 3

DELAY-SENSITIVE AND MULTIMEDIA COMMUNICATION IN COGNITIVE RADIO SENSOR NETWORKS

In this chapter, performance of delay-sensitive and multimedia communication in CRSN are assessed for various smart grid environments. The objective of this work is to point out protocol requirements and design guidelines for delay-sensitive and multimedia CRSN applications specifically in smart grid channel conditions. This work is first presented in [24]. In Section 3.2, real-time communication issues in CRSN, challenges and overview of existing protocols are given. Results of simulation experiments and the effects of cognitive cycle on multimedia and delay-sensitive data delivery in CRSN are presented in Section 3.3. In Section 3.4, firstly, the key points of results discussed in Section 3.3 are outlined to attract attention to emerging challenges, and then, the open research challenges for design of real-time CRSN transport protocols are explored.

3.1 Motivation

Dynamic spectrum access (DSA) schemes have been offered to resolve inefficient overall utilization problem of wireless spectrum. Cognitive radio (CR) [54] is the emerging technology to overcome this challenge and provide DSA capability. With the help of CR, vacant bands in the spectrum can be determined and utilized. In this way, CR can communicate over these vacant spectrum bands opportunistically and increase spectrum utilization efficiency.

In wireless spectrum, some of the bands are reserved to licensed users, and these users have priority to communicate over their allocated channels. CR users must detect the arrival of licensed users and vacate the channel. Then, channels, at which licensed user activity is not

observed, are identified by *spectrum sensing*. Channel selection, i.e., *spectrum decision*, must be made to decide on the channel to continue ongoing communication. Afterwards, CR users should move to this new channel by *spectrum handoff*. Spectrum sensing, spectrum decision and spectrum handoff operations constitute the cognitive cycle [10], and its application is not limited to licensed bands, e.g., it can also be applied among cognitive radio users while accessing unlicensed bands to increase efficiency and capacity.

In addition to improving overall spectrum utilization, capabilities of CR may help to preserve limited resources of sensor nodes in sensor networks. Sensor nodes containing cognitive radios basically can access spectrum opportunistically, and hence sensor network can benefit from the advantages of DSA, and this constitutes a new sensor network paradigm, i.e., cognitive radio sensor network (CRSN) [8]. Multimedia and delay-sensitive applications in CRSN are possible with the integration of low-cost hardware and sensor nodes as in wireless multimedia sensor network (WMSN) [12] case.

Fig. 1.1 depicts a possible configuration of a CRSN, delivering delay-sensitive multimedia data. Real-time CRSN is interconnected with CR equipped sensor nodes that enable retrieval of video and audio streams, images and delay-sensitive data. Sensor nodes are responsible for timely delivery of multimedia and delay-sensitive data from event region to sink, based on spectrum opportunities. Additionally, control data distribution between sensor nodes is needed to perform proper cognitive cycle operation. Overall, the collaborative operation of CRSN brings significant advantages over traditional sensor networks, including opportunistic channel usage, adaptability to reduce power consumption, dynamic spectrum access [8]. The existing and potential applications of CRSN span a very wide range, including real-time target tracking and surveillance, homeland security, multimedia delivery, and smart grid. However, realization of these currently designed and envisioned applications directly depends on real-time transport capabilities of the deployed CRSN.

Recently, there has been considerable amount of research efforts, which have yielded many promising transport layer protocols for wireless sensor networks (WSN) [12, 105]. The common feature of these protocols is that they mainly address the energy-efficient and reliable data communication requirements of WSN. However, in addition to the energy-efficiency and communication reliability, spectrum-aware communication paradigm emerges with CRSN, and cognitive cycle aware protocol design is needed to take advantage of cognitive radio.

Moreover, many real-world CRSN applications, such as multimedia applications, have strict delay bounds and hence mandate timely transport of the event features from the sensor field to the sink node. Real-time communication necessity further amplifies the challenges due to union of cognitive radio and sensor network, and desires careful consideration of communication delays may occur through opportunistic spectrum access in addition to being spectrum-aware. Consequently, the unique features and application requirements of real-time CRSN call for novel transport solutions, and thus, there is an urgent need for understanding the unique challenges of real-time transport in CRSN.

In this chapter, the main design challenges and principles for multimedia and delay-sensitive data transport in CRSN are introduced. The existing transport protocols and algorithms devised for cognitive radio ad hoc networks and WSN are explored from the perspective of CRSN paradigm. Specifically, the challenges for real-time transport in CRSN are investigated in different spectrum environments of smart power grid, e.g., 500kV substation, main power room and underground network transformer vaults. To this end, the wireless channel has been modeled based on experimentally gathered spectrum parameters in different smart power grid environments (shown in our previous study [49]). Through detailed performance evaluations, it is shown that CRSN could be a promising solution to realize delay-sensitive electric utility monitoring and diagnostic systems, with its intelligent processing and DSA capabilities to deal with noise and radio frequency (RF) interference in smart grid environments. In addition, open research issues for the realization of energy-efficient and real-time transport in CRSN are presented. Overall, the performance evaluations provide valuable insights about real-time transport in CRSN and guide design decisions and trade-offs for CRSN applications in smart electric power grid. To the best of our knowledge, this is the first work on the transport layer focusing on real-time event delivery in CRSN and presenting the challenges and performance of delay-sensitive transport in different smart grid environments.

3.2 Real-Time Transport in Cognitive Radio Sensor Networks

In order to realize real-time communication in CRSN, a reliable transport mechanism is imperative. Mainly transport layer is responsible from (a) bridging application and network layers, (b) assuring reliable event transport to the sink while taking application specific QoS requirements into consideration, and (c) regulating the sending rate to prevent and avoid con-

gestion. In order to adapt both the unique characteristics of CRSN paradigm and real-time transport requirements, features of transport layer are contingent on significant modifications to obtain efficient real-time communication in sensor networks. Limited resource nature of CRSN nodes bring consequential constraints on the transport layer protocol design [8]. Moreover, opportunistic spectrum access challenge emerges in CRSN, and brings additional link delays and losses as an expected outcome of variations in spectrum availability due to spectrum mobility.

Furthermore, in addition to the metrics for reliable data transport in CRSN, there exist additional metrics due to the unique characteristics of the real-time transport. These metrics can be outlined as delay and jitter, bandwidth requirement, peak signal to noise ratio (PSNR) for multimedia streaming, and frame delivery probability according to the specific QoS demands of real-time CRSN application.

In this section, we investigate the specific CRSN challenges for multimedia and delay-sensitive data delivery and explore the existing transport solutions developed for WSN and cognitive radio networks together.

3.2.1 CRSN Challenges for Real-Time Transport

In real-time CRSN, sensor nodes should deliver gathered event information in a timely manner. Timeliness gains more importance in real-time communication scenarios than reliability to provide successful event detection and tracking in CRSN. On the other hand, in addition to application-specific requirements such as delay bound, jitter, PSNR, etc., sensor nodes should not interfere with licensed users and use their resources efficiently.

Clearly, real-time CRSN imposes unique challenges due to incorporation of DSA functionalities, which are pointed as follows.

3.2.1.1 Intermittent Connectivity

Upon licensed user arrival, sensor nodes have to vacate the channel. This operation requires periodic sensing of the ongoing communication channel for licensed user activity. After detection of licensed user, spectrum handoff should be performed subsequently. As a result,

communication path to sink is continuously disrupted. Additionally, due to operating channel change, spectrum characteristics also change. This brings new loss rate and delay durations on the network. Therefore, PSNR varies due to changing spectrum characteristics. Furthermore, round-trip time (RTT) estimation gets complicated in behalf of varying jitter.

3.2.1.2 Licensed User Interference

Sensor nodes sequentially sense channel for licensed user activity and deliver their time-critic data to the sink in an hop-by-hop manner. Sequential spectrum sensing and data transmission inherently results in miss detection possibility of licensed users. Licensed user activity can occur at the event delivery duration, which will change the loss rate in the channel as miss-detection occurs. Miss-detected licensed users, if still communicating, can be detected in next spectrum sensing period, and with the detection of licensed user spectrum decision and spectrum handoff sequence will occur subsequently, i.e., cognitive cycle takes place. Consequently, successful frame delivery probability and PSNR varies, and due to erroneous received packets energy is wasted.

3.2.1.3 Spectrum Sensing

Detection of licensed user activities are performed via spectrum sensing functionality of cognitive cycle. Spectrum sensing durations prevent sensor nodes to deliver information to sink since existing radio modules cannot provide sensing and transmitting functionalities at the same time. On the other hand, based on interference limitations with licensed users and noise level of operating channel, spectrum sensing duration may vary [66]. Moreover, heterogeneous spectrum sensing durations can be seen throughout sensor network due to observed heterogeneous licensed user activity in the network. Heterogeneous sensing durations will bring synchronization problems on the path from source to sink. On the other hand, nodes operating at relatively less spectrum sensing duration will have greater ratio of channel access duration to spectrum sensing period, and this will cause in-network asymmetries in utilization of available bandwidth based on rate control algorithm running. Resultant effects will be seen in jitter and delay parameters. Additionally, fairness of bandwidth share between sensor nodes will depend on spectrum sensing duration based on heterogeneous licensed user activity and rate control algorithm.

3.2.1.4 Opportunistic Spectrum Access

Sensor nodes are allowed to communicate only if they find a vacant channel. This means that they have to wait until finding an opportunity to access to a licensed user free channel. Blackouts can occur due to consecutive licensed user arrivals on different channels. This causes abnormal variations in RTT. Moreover, transmitted information may be obsolete by the time it reaches the sink, due to loss of timeliness.

3.2.1.5 Spectrum Mobility

Moving from one channel to another (spectrum handoff) due to detection of licensed user means change of spectrum parameters and also additional delay due to sensing in search of a vacant channel. This causes to fill buffer of sensor nodes with new generated packets and incoming packets from other nodes due to ad-hoc nature. Additionally, variations in the bandwidth and noise levels, and henceforth network capacity is anticipated while moving from one channel to another. Changing spectrum parameters will affect delay, jitter and PSNR values. Previously measured channel conditions will be invalid in new operating channel.

3.2.1.6 Spectrum Coordination

Distribution of control data is essential to keep network synchronized in terms of channel selection and spectrum sensing durations. We assume every sensor node has a single transceiver, therefore, they can only communicate at a single channel at any given time. Thus, spectrum decision and handoff functionalities should be performed with coordination. Moreover, nodes participating in the communication from source to sink should be aware of spectrum sensing durations of the other nodes in the path. This is required to establish a path to the sink. As stated before spectrum sensing nodes cannot communicate with other nodes. This fact brings up energy consumption efficiency due to loss of packets and additional delay due to coordination duration.

Table 3.1: Summary of Existing Transport Protocols

Protocol	***Scope***	***Flow***	***DSA***	***Real-Time***
CODA [104]	WSN	Up	-	-
ESRT [6]	WSN	Up	-	-
PSFQ [103]	WSN	Down	-	-
(RT)^2 [47]	WSN	Up	-	+
RMST [93]	WSN	Up	-	-
TP-CRAHN [33]	CRAHN	Both	+	-

3.2.2 Overview of Existing Approaches for Real-Time Transport in Sensor Networks

Recently, there has been many research efforts, which have yielded many promising transport protocols for wireless sensor networks (WSN) [105]. Existing transport protocols are classified in Table 3.1 according to their scope, packet flow, cognitive radio and real-time communication support, respectively. Albeit providing energy-efficient reliable event delivery functionalities as well as congestion detection mechanisms, none of the existing transport protocols considers both challenges of DSA and constraints of sensor network.

Congestion Detection and Avoidance (CODA) protocol [104] aims preventing possible congestion to keep energy-efficient operation by using hop-by-hop congestion detection algorithm based queue length of intermediate nodes on source-to-sink path, and hence, source node can regulate its rate with a incurred additional delay in congestion control. Event-to-Sink Reliable Transport (ESRT) [6] and Real-Time and Reliable Transport ((RT)^2) [47] protocols provide event-based reliability by exploiting spatio-temporal correlation of generated packets by source nodes, and are equipped with congestion avoidance, which performs based on previous decision interval and control is centralized at sink. Additionally, (RT)^2 support delay-bounded reliability. On the other hand, Pump Slowly Fetch Quickly (PSFQ) [103] address sink-to-sensor transport reliability, e.g, aims to deliver packets from sink to sensor nodes in the network reliably, and in order to retrieve missing packets uses hop-by-hop retransmissions. Reliable Multi-Segment Transport (RMST) protocol [93] provides reliable communication on sensor-to-sink path, supports negative acknowledgement (NACK) oriented 100% reliability like PSFQ, and both of them point out the importance of hop-by-hop retransmissions of lost packets.

Recently, a TCP enhancement for CRAHN, Transport Protocol for Cognitive Radio Ad-

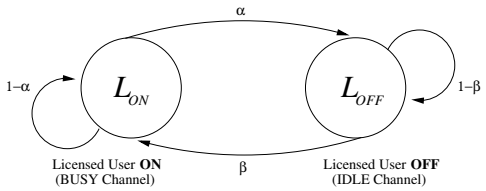

Figure 3.1: Two-state Markov chain for licensed user activity model.

Hoc Networks (TP-CRAHN) [33], which is aims to address challenges of DSA in cognitive radio ad hoc networks, is proposed. Even though its algorithm incorporates spectrum sensing and handoff functionalities, it occupies TCP's window-based congestion control mechanism, which has clearly been shown to have very poor performance in sensor networks [105].

With the unique characteristics and emerging challenges of real-time transport in CRSN is far beyond the scope of existing protocols, i.e., they are not designed with the consideration of real-time communication in CRSN. Packets are usually consist of non-redundant data, e.g., carried information is highly compressed. Therefore, providing end-to-end congestion control acquire significance in order to satisfy real-time multimedia streaming and high data rate delay-sensitive applications' QoS requirements in CRSN. Since equation based rate control is a broadly well-known rate control mechanism for streaming [41, 40, 97, 28], and thus, in order to assess the characteristics of transport layer in CRSN, we prefer to employ an equation-based rate control algorithm, e.g., TCP-Friendly Rate Control (TFRC) algorithm [41], which uses the following formula to determine throughput in packets per second as a function of packet loss rate and round-trip time:

$$T = \frac{1}{RTT\left[\sqrt{\frac{2p}{3}} + 12\sqrt{\frac{3p}{8}}p(1+32p^2)\right]} \tag{3.1}$$

where RTT is round-trip time, p is packet loss rate, which is ratio of number of lost packets to transmitted ones. Next, a wide range of simulation experiments are performed to reveal multimedia and delay-sensitive data transport challenges in CRSN.

3.3 Multimedia and Delay-Sensitive Data Delivery of Cognitive Radio Sensor Networks in Smart Grids : A Case Study

In order to reveal real-time CRSN challenges for delay-sensitive and multimedia communication, extensive simulations are studied in two parts, namely delay-sensitive data transport and real-time video streaming in CRSN. Before moving discussion of simulation results, first we explain details of CRSN network architecture and simulation environment as follows.

Performance of CRSN is closely related to licensed user activity. Therefore, determination and prediction of licensed user activity is an acute necessity. Licensed user arrivals are assumed to be independent, hence, inter-arrivals are modeled with exponential distribution. Therefore, licensed user activity can be modeled as two-state birth-death process with birth rate β and death rate α as in Fig. 3.1 , and moving from one state to another follows Poisson arrival process, which implies that length of ON and OFF periods are exponentially distributed [92]. Licensed user ON state means channel is occupied by licensed user and OFF state means channel is vacant and it can be accessed by cognitive radio users [29, 30]. By the help of assumed licensed user activity model, *posteriori* probabilities can be estimated using renewal theory [35] as:

$$P_{ON} = \frac{\beta}{\beta + \alpha} \qquad P_{OFF} = \frac{\alpha}{\beta + \alpha} \tag{3.2}$$

where P_{ON} is the licensed user being active(ON), e.g., using the channel, probability, and P_{OFF} is the licensed user being inactive(OFF), e.g., not using the channel probability. We assume spectrum sensing mechanism works perfectly, e.g., no miss detections and false alarms occurs. Therefore, licensed user activity detection probabilities are taken as directly equal to licensed user activity probabilities in simulations.

The collaborative and low-cost nature of wireless sensor networks (WSN) brings significant advantages over traditional communication technologies used in today's electric power systems. Recently, WSN has been widely recognized as a promising technology that can enhance various aspects of today's electric power systems, including generation, delivery, and utilization, making them a vital component of the next generation electric power system, the smart grid [49, 16, 27, 55, 48, 53, 102, 80]. To realize reliable and delay-sensitive electric utility monitoring and diagnostic systems, CRSN is a promising solution, with its opportuni-

Table 3.2: Log-normal shadowing path loss model parameters for different smart grid environments

Power System Environment	***Path Loss*** (η)	***Shadowing Deviation*** (σ)	***Noise Level***(dBm)
500 kV Substation	2.42	3.12	-93
Main Power Room	1.64	3.29	-88
Underground Network Transformer Vault	1.45	2.45	-92

ties to deal with radio frequency (RF) interference and varying spectrum parameters due to DSA capability [49].

In order to simulate wireless channel in smart grid environments, we have used the wireless channel model and parameters determined in our previous study via field-test experiments [49]. Specifically, as channel model, log-normal shadowing path loss model, which calculates path loss with respect to formula in Eq. 3.3, is utilized. In this model, signal to noise ratio $SNR(d)_{dB}$ at a distance d from the transmitter is given by:

$$SNR(d)_{dB} = P_t - PL(d_0) - 10\eta log_{10}(\frac{d}{d_0}) - X_\sigma - P_n \tag{3.3}$$

where P_t is the transmit power in dBm, $PL(d_0)$ is the path loss at a reference distance d_0, η is the path loss exponent, X_σ is a zero mean Gaussian random variable with standard deviation σ, and P_n is the noise power in dBm. Experimentally determined log-normal channel parameters for different power system environments are given in Table 3.2.

For power grid environment, licensed user activity can be perceived as wireless channel conditions that restricts communication of sensor nodes. Although, along the paper licensed user term is used, these results can be applied to challenged spectrum environments of power grid.

We have performed simulations by extending the ns-3 network simulator [4] to enable dynamic spectrum access in sensor networks. 200 nodes and a sink are placed randomly in a 100m x 100m field. 10 source nodes are randomly selected within an event area of radius 15m, and transmit power (P_t) is set to $10dBm$. Packet size is limited to 100 bytes due to energy efficiency issues stated in [84] and nodes are equipped with a single transmitter/receiver with a CSMA/CA based simple medium access control layer.

Sensor node behavior is modeled with data transmission (τ_S^d), spectrum sensing (τ_S^s) and spectrum handoff (τ_S^h) periods. TFRC [41] is used as transport protocol in the simulation experiments. 10 channels are created for each power grid spectrum environment, e.g., 500kV substation, main power room and underground network transformer vault, given in Table 3.2. Lastly, each simulation configuration is run 10 times and results are averaged.

In the following sections, to gain more insights regarding the challenges of real-time transport in CRSN, comparative performance evaluations are presented for delay-sensitive data and multimedia transport, respectively.

3.3.1 Delay-Sensitive Transport in CRSN

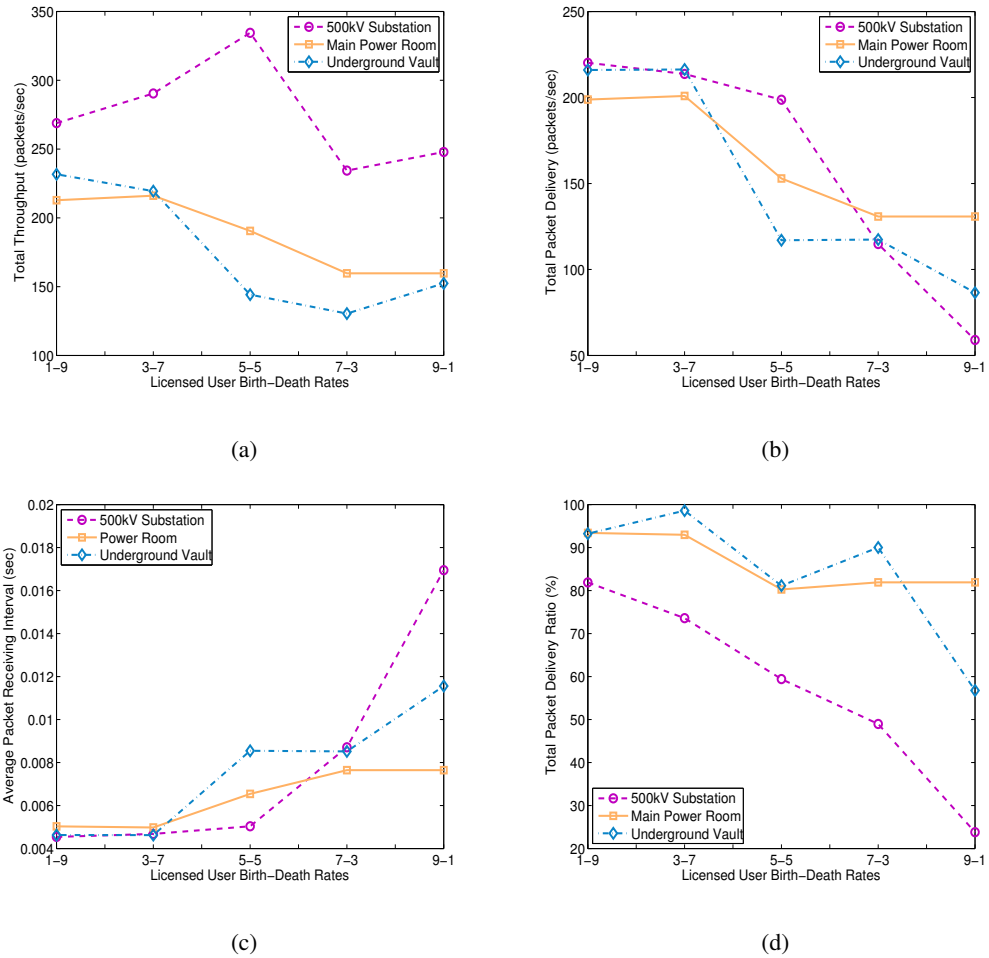

Figure 3.2: Variation of throughput(a), packet delivery(b), packet receiving frequency(c) and packet delivery ratio(d) with respect to increasing P_{ON} for τ_S^d of 1.5 sec and τ_S^s of 0.5 sec.

Timely delivery of event information is necessary for delay-critical applications in CRSN. To evaluate delay-sensitive transport issues in CRSN, we have performed simulations for different licensed user activity probability and spectrum sensing duration to data transmission duration ratio values in different spectrum environments of a power grid. In order to assess effects of licensed user activity, firstly, we have used constant spectrum sensing duration for all ten channels and changed licensed user state transition rates in Fig. 3.2 and 3.3, then, kept licensed user activity constant and changed τ_S^s/τ_S^d ratio while assessing spectrum sensing duration's effects in Fig. 3.4 and 3.5. We have measured average throughput, packet delivery, packet inter-arrival time per second and packet delivery ratio to assess performance.

3.3.1.1 Throughput

Variation of throughput with respect to different licensed user activities and spectrum sensing parameters is given in Fig. 3.2(a), Fig. 3.3(a), Fig. 3.4(a) and Fig. 3.5(a). In Fig. 3.2(a), with the increasing licensed user ON probability, different throughput patterns are observed for $\tau_S^s = 0.5sec$ and $\tau_S^d = 1.5sec$. In 500kV substation environment, throughput initially increases due to wrong measurement of RTT and packet loss probability. Packet loss probability is measured at the sink for each source and send in acknowledgement feedback packets to the source nodes. Due to its harsh spectrum conditions, in 500kV substation environment higher path loss exponent is measured, and hence, higher number of packet drops are expected. However, due to fact that acknowledgement packets from sink are not timely received packet loss rate could not being set to its desired value. Moreover, rate is regulated by time-out events in TFRC, however, as RTT gets larger TFRC source waits more for acknowledgement packets to come. Therefore, timely reception of acknowledgement packets is crucial for rate control in CRSN. On the other hand, as P_{ON} keeps increasing, throughput decays for 500kV substation environment, since RTT becomes dominant factor for controlling throughput. In main power room environment, which has a less path loss exponent than 500kV substation environment, throughput starts to decrease immediately with the licensed licensed user on probability. RTT becomes dominant factor for throughput calculation in main power room and underground network transformer vault environments. Additionally, throughput slightly increases for underground transformer vault environment while moving from $P_{ON} = \frac{7}{10}$ to $P_{ON} = \frac{9}{10}$, since rate reductions due to time-outs results in less throughput degradation with respect to degradation due to bursty losses in sensor network.

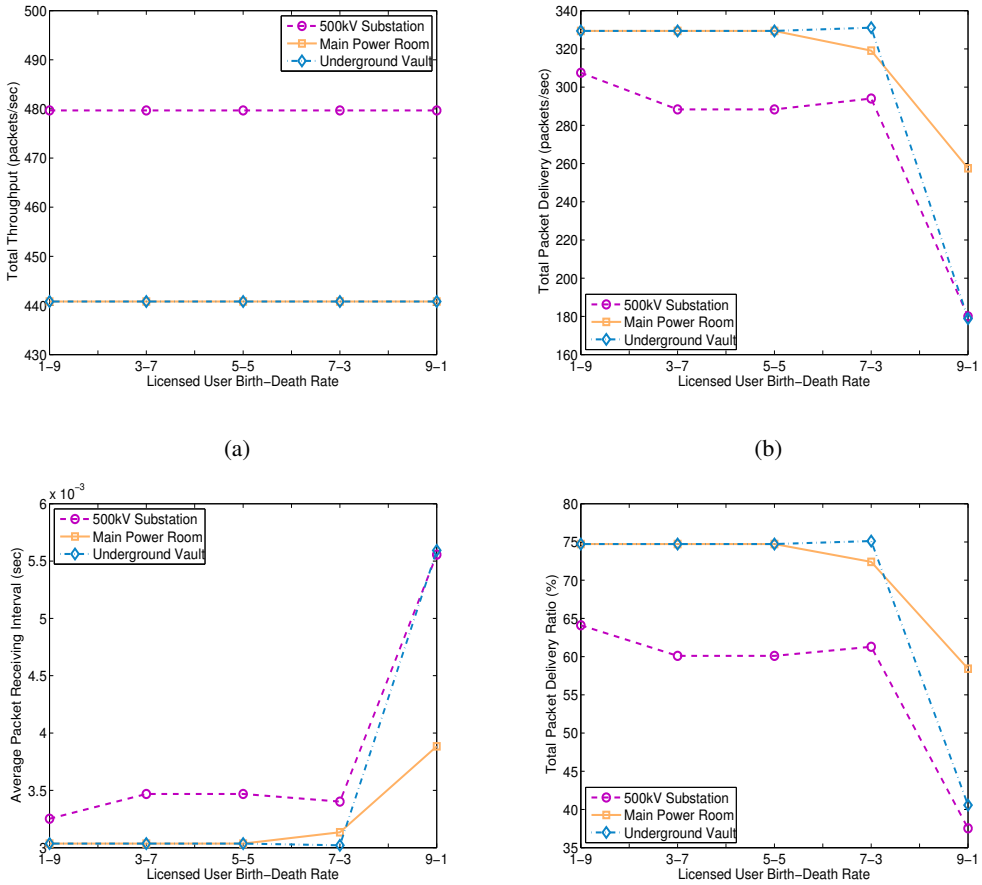

Figure 3.3: Variation of throughput(a), packet delivery(b), packet receiving frequency(c) and packet delivery ratio(d) with respect to increasing P_{ON} for τ_S^d of 1.5 sec and τ_S^s of 0.2 sec.

In Fig. 3.3(a), throughput stays constant for all licensed user birth-death rates for $\tau_S^s = 0.2$ sec and $\tau_S^d = 1.5$ sec. It shows us that as τ_S^d gets larger with respect to τ_S^s, licensed user activity does not effect throughput performance of sensor nodes. As τ_S^s is shorter relative to τ_S^d, spectrum handoff durations do not cause any change in throughput pattern.

As it can be seen from Fig. 3.2(a), TFRC throughput is not strictly decreasing with increasing licensed user birth rate. However, erroneous measurements of packet losses and RTT cause throughput to take undesirable values. Since injection of more packets cause congestion and leads to packet drops, robust throughput control is essential in real-time CRSN

In Fig. 3.4(a) and 3.5(a), variation of throughput is given for different τ_S^s/τ_S^d ratio while P_{ON} kept constant. In addition to problems in estimation of RTT and p, with the variation

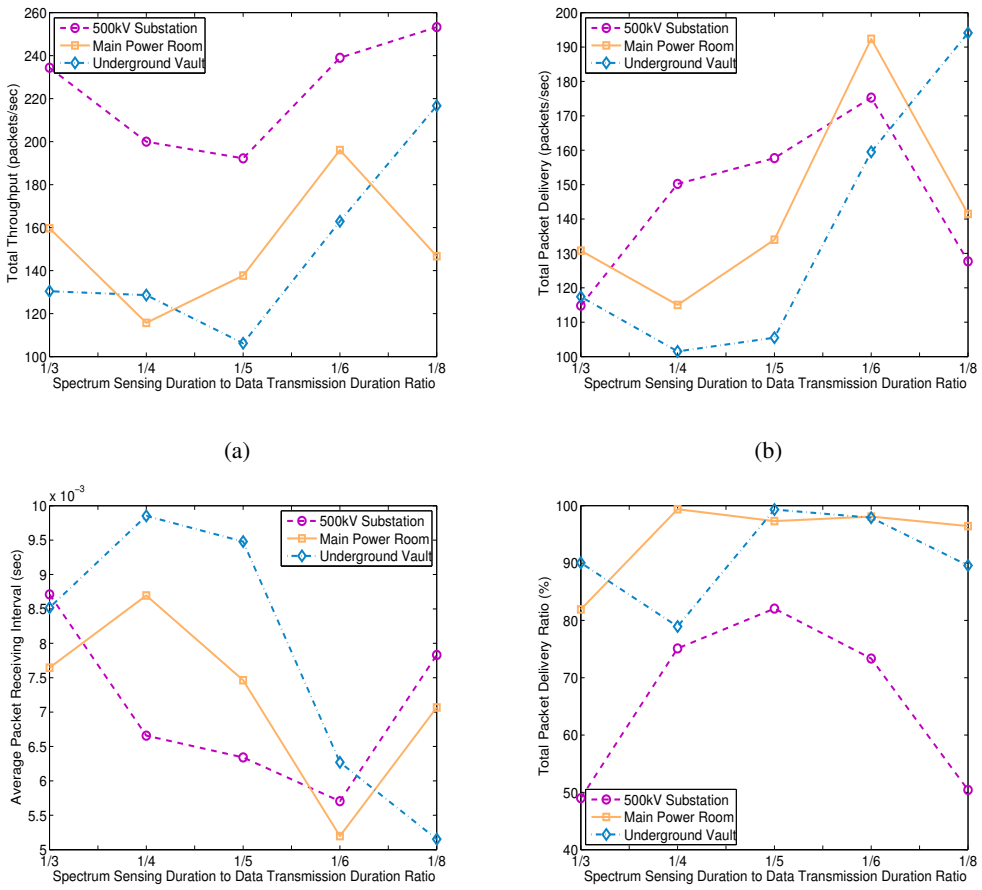

Figure 3.4: Variation of throughput(a), packet delivery(b), packet receiving frequency(c) and packet delivery ratio(d) with respect to decreasing τ_S^s/τ_S^d ratio, for $\beta = 7$ and $\alpha = 3$.

of τ_S^d congestion problem in sensor network emerges. In Fig. 3.4(a), it can bee seen for $P_{ON} = \frac{7}{10}$ that decreasing τ_S^s/τ_S^d ratio results in congestion. For the same packet generation rate, when nodes have more τ_S^d, more packets are injected into network. Therefore, decreasing τ_S^s creates bottlenecks in the network. However, with the further decreasing τ_S^s, increases in the throughput pattern are observed due to the fact that sensor nodes gain enough τ_S^d to deliver delay-critical data to sink. Same pattern for throughput is also seen in Fig. 3.5(a). However, this time sharper decreases are seen due to P_{ON} is decreased to $\frac{3}{10}$. Since less spectrum hand-offs occur because of decreased licensed user activity, more packets are injected into network in simulations of Fig. 3.5(a), and hence, congestion severity is increased. Additionally, with the decreased P_{ON} in Fig. 3.5(a) throughput reaches higher values than in Fig. 3.4(a).

With the decrease of τ_S^s, τ_S^d increases relatively, and as a result of this congestion occurs in

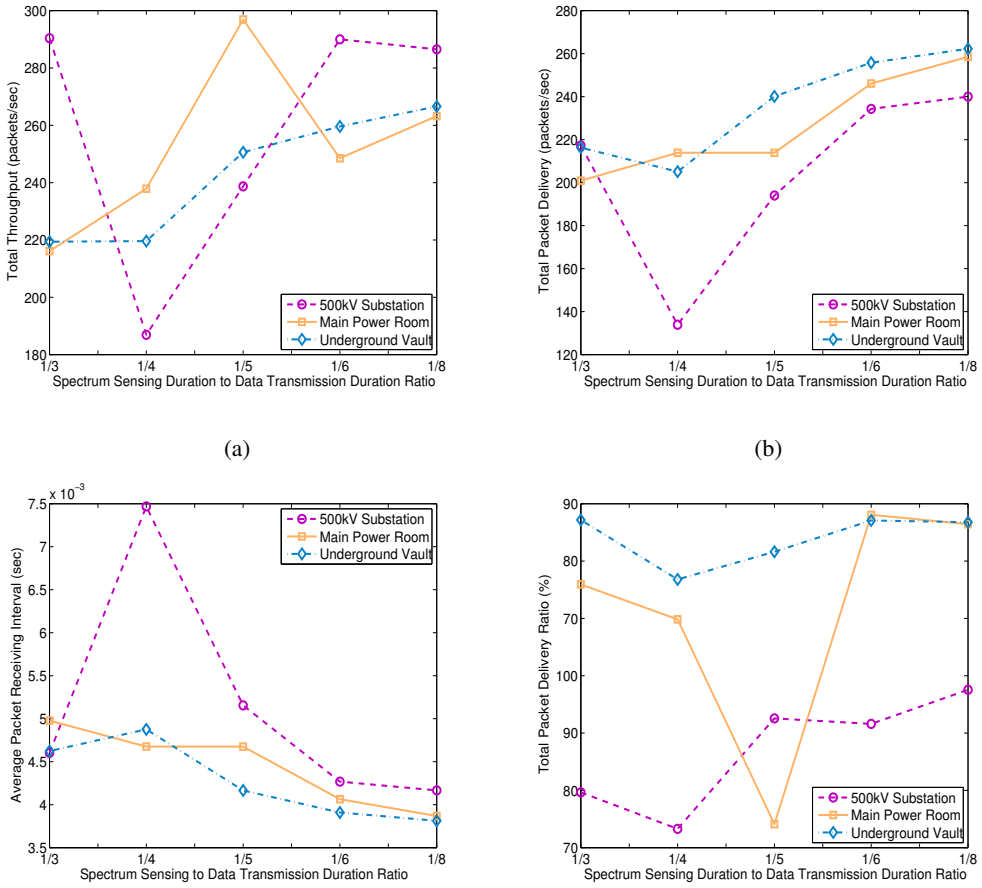

Figure 3.5: Variation of throughput(a), packet delivery(b), packet receiving frequency(c) and packet delivery ratio(d) with respect to decreasing τ_S^s/τ_S^d ratio, for $\beta = 3$ and $\alpha = 7$.

the network. From this point, increasing τ_S^s can be seen as the decrease of the packet injection into network. Therefore, with the decreasing τ_S^s, we increase the number of packets injected into network, and hence, create bottlenecks and amplify RTT. While keeping to decrease τ_S^s, these bottlenecks can be diminished as in 500kV substation environment in Fig. 3.5(a) while moving from ratio $\frac{1}{4}$ to $\frac{1}{6}$, or bottlenecks can be generated as in main power room example in 3.4(a) while moving from ratio $\frac{1}{6}$ to $\frac{1}{8}$. The relationship between throughput and τ_S^s varies depending on the spectrum environment, licensed user activity pattern and τ_S^d.

3.3.1.2 Packet Delivery

Packet delivery is given in Fig. 3.2(b) and Fig. 3.3(b) for varying P_{ON}, while τ_S^s and τ_S^d are kept constant. In Fig. 3.4, number of packets delivered to sink strictly decreases even if throughput increases. With the increasing probability of licensed user being ON, spectrum handoffs due to detection of licensed user activity are performed more frequently and exposed delay increases. Additionally, disruption of event delivery by frequent licensed user activity prevents source and intermediate nodes to deliver packets to sink in a timely manner. In Fig. 3.2(b), although throughput increases while changing P_{ON} from $\frac{3}{10}$ to $\frac{1}{2}$, packet delivery continues decreasing. Inaccurate throughput values can increase the congestion level in the network. Additionally, discrimination of wireless losses and losses due to congestion is required to efficiently control the sending rate of sensor nodes. With its high path loss exponent with respect to other environments, while licensed user ON probability is increased, 500kV substation environment's throughput decays more drastically than the throughput of other environments even its throughput increases due to wrong determination of RTT and packet loss rate. On the other hand, in Fig. 3.2(b), for a lower τ_S^s/τ_S^d ratio, packet delivery stays near constant for all three environments until P_{ON} is increased to $\frac{9}{10}$. With the decreasing τ_S^s/τ_S^d, number of delivered packets at the sink become more resistant to increasing P_{ON}, in Fig. 3.5(b). Although throughput is constant as seen in 3.5(b), delivered packets start to decay for 500kV substation environment, main power room and underground network transformer vault, respectively. Its lossy spectrum conditions make 500kV substation have less number of packets delivered at the sink with the retransmitted packets. Feedback packets are sent to regulate rate and recover missing packets in case of errors, however, on the average throughput stays constant due inaccurate measured RTT and packet loss rate.

In order to understand effect of τ_S^s/τ_S^d ratio on packet delivery, simulation results are presented in Fig. 3.4(b) and 3.5(b), for $P_{ON} = \frac{7}{10}$ and $P_{ON} = \frac{3}{10}$, respectively. Packet delivery is disrupted by congestion with the decreasing τ_S^s/τ_S^d ratio due to injection of more packets to the sensor network, in Fig. 3.4(b) and Fig. 3.5(b) for underground network transformer vault environment, which has the lowest path loss exponent in all three environments. However, as τ_S^d gets larger values than τ_S^s, delivered packets start to increase due to depleting congestion. This is due to fact that τ_S^d becomes dominant over τ_S^s. Therefore, it is not possible to say packet delivery immediately increase with the decreasing τ_S^s/τ_S^d ratio, since it is possible to

cause congestion with the increasing number of packet injections in densely deployed sensor network. Throughput, i.e., number of packets are being sent, is critical for maximizing packet delivery. Thus, accurate measurement of RTT and packet loss rate once more gains importance. On the other hand, it is certain that decreasing τ_S^s/τ_S^d ratio sufficiently has a potential improvement impact on packet delivery as it can be seen in Fig. 3.4(b) for main power room while moving from ratio $\frac{1}{4}$ to $\frac{1}{6}$ and in Fig. 3.5(b) for 500kV substation while moving from ratio $\frac{1}{4}$ to $\frac{1}{8}$, for large and small P_{ON} values, respectively.

Overall, there is a delicate balance between number of injected packets into network and congestion in sensor networks. Hence, received number of packets are depending on congestion, spectrum conditions and cognitive radio parameters such as spectrum sensing and henceforth licensed user activity.

3.3.1.3 Average Packet Receiving Interval

Due to spatial and temporal correlation of the information delivered by sensor nodes [100], it is important to receive required amount of packets in a predefined delay bound in delay-sensitive applications [47]. In Fig. 3.2(c), 3.3(c), 3.4(c) and 3.4(c) average inter-arrival time of incoming packets at the sink is given in order to assess timeliness of event detection in delay-critical applications. Each of 10 source nodes was set to generate $100bytes$ packets per $25msec$. Therefore, average packet generation inter-arrival by source nodes in the sensor network is considered to be about $2.5msec$.

In Fig. 3.2(c) and 3.3(c), average inter-arrival time of received packets is strictly increases. Increasing P_{ON} disturbs the delay-sensitive data transport of event. Although sending interval was 0.025 for each of 10 source nodes, e.g., 400 packets are generated per second by all source nodes, sink receives about 250 packets per second, e.g., an average inter-arrival duration of 0.004 sec., for $P_{ON} = \frac{1}{10}$, and τ_S^s and τ_S^d are equal to 0.5 and $1.5sec$, respectively. For 500kV substation spectrum environment, it increases rapidly up to 0.017 sec. in Fig. 3.2, which is undesirable when real-time delivery of event is thought. For a lower τ_S^s, e.g., 0.2 sec., in Fig. 3.3(c), average packet inter-arrival also increases sharply with increasing P_{ON}, however, it is relatively smaller than the one observed in previous case, e.g., it has a maximum packet inter-arrival duration about $\frac{1}{3}$ of the one in 3.2(c) for all three spectrum environments.

Due to the variation of both throughput and congestion level in the network, average packet receiving interval at the sink does not follow a simple pattern with the decreasing τ_S^s/τ_S^d in Fig. 3.4(c) and Fig. 3.5(c) for constant P_{ON}, $\frac{7}{10}$ and $\frac{3}{10}$, respectively. For decreasing τ_S^s/τ_S^d ratio, average packet inter-arrival time follows different patterns. It takes values up to 400% and 300% of sending inter-arrival duration, in Fig. 3.4(c) and Fig. 3.5(c), respectively. This points out the heavily congested sensor network due to load of 40 packets per source node in a second, and variation of τ_S^s/τ_S^d can cause this congestion deplete or overwhelm sensor network based on P_{ON}. Therefore, consideration of congestion prone densely deployed sensor network's constraints is essential in order to satisfy real-time QoS requirements.

3.3.1.4 Packet Delivery Ratio

In terms of energy efficiency, packet delivery ratio is an important metric for sensor networks with high communication load due to their resource limited nature. We measure packet delivery ratio as the ratio of total received packets by sink to total sent packets by source nodes in the network. Dropped packets in lower layers of source node or in forwarding intermediate nodes and lost packets due to spectrum environment are not received by sink.

In Fig. 3.2(d), packet delivery ratio decays with the increasing P_{ON}. In addition to its lossy propagation environment, frequent spectrum handoffs cause packet delivery ratio in 500kV substation environment to decay from 0.8 to 0.22, in Fig. 3.2(d). In Fig. 3.3, packet delivery ratio is kept constant (as it was in throughput and packed delivery plots in Fig. 3.3(a) and in Fig. 3.3(b), respectively) about 0.7. Packet delivery ratio is about 75% and 60% for underground network transformer vault and 500 kV substation, respectively. Which means that, at least one quarter of created packets, together with retransmissions, could not be delivered to the sink due to packet drops or propagation errors. This points out the need for adequate flow control algorithms in CRSN for use with energy limited sensor nodes.

Since lower τ_S^s/τ_S^d ratio enables source nodes to inject more packets into network to be delivered to sink, congestion spreads from source nodes to intermediate nodes, which forward packets toward sink. In Fig. 3.5(d), due to low P_{ON} relative to Fig. 3.4(d), packet delivery ratio does not drop below 70%. Initially packet delivery decreases, afterwards, it starts to increase since less spectrum handoff delay is exposed due to lower P_{ON}, e.g., for main power room environment packet delivery ratio firstly decreases due to congestion and then with the

decreasing τ_S^s/τ_S^d ratio, packet delivery ratio starts to increase in Fig. 3.5(d). On the other hand, in Fig. 3.4(d), packet delivery initially decreases while τ_S^s/τ_S^d ratio decreases, then it turns to be increasing for underground network transformer vault environment.

Based on spectrum environment and communication load on sensor nodes, packet delivery ratio can decrease with decreasing τ_S^s/τ_S^d ratio. Packet delivery ratio also can be seen as an indicator of energy efficiency, and hence, flow control gains crucial importance in delay-sensitive CRSN applications to both preserve energy and deliver events timely. In order to keep network away from congestion and prevent energy wastage, τ_S^s/τ_S^d ratio should be taken into consideration deliberately with according P_{ON} and spectrum environment while controlling rate of source nodes.

3.3.2 Real-time Video Streaming in CRSN

In simulations a sample MPEG-4 stream of $10sec$ ($30fps$, $289.58Bytes$ average frame length, $35.39dB$ average frame peak signal-to-noise ratio) is used to assess real-time video streaming challenges in CRSN and simulations are run for $11sec$. Since, in [84] it is shown that energy efficiency reduces after a packet size threshold of $100bytes$, frames are packeted into $100bytes$ chunks. Evalvid [1] is used to extract results of simulations to assess video streaming performance. For the received video, while lost packets are zero padded, during decoding lost sections are extrapolated from already reconstructed frames.

3.3.2.1 Throughput, Packet Delivery and Energy Efficiency

Throughput, packet delivery and energy efficiency results of CRSN nodes using TFRC for different power grid environments are given in Fig. 3.6(a), 3.6(b) and 3.6(c), respectively. Throughput and packet delivery results represent the total amount of packets sent by sources and delivered to sink, respectively. Since loss of packets means waste of energy in sensor networks, we measured energy efficiency as ratio of delivered packets to sent packets.

While the number of transmitted packets are above $650pakcets/sec$ between 0 and $8sec$ in Fig. 3.6(a), it can be seen from Fig. 3.6(b) that received packets at sink are always below $500packets/sec$. Varying RTT due to spectrum sensing and spectrum handoff functionalities causes TFRC throughput to fluctuate frequently. Varying RTT due to spectrum sensing and

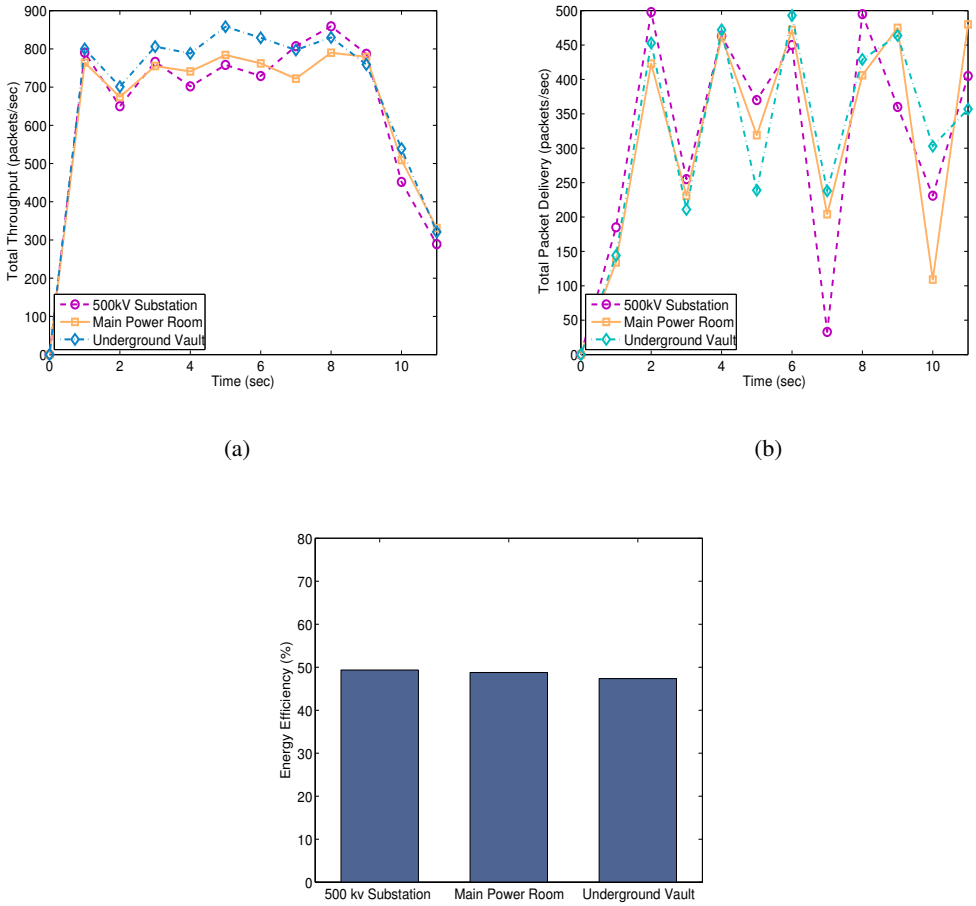

(a) (b)

(c)

Figure 3.6: Throughput (a), packet delivery(b) and energy efficiency(c) for video streaming in CRSN.

spectrum handoff functionalities causes TFRC throughput to fluctuate frequently. In addition, smaller RTT values result in larger throughput values, since TFRC throughput is inversely proportional to square root of RTT [42]. TFRC throughput is inversely proportional to square root of RTT. Therefore, smaller RTT values will result in larger throughput values.

On the other hand, due to dense deployment and multi-source nature of sensor networks, while the number of injected packets into network are getting larger and larger, number of delivered packets at the sink decreases. It can be seen in Fig. 3.6(a) and 3.6(b) at first, second, third and forth seconds clearly. In addition to silent spectrum sensing periods, another reason for fluctuation of received packets at the sink is bursty nature of sensor network. After silent periods, intermediate nodes on the path to sink are exposed to high load with incoming pack-

ets. This results in drop of excessive amounts of packets. Even more, at some instants, e.g., sixth second, received packets per second drops below one third of the sent packets (throughput), e.g., while total sending rate of source nodes are 710 packets per second, receiving rate of sink node is about 220 packets per second. Moreover, more than half of the energy is wasted for all different power grid environments as given in Fig. 3.6(c).

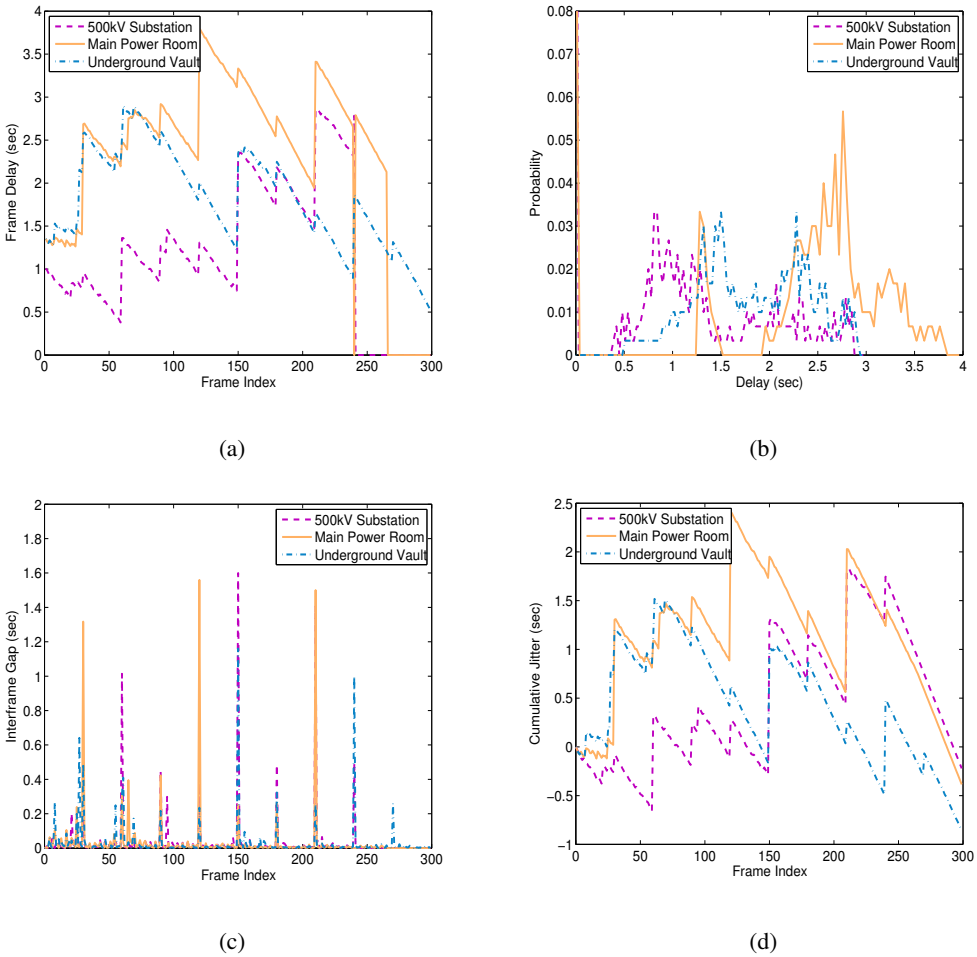

Figure 3.7: End-to-end packet packet delay(a), pdf of end-to-end packet delay(b), interframe gap of received frames(c) and cumulative jitter(d) for video streaming in CRSN.

3.3.2.2 Frame End-to-end Delay and Jitter

In Fig. 3.7(a), (b) and (c) frame end-to-end delay measurements per frame are given for 500kV substation, main power room and underground transformer vault, respectively. Only in underground transformer vault all of the frames could be delivered to sink at the end of 11th second. However, frame end-to-end delay measured for underground transformer vault envi-

ronment mostly stays above of 1*sec* and reaches over 2.5*sec* for some frames in Fig. 3.7(c), which is inappropriate for real-time video application considerations in sensor network. On the other hand, although more than 50 of last frames are not delivered, frames are exposed to less delay at 500kV substation environment, in Fig. 3.7(a), with respect to other environments, in Fig. 3.7(b) and (c). Due to the tough spectrum environment of 500kV substation with respect to other power grid environments, more packets are lost on the way to sink because of wireless propagation. Although this incurs retransmission of lost packets, it resolves the bottleneck on the sink path. However, this is not an efficient solution to reduce end-to-end delay, since energy is wasted in this way. On the other hand, it can be seen from Fig. 3.6(c) most energy efficient operation is obtained in 500kV substation environment. Consecutive timeouts due to not arriving acknowledgement packets from sink is the main reason for rate reduction for source sensor nodes, while this leaves some of the sensor nodes out of event delivery, it helps others to deliver their packets to sink better, however, the resultant picture is still far from meeting timely delivery requirement of real-time applications. End-to-end frame delay reaches values over 3*sec* around frame index 150 for main power room environment in Fig. 3.7(b), afterwards it decreases up to 2*sec* due to timeout events and packet drops with reduction in rate. However, in addition to excessive amount of delay, around 30 of the frames could not be delivered to the sink.

Probability distribution function of delay is given in Fig. 3.7(b) for 500kV substation, main power room and underground transformer vault environments, respectively. Probability reaches its peak value around delay values frequently measured. In Fig. 3.7(b), for substation environment exposed end-to-end packet delay is mostly around 1*sec*. When compared main power room and underground network transformer vault environments, which have a exposed delay mostly around 2.7*sec* and 1.5*sec*, respectively, 500kV substation environment is likely to sustain less delay. However, it is still far from allowing real-time communication in CRSN, and takes values up to 2.8*sec*. End-to-end delay values around 2.7*sec* are more frequently observed in Fig. 3.7(b) for main power room environment. Additionally, in Fig. 3.7(b) end-to-end delay measurements around 1.5*sec* get higher probability for underground network transformer vault environment, again it is very high for real-time video streaming considerations.

The difference between frame arrivals are pointed out in Fig. 3.7(c) for 500kV substation, main power room and underground transformer vault. High inter-frame gaps cause freezing,

e.g. decreases quality, of the video, and prevents real-time streaming. However, in all of three environments inter-frame gap reach to 1*sec* and over. Spectrum sensing durations and spectrum handoff intervals are also important for inter-frame gap minimization. Intermittent connectivity due to licensed user activity makes it hard to satisfy application specific quality of service (QoS) requirements of CRSN. This property makes CRSN extremely challenging for real-time video streaming.

Variance of the inter-frame time is named as cumulative frame jitter. In Fig. 3.7, jitter values are acceptable only for the frames at beginning of the video. Then jitter starts to fluctuates and reaches 1.8, 2.4 and 1.5*sec* as maximum values for 500kV substation, main power room and underground transformer vault, respectively. Injection of more packets into network in sensor network increases the congestion in the network and causes bursty frame losses which boosts the difference between successful frame arrivals. Moreover, periodic spectrum sensing intervals and spectrum handoffs based on licensed user activities contribute to increase in jitter. In addition to traditional sensor network challenges, challenges introduced by CRSN, e.g., spectrum sensing durations and spectrum handoff intervals, amplifies the jitter and should be inspected deliberately to satisfy delay constraints of running application.

3.3.2.3 Peak Signal to Noise Ratio (PSNR)

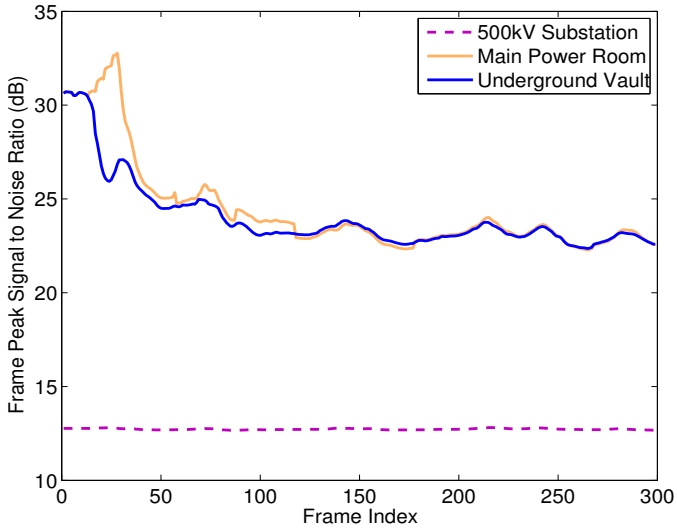

Figure 3.8: Frame PSNR values of received video in different power grid environments.

In order to have acceptable quality, real-time video streaming should have an average PSNR more than $30dB$ for each frame. In Fig. 3.8, obtained PSNR of the delivered frames are shown for different spectrum environments in power grid. Since as time goes on, i.e., as more packets are released by source nodes to be delivered at sink, network tends to get more congested, and hence, for higher frame indexes resultant PSNR is lower than previous ones. In 500kV substation environment lowest PSNR values for received frames are observed, i.e., $12.6dB$. In relatively better spectrum conditions having main power room and underground network transformer vault environments PSNR values of frames start above $30dB$, however as frame index increases PSNR values decreases to below $25dB$, which implies received video quality is poor.

3.4 Observations and Future Research Directions

Energy-efficiency has been the main focus of transport layer solutions proposed for sensor networks thus far [105]. For this aim, designed solutions mainly concentrated on rate control algorithms that provide reliability while keeping network away from congestion. However, with the sensor nodes equipped with cognitive radio, in addition to energy efficiency, dynamic spectrum access (DSA) should be transparent to event delivery. Additionally, many real-world applications, such as multimedia applications, have strict delay bounds and hence mandate timely transport of the event features from the sensor field to the sink node. Dynamic spectrum management also brings additional challenges to sensor network characteristics for real-time transport in CRSN. Overall, performance evaluations in Section III provide valuable insights to clarify challenges posed by DSA combined with the unique characteristics of sensor networks. In this section, the main results of the simulations are outlined and open research issues for multimedia and delay-sensitive data transport in CRSN are summarized.

3.4.1 Overview of Simulation Results

Extensive simulations address the existing challenges in the design of transport protocols, and show that transport layer performance suffers from cognitive cycle introduced with DSA. Results are outlined briefly as follows.

- Spectrum sensing, one of the main functionalities in cognitive radio, causes silent peri-

ods that nodes sense the channel. In these silent periods packet delivery to sink stops. Therefore, extra delays induced on event information carrying and feedback packets.

- Varying the τ_S^s/τ_S^d ratio causes network change its congestion condition. While larger τ_S^s/τ_S^d ratio allows source nodes to send less packets in a given time, in this case congestion is mainly concentrated on source nodes. However, as the τ_S^s/τ_S^d ratio decreases more packets are injected into network, and hence, drops on the path to sink are observed until τ_S^s/τ_S^d ratio decreases sufficiently to allow all nodes attending real-time transport from source nodes to sink as in 3.4(b) and 3.5(b).

- Accurate RTT and packet loss rate measurements gain importance in analytical rate control schemes, since extra delays and packet drops caused by cognitive radio reduces the quality of multimedia streaming (Fig. 3.7 and 3.8) and timeliness of delay-sensitive data (Fig. 3.4(c) and 3.5(c)).

- With the detection of licensed user activity, sensor nodes are required to leave the channel and must find a vacant channel to maintain ongoing communication. This brings disruptions on the source to sink path. Due to unawareness of licensed user detection and spectrum handoff functionality, transport layer continues to send packets. Due to this fact packet delivery ratio decreases drastically in Fig. 3.2(d) and 3.3(d) for $P_{ON} = \frac{9}{10}$.

- Timeliness of delivered packets are critical in real-time applications. In delay-sensitive data delivery simulations (Fig. 3.2(c) and 3.3(c)) and multimedia simulations (Fig. 3.7), it is shown that exposed delay is very high satisfying real-time QoS requirements. Therefore, minimization of incurred delays is essential while taking resource limited nature of sensor nodes into consideration.

DSA causes to have variations in packet delivery and delay in CRSN for different spectrum characteristic. This points out the need for spectrum-aware transport layer solutions for real-time and energy efficient communication requirement for multimedia and delay-sensitive transport in CRSN. Effects of resultant extra delays and packet losses due to incorporation of cognitive radio in sensor network are investigated in simulation results, and these results show the need for DSA-aware transport protocols considering bursty many-to-one flow in CRSN.

3.4.2 Open Research Issues

Multimedia and delay-sensitive data transport in CRSN requires consideration of inherent characteristics of sensor network and cognitive radio challenges together to enable timely energy-efficient communication in CRSN. Overall, design of novel spectrum adaptive real-time transport solutions for CRSN is needed and spectrum awareness is the key factor to increase performance of desired transport solution. Multimedia and delay-sensitive data transport in CRSN requires special attention due to varying spectrum conditions, induced delays by spectrum sensing and spectrum handoff functionalities, and sensor network's tend to congestion. In order to enlighten further research on multimedia and delay-sensitive data transport in CRSN, we point out open research issues of transport layer as follows:

- Novel transport protocols taking DSA functionalities and challenges into consideration is required to enable energy efficient and timely delivery of multimedia and delay-sensitive data to sink. Collaboration of cognitive cycle and rate control algorithm is needed. Adaptive transmission strategies regulated by the licensed user activity and cognitive radio functionalities is essential for delay-critic applications in CRSN.

- Predictive frameworks can be developed based of probabilistic behavior pattern of licensed users. As in TFRC case, analytic models can be developed including cognitive radio parameters, spectrum conditions and licensed user activity pattern in addition to sensor network characteristics.

- Designed protocols should adapt rapidly to dynamically varying network capacity due to spectrum handoff. With the union of the cognitive radio and sensor networks, network capacity problem is further amplified and estimation of it becomes extremely challenging.

- Cross layer interactions are essential with cognitive cycle in order to benefit from cognitive radio and utilize limited resources of sensor nodes efficiently. Therefore, cross-layer rate control algorithm integrating cognitive radio functionalities and rate control algorithm is necessary to real-time communication demand in CRSN.

- Based on varying licensed user activity, spectrum sensing duration and spectrum environment, novel real-time and energy efficient algorithms required to control rate of source nodes. With spectrum handoff, in addition to introduced extra delay, spectrum

environment and cognitive radio parameters such as spectrum sensing and data transmission period are changes. Novel techniques should be developed to enable seamless multimedia streaming and delay-sensitive data delivery in CRSN.

CHAPTER 4

SPECTRUM-AWARE AND ENERGY-ADAPTIVE RELIABLE TRANSPORT IN COGNITIVE RADIO SENSOR NETWORKS

In this chapter spectrum-aware and energy-adaptive reliable transport (SERT) protocol is presented for collaborative event sensing in CRSN. The objective of SERT is to adapt the reporting rate of sensors based on spectrum opportunities and determine the desired number of sources, i.e., event reporting, nodes via estimation theory to achieve adequate reliability in event sensing. The SERT protocol is introduced in [21]. A review of related work is presented in Section 4.2. Network architecture is given in Section 4.3. The effects of the intermittent communication and OSA on the reliable event transport performance are investigated in Section 4.4. The spectrum-aware and energy-adaptive reliable transport protocol for opportunistic distributed sensing is given in detail in Section 4.5. The simulation experiment results and performance evaluation of SERT are discussed in Section 4.6.

4.1 Motivation

Cognitive radio (CR) is the key enabling technology to provide opportunistic spectrum access (OSA) and mitigate inefficient utilization of overall wireless spectrum. Cognitive radio networks (CRN) are characterized by opportunistic access of unlicensed users to vacant bands of the licensed spectrum. In order to overcome spectrum scarcity and increase utilization efficiency, CR can detect and communicate over spectrum holes opportunistically [54]. Therefore, the opportunistic spectrum access (OSA) capability provided by CR enables communication over a licensed spectrum for sensor networks under limited spectrum availability conditions such as emergency and warfare. Sensor nodes equipped with cognitive radios ba-

sically can access spectrum opportunistically via utilizing OSA, and this constitutes a new sensor network paradigm, i.e., cognitive radio sensor networks (CRSN) [8].

CRSN consists of interconnected CR equipped sensor nodes that perform collaborative event sensing. Sensor nodes are responsible for the reliable delivery of event observations based on spectrum opportunities from the event region to sink in a multi-hop manner. Overall, CRSN brings significant advantages over traditional WSN, including opportunistic channel usage and adaptability to reduce power consumption [8]. CRSN can be used to provide ubiquitous distributed sensing for a very wide range of cyber-physical systems, including agriculture, homeland security, disaster relief, and smart grid applications. However, realization of these envisioned applications depends on reliable and energy-efficient event transport capabilities of the CRSN.

A typical CRSN architecture is represented in Fig. 1.1. In this architecture, CRSN nodes can be in the communication range of different licensed users. CRSN is expected to provide spectrum-aware and spectrum mobility transparent distributed sensing as well as collaborative energy-efficient reliability. The CRSN poses various challenges for reliable event transport as:

- **Intermittent Communication**: CRSN is required to sense the spectrum regularly, and event reporting is paused while spectrum sensing, since the existing communication modules cannot perform spectrum sensing and event reporting simultaneously.
- **Spectrum Mobility**: CRSN nodes must reconfigure their spectrum sensing durations and schedules based on new spectrum characteristics.
- **Network Life-time**: Both the number of source, i.e., event reporting, nodes and individual reporting rate of sensor nodes should be carefully devised to achieve utmost network life-time with reliability in CRSN.

All these challenges coupled with the processing limitations, dense deployment and bursty communication nature of sensor nodes call for a versatile, efficient, and flexible transport layer to realize opportunistic distributed sensing for cyber-physical systems. Energy-efficient congestion avoidance [104, 112, 115, 106] and collaborative reliable event sensing [93, 6, 47] have been the main approaches in transport protocol design for wireless sensor networks (WSN). While these solutions have been adequate for distributed event sensing in WSN, their

performance in CRSN was shown to be not adequate [20] with regard to intermittent communications, spectrum mobility, and network life-time challenges in CRSN. Recently, there has been some research incorporating cognitive radio functionalities into transport layer for single hop as well as multi-hop ad hoc networks [33, 76, 86]. In these studies, traditional transmission control protocol (TCP) has been the design basis, which has been demonstrated to be unsuitable for WSN [105, 6]. Therefore, incorporation of cognitive radio capability and inherited features from WSN require a new event transport protocol to overwhelm exceptional challenges of CRSN.

In this chapter, spectrum-aware and energy-adaptive reliable transport protocol (SERT) which dynamically adjusts its parameters to adapt heterogeneous spectrum opportunities, i.e., varying spectrum sensing and data transmission durations after spectrum handoff, is presented. Furthermore, SERT selects source nodes in the event region according to spectrum opportunities and sensed event signal characteristics while adapting energy constraints. To the best of our knowledge, this is the first work on the transport layer focusing on reliable event transport for opportunistic distributed sensing over CRSN. The distinctive features of SERT are as follows:

1. **Spectrum Awareness**: SERT adapts the reporting rate of sensor nodes to heterogeneous spectrum sensing durations and mitigates oscillations in the total number of received packets at sink, which are caused by interruptions due to silent spectrum sensing periods.

2. **Opportunistic Reliability**: Source nodes and their reporting rates are dynamically adapted to spectrum opportunities and event signal characteristics to achieve reliability under spatio-temporally varying licensed user presence and spectrum coordination failures.

3. **Reliable Network Life-time**: SERT provides network life-time preservation via limitation on reporting rates of source nodes to conform to energy expenditure constraint and continue its operation reliably during the planned network life-time.

4. **Low Complexity**: SERT is tailored based on a simple and universal distributed sensing model that does not rely on any specific type of data or application. Reporting rate updates and selected source nodes are broadcast by the sink to avoid delays on the sink-to-sensor path and to provide agility on rate control.

4.2 Related Work

CRSN has been receiving increasing interest from the community. To minimize total power consumption, a joint event and spectrum sensing scheme is proposed in [119]. Delay performance of CRSN is assessed in [70] for different types of traffic, and periodic and triggered channel switching mechanisms. To address licensed user interference, reliable detection requirements, and energy efficiency, packets size optimization is studied in [83]. Using partially observable Markov decision process framework, an energy-efficient channel assignment is studied in [52]. In [120], the authors propose a spectrum-aware clustering algorithm to reduce power consumption via having low distance among nodes in a cluster. However, an event transport protocol that adapts itself to spectrum opportunities has yet to be developed for CRSN.

Energy efficiency has been the main objective in proposed transport protocols for WSN as well as providing reliable event transport functionality [105]. In [104, 112, 115, 106], proactive and predictive congestion avoidance approaches are proposed to prevent inefficient utilization of limited energy resources of sensor nodes. In [93], the authors proposed an end-to-end solution approach for WSN. In [6, 47], the reliability notion in WSN is re-defined based on event tracking accuracy objective at sink, and instead of end-to-end packet-based reliability, the collection of a certain number of packets in a decision interval is proposed. Although these protocols address WSN requirements, they are shown to have very poor performance in CRSN [20].

Recently, there have been TCP-based studies on transport protocol design for CRN. Through tuning TCP for CR compability, a set of transport protocols were derived from TCP in [86] to serve delay-tolerant applications. In [33], the authors proposed a transport protocol for cognitive radio ad hoc networks (TP-CRAHN), which incorporates the channel information and spectrum sensing function into the TCP rate control algorithm. Jointly addressing CR functionalities, modulation, coding, and frame size, a cross-layer optimization scheme is proposed in [76] to maximize TCP throughput. TCP-based works are devised mainly to improve end-to-end reliability and congestion control performance in CRN. Many-to-one communication and collaborative event reporting challenges of sensor networks are not addressed in these works.

Despite the significant amount of research in transport protocols for WSN and rate control schemes for CRN, none of these works address challenges regarding event transport in CRSN. Thus, a spectrum-aware transport protocol is needed to address both OSA challenges and distributed sensing requirements in energy-constrained CRSN.

4.3 CRSN Architecture

For the transport protocol design, we used a distributed sensing network composed of cognitive radio capable sensor nodes. A simple topology for CRSN is shown in Fig. 1.1. Such a topology is representative for cyber-physical systems consisting of sensor nodes data gathering about the structure health information in buildings or soil conditions in agriculture.

4.3.1 Spectrum Management Model

Each sensor node has a single transceiver with capability of spectrum sensing and handoff. The licensed user ON state means the channel is occupied by a licensed user, and OFF state means the channel is vacant and can be accessed by CRSN nodes. The sensor nodes employ periodic spectrum sensing to detect licensed user communication, and cannot communicate during spectrum sensing. Sensor node behavior in a channel c is modelled with data transmission (τ_t^c), and spectrum sensing (τ_s^c) periods as shown in Fig. 4.1.

The sink is responsible for spectrum decision and coordination. After the start of event reporting, the selected source and intermediate, i.e., forwarding, nodes are excluded from spectrum sensing. When there is not any reported event, spectrum handoff is performed immediately with licensed user detection. During event reporting, if licensed user communication is detected by a subset of source nodes, the sink replaces them with sensor nodes in the event region that have not detected licensed user activity, i.e., that have spectrum opportunity. To facilitate this operation, SERT employs an energy-adaptive source node replacement procedure for spectrum opportunity variations in the event region to prevent excessive consumption of limited energy resources of CRSN nodes, which will be explained in Section 4.5.3.

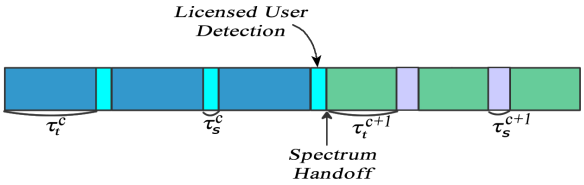

Figure 4.1: CRSN node activity pattern with time.

4.3.2 Event-to-sensor Dispersion and Distributed Sensing Model

To estimate the event signal, the best linear unbiased estimator (BLUE) [78] is employed at the sink, since the estimator is made comprehensive and does not depend on distribution of a specific sensing noise apart from second-order moment. Therefore, we do not assume any specific distribution for sensed signal and noise. Observation $s_m(t)$ is the distorted version of event signal $\theta(t)$ by observation noise $\eta_m(t)$ and dispersion loss in signal power $\gamma_m(t)$ through the sensor due to the distance between the sensor and the event source, i.e., $s_m(t) = \gamma_m(t) \cdot \theta(t) + \eta_m(t)$, at sensor m and time t. Each sensor sends a measured signal $s_m(t)$ to the sink, where θ is estimated from the received version of $\theta(t)$. We also assume that both $\theta(t)$ and $\eta_m(t)$ are i.i.d. over time, and $\theta_m(t)$ and $\eta_m(t)$ have zero mean and power of σ_θ^2 and ξ_m^2, respectively. Under independence over time and space assumption, indices are ignored for all variables.

The sink collects samples during estimation interval (τ_d) and generates an estimate of the event at the end of each τ_d. The number of received samples during an estimation interval is as

$$X = \tau_d \cdot \sum_{m=1}^{M} G_m \cdot S_p \tag{4.1}$$

where M is the number of the source nodes, G_m is the packet reception rate from sensor m, S_p is the number of samples contained in a packet. The received sample vector is a combination of sensing noise and sensed signal as $\mathbf{r} = \boldsymbol{\gamma} \cdot \boldsymbol{\theta} + \mathbf{n}$, where $\mathbf{r} = [r_1, \cdots, r_X]^{\mathrm{T}}$, $\boldsymbol{\gamma} = [\gamma_1, \cdots, \gamma_X]^{\mathrm{T}}$, $\boldsymbol{\theta} = [\theta_1, \cdots, \theta_X]^{\mathrm{T}}$, and $\mathbf{n} = [n_1, \cdots, \eta_X]^{\mathrm{T}}$. The estimate of event signal using BLUE is as [78]

$$\hat{\theta} = \left[\boldsymbol{\gamma}^T \mathbf{R}^{-1} \boldsymbol{\gamma}\right]^{-1} \boldsymbol{\gamma}^T \mathbf{R}^{-1} \mathbf{r} \tag{4.2}$$

where $\mathbf{R}$ is M-dimensional diagonal covariance matrix of the received samples at sink, whose diagonal entries are ξ_m^2, and other entries are 0. The mean square error (MSE) for BLUE is

[78]

$$D = Var\left[\hat{\theta}\right] = \left[\boldsymbol{\gamma}^T \mathbf{R}^{-1} \boldsymbol{\gamma}\right]^{-1} = \left(\sum_{n=1}^{X} \frac{\gamma_n^2}{\xi_n^2}\right)^{-1} = \left(\sum_{n=1}^{X} \frac{\sigma_\theta^2 \gamma_n^2}{\sigma_\theta^2 \xi_n^2}\right)^{-1} \tag{4.3}$$
$$= \sigma_\theta^2 \left(\sum_{m=1}^{M} \tau_d G_m \cdot S_p \psi_m\right)^{-1} = \frac{\sigma_\theta^2}{\tau_d S_p} \left(\sum_{m=1}^{M} G_m \psi_m\right)^{-1}$$

where ψ_m is the signal-to-noise ratio ($\frac{\gamma_m^2 \cdot \sigma_\theta^2}{\xi_m^2}$) for samples of node m. We assume that during an estimation interval τ_d, ψ_m of a sensor does not change. SERT uses (4.3) in formulation of energy-adaptive source node selection problem (4.6) to calculate distributed estimation distortion D for a set of selected source nodes and compare D with desired distortion level D_0. We now discuss the effects of OSA on event transport in CRSN and explain SERT design principles.

4.4 SERT Design Principles

Here, we discuss the the main design constituents of SERT in detail via a case study and numerical results to gain more insight regarding the SERT protocol operation. In the following subsections, we first describe the impact of intermittent communication and spectrum heterogeneity on reliable event estimation. Then, we analyze the effect of loss of spectrum opportunity and source node selection on distributed sensing reliability and network life-time in CRSN.

4.4.1 Impact of OSA and Spectrum Heterogeneity on Reliable Event Transport

To investigate the effects of spectrum handoff among heterogeneous spectrum sensing and data transmission duration having channels, we study the reliability level oscillations and decrease caused by these interruptions. We perform simulations by extending *ns-3* [4]. A total of 100 sensor nodes and a sink are placed randomly in a 500 m x 500 m field. Source nodes are selected from an event area of radius 30 m, and transmit power (P_t) is set to 10 dBm. While calculating received power, log-normal shadowing path loss model is used, which is accurate for propagation in sensor networks [123]. The packet size is limited to 64 Bytes due to energy efficiency issues stated in [83]. Simulations are repeated 10 times and results are averaged. τ_h^c is set to 0.005 sec for each channel c. Two different estimation intervals (τ_d) are

Table 4.1: Lengths of τ_s^c and τ_t^c, and Spectrum Handoff Instants (t_c) Used in Experimental Analysis for Each Channel c

$\boldsymbol{c}$	1	2	3	4	5	6	7	8	9	10
$\tau_{\mathbf{t}}^{\mathbf{c}}$	0.6	0.3	0.6	0.3	0.2	0.6	0.3	0.4	0.2	0.6
$\tau_{\mathbf{s}}^{\mathbf{c}}$	0.1	0.2	0.05	0.2	0.05	0.05	0.2	0.1	0.1	0.1
t_c	0	3	5	11	14	15	17	22	25	28

used to investigate reliability level oscillations and reduction due to spectrum heterogeneity and spectrum handoff. X_d is the number of required samples per estimation interval to reliably estimate and track event features, and required number of packets per τ_d is found via X_d/S_p. The reliability requirement for different τ_d values of 0.5, and 1 sec are set as 25, and 50 packets per τ_d, respectively. τ_s^c duration, τ_t^c duration, and spectrum handoff instants t_c for each channel c used in the simulations are summarized in Table 4.1.

In our experimental analysis, sensors update their reporting rate independent of underlying protocol stack via a simple and reliability-oriented yet practical scheme. One such mechanism based on event observation reliability Γ_k at sink can be as

$$J_{k+1} = J_k \cdot 1/\Gamma_k \tag{4.4}$$

where J_k is the reporting rate of sensors for the k^{th} estimation interval, and Γ_k is the reliability level at sink for k^{th} estimation interval, which is determined by the ratio of received samples (X) to the desired number of samples (X_d). At the start of each estimation interval, Γ_k is broadcast by sink to source nodes for reporting rate update.

Results regarding the transient reliability performance with OSA and without OSA cases are presented in Fig. 4.2. Under OSA, event observation reliability at sink experiences significant oscillations compared to the non-OSA case due to heterogeneous spectrum conditions, i.e., varying τ_t^c and τ_s^c with spectrum handoff. In Fig. 4.2, the reliability level oscillates about 20%, and 40% in case of OSA for estimation intervals of $\tau_d = 0.5$ and 1 sec, respectively. The magnitude of oscillations in the reliability level for $\tau_d = 0.5$ sec is smaller compared to $\tau_d = 1$ sec, since smaller τ_d reduces the time elapsing until the rate update after the spectrum handoff. Longer τ_d defers adapting the reporting rate to heterogeneous spectrum conditions due to spectrum handoff. From this point of view, reporting rate updates must be performed immediately after spectrum handoff. This points out the impact of concurrent reporting rate updates with spectrum handoff under heterogeneous spectrum conditions for reliable and ef-

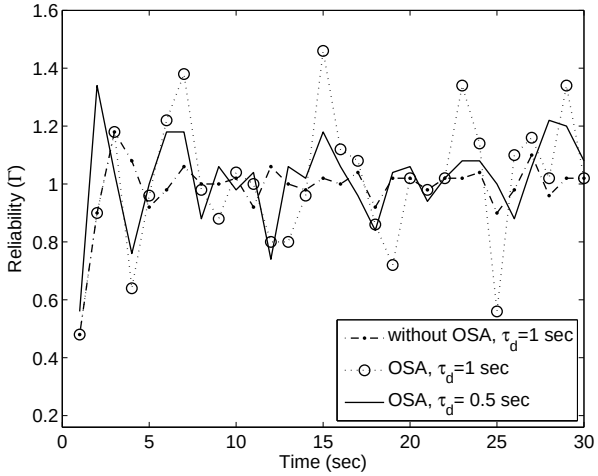

Figure 4.2: Reliability performance at sink for $\tau_d = 0.5$ sec with OSA and $\tau_d = 1$ sec with OSA and without OSA.

ficient distributed sensing in CRSN.

The ratio of data transmission to cognitive cycle duration in channel c, i.e., $\tau_t^c/(\tau_t^c + \tau_s^c)$, is defined as r_c. In Fig. 4.3, the reporting rate update performed by sink after spectrum handoff is presented for varying r_c, i.e., r_{c+1}/r_c for different τ_d. If a spectrum handoff is performed among homogeneous channels, i.e., r_{c+1}/r_c is about unity, then the rate update at the end of the estimation interval is about unity as well. However, as r_{c+1}/r_c ratio decreases, the reporting rate is increased significantly, e.g., reporting rate doubles for $r_{c+1}/r_c = 0.5$. Using the obtained rate regulation behavior in Fig. 4.3 for different τ_d, reporting rate scaling after spectrum handoff for the rate update mechanism in (4.4) is found as

$$\frac{1}{\Gamma_k} \approx \frac{r_{c+1}}{r_c} \tag{4.5}$$

These results motivate us to devise a spectrum-aware transport layer protocol that maintains the desired reliability in heterogeneous spectrum conditions for various estimation intervals. To achieve seamless distributed sensing reliability, reporting rate updates should be decoupled from event estimation intervals. The reporting rate is updated after the spectrum handoff via spectrum-aware rate update approach. The spectrum-aware rate update policy provides a sufficient approximation for rate updates in case of different estimation intervals. Since we do not seek the exact model of reporting rate oscillations in CRSN, we use this approach for regulation of the reporting rate in SERT and evaluate its performance in Section 4.6.

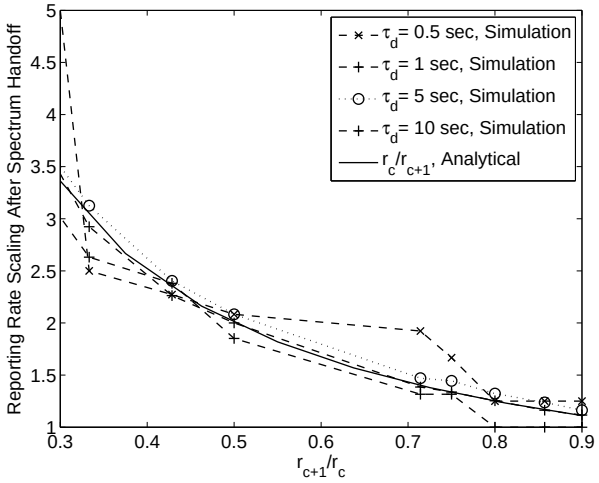

Figure 4.3: Report rate updates after spectrum handoff for various τ_d values.

4.4.2 Impact of Spectrum Opportunity Loss and Source Node Selection on Reliable Event Transport

As illustrated in Fig. 1.1, the number of sensor nodes that can report an event is limited by the spectrum opportunities. Some portion of the source nodes in the event region may lose their spectrum opportunity due to spatially varying licensed user communication. These source nodes must be replaced by other nodes in the event region that have spectrum opportunity. We investigate the effect of the distortion requirement on source node selection and discuss its implications on event transport in CRSN. Distortion formulation developed in (4.3) is used for the numerical evaluation. Dispersion loss γ_m is selected randomly from the interval between $[0, 1]$ for the source nodes in the event region. The sensing noise ξ_m is 0.01 for all m. The number of sensors in the event region is 100. The average packet reception rate G_m, and number of samples in a packet S_p is set to 4 packets/sec for all m and 10 samples for all packets, respectively. Simulations are performed 1000 times, and results are averaged. Using developed distortion function (4.3), the minimum required number of source nodes to satisfy estimation distortion constraint is given in Fig. 4.4 for estimation intervals of 0.5, 1, 5, and 10 sec.

The number of source nodes varies significantly based on distortion constraint and estimation interval. As the τ_d decreases, the number of source nodes increases in bursts, e.g., from

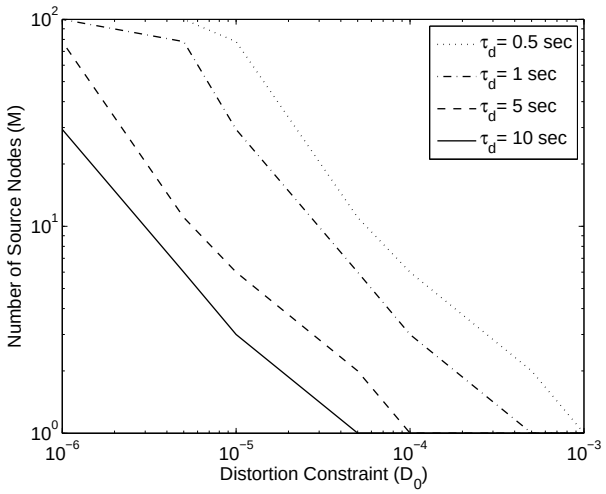

Figure 4.4: Number of source nodes with respect to distortion constraint (D_0).

about 5 to 90 when τ_d is decreased from 10 to 0.5 sec for $D_0 = 10^{-5}$. Especially under low D_0 and τ_d requirements, inefficacious and inefficient source node selection would inevitably yield degradation of reliability performance and depletion of limited energy resources of sensor nodes in CRSN. Additionally, in case of spectrum coordination failures, the sensor nodes remaining uncoordinated cannot participate in event communication. In [20], simulation experiments regarding the performance of event delivery are presented in the act of spectrum coordination failure. While reliability-oriented protocols [6, 47] update their reporting rate to satisfy reliability objectives, congestion control oriented protocols [104, 33] regulate their reporting rates irrespective of reliability requirements and fail to provide reliability. However, in reliability-oriented approaches, the energy consumption of source nodes remaining coordinated increases significantly due to enhanced reporting rates. Therefore, achievement of reliable event transport under variations in spectrum opportunities and spectrum coordination failures in the event region necessitates an energy-adaptive source node selection scheme. In the design of SERT, we jointly address energy expenditure per estimation interval and estimation distortion constraints. SERT performs energy-adaptive source node selection according to signal-to-noise ratio (SNR) of event sampling sensor nodes, so as to mitigate adverse effects of spectrum opportunity losses and coordination failures.

4.5 Spectrum-aware and Energy-adaptive Reliable Transport

To provide reliability in varying heterogeneous spectrum environments while conforming energy expenditure constraints, SERT is equipped with four main components, namely, an initial source node selection algorithm based on sensed signal characteristics, a spectrum-aware reporting rate update mechanism adapting itself to heterogeneous spectrum conditions, an energy-adaptive source node replacement scheme addressing limitations on energy consumption of sensor nodes, and a proactive local congestion detection mechanism.

4.5.1 Instant Start

Upon event detection, a sensor network must instantly start event reporting such that the sink can reliably estimate and track event features. When limited energy resource and dense deployment of sensor nodes are examined, the number of source sensors and their reporting rate must be limited and configured to achieve reliability requirements at the sink.

Therefore, event detecting sensor nodes send their sensing signal-to-noise ratio (SNR) to the sink for source node selection and reporting rate configuration. The initial reporting rate is set uniformly among source nodes by sink according to initial energy consumption constraint per estimation interval E_{τ_d}. The initial reporting rate is determined via $J_0 = E_{\tau_d}/E_p$, where E_p is the energy consumed to transmit a packet. Using the estimation distortion formulation in (4.3), the minimum number of nodes are selected to satisfy D_0 with $G_m = J_0$ from all event detecting nodes m. To this end, sensing SNR (ψ_m) values of event detecting sensor nodes are sorted in the descending order and inserted into (4.3), until $D \leq D_0$ is achieved. The subset of event detecting nodes achieving $D \leq D_0$ are assigned as source nodes. After the instant start phase, the spectrum-aware rate control algorithm is executed for regulation.

4.5.2 Spectrum-aware Rate Control

Fig. 4.2 shows that when multiple spectrum handoffs take place during event estimation, reporting rate updates become inaccurate. Furthermore, for large τ_d, waiting for the end of τ_d for a reporting rate update fails reliable distributed sensing. Thus, the reporting rate updating is performed after each spectrum handoff as well as at the end of each τ_d.

Recall that we previously defined Γ_k as the reliability level indicator based on the received number of samples at a τ_d, i.e., the ratio of the number of received samples during a τ_d (X) to the required number of samples per τ_d (X_d). For simple rate update mechanism (4.4) applied at the end of each τ_d, it is shown in Fig. 4.3 that the reporting rate scaling approximately equals to (4.5). To determine the proper event reporting rate update policy after spectrum handoff under heterogeneous spectrum conditions, motivated from the results in Fig. 4.3, reporting rates of source nodes are scaled with the reciprocal of the r_c/r_{c+1} after spectrum handoff. Overall, the spectrum-aware rate updating policy can be formulated as $J_{i+1} = r_c/r_{c+1} \cdot J_i$, where $J_{\mathrm{i+1}}$ is the reporting rate after update, and J_{i} is the current rate. We perform performance evaluations of SERT to assess the spectrum-aware rate update policy's effectiveness to maintain reliability at the desired level for different τ_d.

4.5.3 Energy-adaptive Source Node Selection for Collaboration

To design the selection and reporting rate of collaborating sensors in the event area, we assume that CRSN is employed with a pre-determined value on energy expenditure per τ_d (E_{τ_d}) to enable the distributed sensing operation over the desired network life-time. However, the main concern of SERT is reliability. Although energy efficiency is one of the main design objectives in CRSN, reliability and timely distributed sensing should not be compromised for energy conservation. Therefore, apart from the strict distortion requirement, E_{τ_d} is advisory and used for initial node selection, spectrum coordination failures, and spectrum opportunity losses. Section 4.4.2 points out that instead of blind selection of source nodes, a scheme utilizing sensing signal-to-noise ratio (SNR) would increase efficiency in distributed sensing. Therefore, SERT adapts the selection of source nodes from the event region to energy constraints of sensor nodes, i.e., E_{τ_d}.

In addition to the source node selection upon event detection described in Section 4.5.1, we devise an energy-adaptive approach to select source nodes in case of spatial spectrum opportunity variations and spectrum coordination failures where bursts in energy consumption can be experienced as previously elaborated in Section 4.4.2. Using the estimation distortion

formulated in (4.3), the energy-adaptive source node selection problem is stated as

$$\begin{aligned} \textbf{min} \quad & M \\ \textbf{s.t.} \quad & \frac{\sigma_\theta^2}{\tau_d \cdot S_p} \left(\sum_{m=1}^{M} J_0 \cdot \psi_m \right)^{-1} < D_0 \end{aligned} \tag{4.6}$$

To solve this problem, the sink sorts source nodes according to their sensing SNR ψ_m in the descending order. Then, using ψ_m in (4.3), it checks if distortion constraint is satisfied, i.e., $D \leq D_0$ is achieved. When the desired distortion level is achieved, the set of sensor nodes with a greater SNR than the latest one used in (4.3) are selected as source nodes for event reporting.

4.5.4 Proactive Local Congestion Detection

SERT includes a buffer occupancy-based local congestion detection component. To detect congestion, each sensor m measures the moving average of the total incoming packet rate λ_m due to packet generation and relaying, and the outgoing packet rate β_m for its local buffer. For congestion detection, SERT monitors buffer occupancy level, i.e., the number of empty slots in the buffer, for a time period equal to the sum of data transmission and spectrum sensing interval ($\tau_t^c + \tau_s^c$) to prevent overflow. If the empty slots of the local buffer are expected to be filled in the next $\tau_t^c + \tau_s^c$, i.e., congestion is detected, the sensor node pauses packet generation and relaying. The congestion detection condition is formulated as

$$Q_m^{\text{left}} < (\tau_t^c + \tau_s^c) \cdot (\lambda_m - \beta_m) \tag{4.7}$$

where Q_{left} is the size of empty slots in the buffer of node m assuming fixed packet size, and τ_s^c is the spectrum sensing duration for currently access channel c. Taking advantage of the broadcast nature of the wireless channel, congestion detection information is piggybacked in the header of packets. With omni-directional antenna, relayed nodes can capture such information when packets with Congestion On the Way (COW) flag are transmitted by their relay nodes towards the sink. They generate COW for back-pressure if (4.7) is satisfied, since all nodes run a proactive local congestion detection algorithm on itself as well.

4.6 Performance Evaluation

To study the performance of SERT, we developed an evaluation environment using *ns-3*[4]. We use the same sensor node and simulation configurations described in Section 4.4.1 and 4.4.2. We run simulation experiments for spectrum mobility, and spectrum opportunity loss under heterogeneous spectrum conditions, and spatially varying licensed user activity, respectively.

4.6.1 Spectrum Mobility

We first analyze the performance of SERT for varying cognitive cycle parameters under heterogeneous spectrum conditions. To the best of our knowledge, there is no existing transport protocol that addresses challenges due to incorporation of CR functionality into sensor nodes, and protocols devised for conventional sensor networks cannot be compared with SERT in a fair manner. We use $(RT)^2$ [47] for comparison due to its reliability-oriented rate control which conforms with SERT's rate control approach and investigate how SERT adapts itself to maintain reliability after spectrum handoff and transiently. For analysis of reliability variation after spectrum handoff, we investigate the effect of spectrum handoff to the lower r_c value having channels, which results in reduction of data communication duration in an event estimation interval. r_{c+1}/r_c value is varied from 0.2 to 0.9. For transient reliability analysis, τ_t^c durations are set to 0.4, 0.2, 0.5, 0.3 sec for channel 1 to 4, respectively, while τ_s^c durations are set to 0.1 for all channels. Licensed user arrivals are scheduled randomly between estimation intervals 1 - 3, 3 - 4, 4 - 6, and 6 - 8 for channels 1 to 4, respectively, for $\tau_d = 0.5$ sec. For $\tau_d = 1$ sec licensed user arrivals are scheduled randomly between estimation intervals 1 - 3, 3 - 5, and 5 - 7 for channels 1,2, and 4, respectively. The reliability requirement for $\tau_d = 0.5$, 1, 5 and 10 sec are set as 25, 50, 250, and 500 packets per τ_d, respectively.

4.6.1.1 Reliability Performance After Spectrum Handoff

Fig. 4.5 shows the reliability performance of SERT after spectrum handoff among heterogeneous channels with different r_c values. Reliability loss after spectrum handoff sharply decreases with increasing r_{c+1}/r_c ratio, since the data communication duration variation between different channels is reduced. SERT incorporates changing cognitive cycle parameters

to rate control algorithm and updates its rate at spectrum handoff, while $(RT)^2$ waits for the end of estimation interval for the rate update and attributes the reliability decrease to node failures and packet losses. Therefore, SERT reduces the experienced loss in reliability after spectrum handoff with its spectrum-aware rate control scheme. Furthermore, SERT experiences no reliability loss for r_{c+1}/r_c values greater than 0.5 and 0.7 for $\tau_d = 5$ sec and $\tau_d = 10$ sec, respectively. The variation of reliability after spectrum handoff against r_{c+1}/r_c ratio in Fig. 4.5 shows that SERT responds to the varying r_c with reduced reliability decrease, and the reliability decrease can even be completely mitigated after the scaling.

In Fig. 4.5, rate adaptation via SERT improves achieved reliability. Furthermore, the performance of SERT increases when the difference of r_c values of accessed channels is small, i.e., r_{c+1}/r_c is near unity, implying that the forced scaling of the rate is effective in achieving reliability.

4.6.1.2 Transient Reliability Performance

Here, we study the performance improvement provided by SERT for transient reliability in consecutive spectrum handoff scenarios. In addition to $(RT)^2$, we use exponentially weighted moving average (EWMA) as an alternative conservative rate update policy to compare with transient reliability performance of SERT, which is defined as

$$J_{\mathrm{i}+1} = \alpha \frac{r_c}{r_{c+1}} J_{\mathrm{i}} + (1 - \alpha) J_{\mathrm{i}} \tag{4.8}$$

where $J_{\mathrm{i}+1}$ is the reporting rate after update, J_{i} is the current rate, α is the smoothing factor. In the evaluations, α is set to 0.25 for EWMA rate update policy. The SERT rate update can also be derived from EWMA via setting $\alpha = 1$.

In Fig. 4.6, the transient reliability performance of SERT is presented with the $(RT)^2$ and EWMA scheme. Consecutive spectrum handoffs cause a change of cognitive cycle parameters, and hence, the received number of samples from sensors varies at the sink. This change dominates the reliability performance. It prevents fixing the reporting rate of sensors at a constant level. However, SERT achieves reduced reliability variations around ± 0.2 and less than ± 0.1 for $\tau_d = 0.5$ and 1 sec, respectively. The reliability improvement provided by SERT increases especially for a higher τ_d value compared to $\tau_s^c + \tau_t^s$ value, which varies from 0.3 to 0.6 sec for different channels used in simulations. For $\tau_d = 1$ sec in Fig. 4.6 (b), SERT

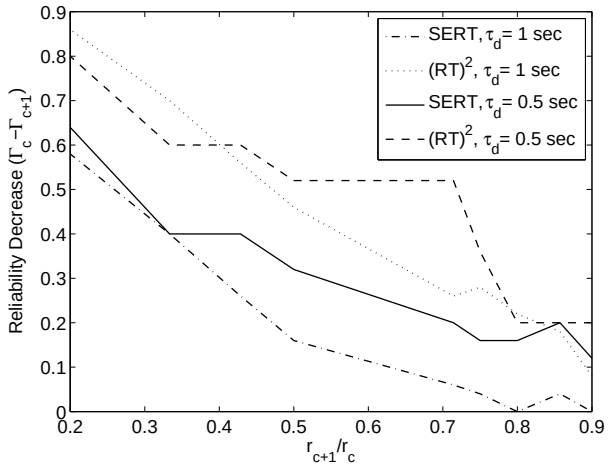

(a)

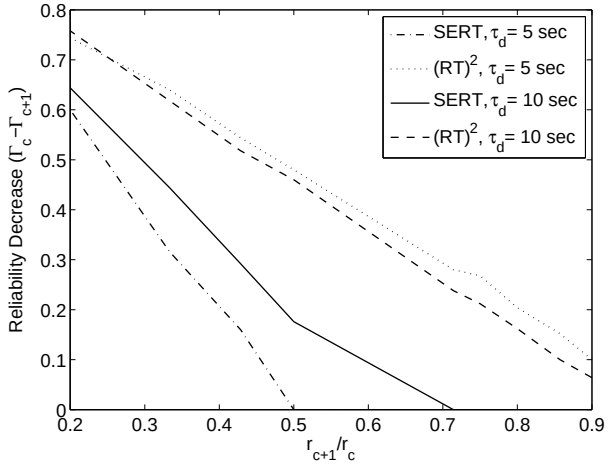

(b)

Figure 4.5: Reliability performance of SERT after spectrum handoff for various τ_d values.

achieves a significantly higher reliability performance due to the spectrum-aware rate control mechanism. Although EWMA rate update scheme performs close to SERT for $\tau_d = 0.5$ sec, its conservative policy does not provide sufficient adaptation capability to changing spectrum conditions, and for $\tau_d = 1$ sec, it performs far below SERT and close to (RT)^2. (RT)^2 updates reporting rate of sensors at the end of each estimation period in accordance with its rate regulation policy. It fails to adapt changing spectrum conditions, and as the estimation interval gets higher compared to $\tau_t^c + \tau_s^c$, its reliability performance falls behind SERT dramatically.

The effect of the spectrum-aware rate control results in higher transient reliability performance for SERT as seen in Fig. 4.6. Furthermore, the performance improves when the

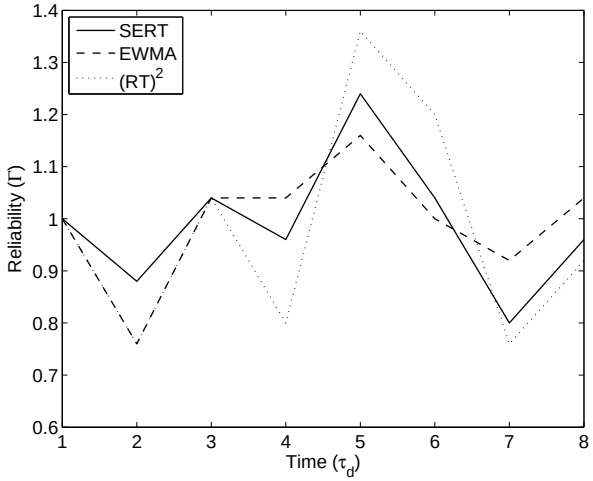

(a)

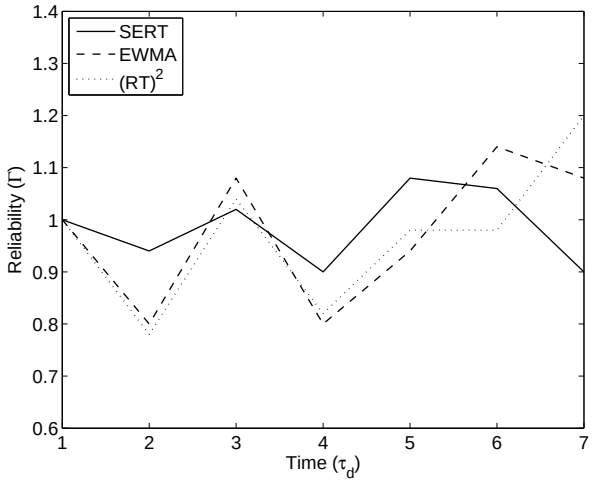

(b)

Figure 4.6: Transient reliability performance of SERT for τ_d values of 0.5 and 1 sec, in (a) and (b), respectively.

difference in the difference between the r_c value of the channels is higher, implying that spectrum-aware rate control is effective in achieving reliability. The transient variation of the reliability in Fig. 4.6 shows that SERT responds to spectrum handoff functionality immediately, and after the rate update, the reliability is achieved in most of the cases, while oscillations are reduced.

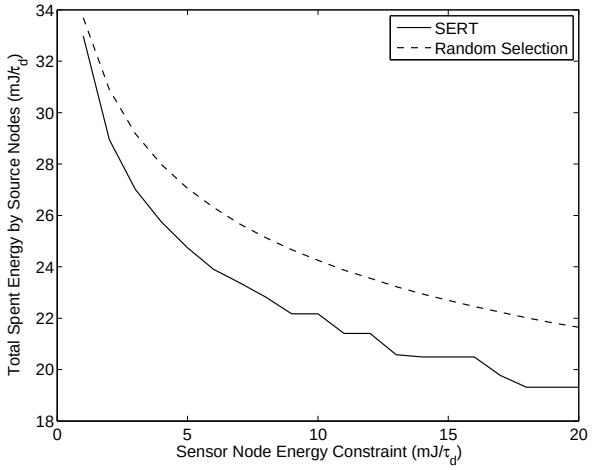

Figure 4.7: Total energy consumption of source nodes in CRSN for different sensor node energy constraint levels.

4.6.2 Spectrum Opportunity Loss

SERT performance is examined for total energy consumption per τ_d with respect to different per node energy constraint and the number of new source nodes used in case of loss nodes due to spectrum opportunity loss or coordination failure. Energy-adaptive source node selection is performed via SERT as described in 4.5.3. We calculate energy consumption for active mode E_a and transmission of a packet (E_t) as $E_a = \tau_d \cdot I_a \cdot V_s$ and $E_t = T_b \cdot L_p \cdot I_t \cdot V_s$, respectively. I_a is the active mode current, I_t is the transmitting current, T_b is the byte transmission time, L_p is the packet size, and V_s is the supply voltage of the sensor nodes. V_s is set to 3 V, I_a is set to 8 mA, I_t is set to 17.4 mA, T_b is set to 32 μsec[62]. L_p is equal to 64 Bytes [83].

Fig. 4.7 gives the relationship between per node energy constraint (E_{τ_d}) and total energy consumption per τ_d. Distortion constraint D_o is set to 10^{-4}. While the energy level per node increases, the total energy consumption in network decreases, since the number of selected source nodes is decreased. Furthermore, SERT provides about 15%, i.e., 3 mJ, energy saving per estimation interval for 20 mJ sensor node energy constraint level per estimation interval against random selection with its energy-adaptive source node selection scheme algorithm. The source sensor selection with respect to sensing SNR provided by SERT extends the network life-time. As the higher node energy level enables operating with a higher report rate per sensor node, the required number of collaborating source nodes for reliable event estimation

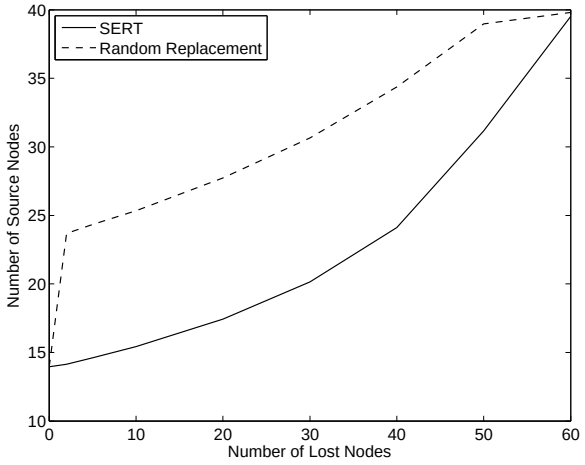

Figure 4.8: Number of selected source nodes for different number of spectrum opportunity lost nodes.

is also decreased, which prevents activation of new source nodes. Therefore, increasing the energy level per node decreases energy consumption per estimation interval by the CRSN.

We also analyze the performance of SERT for opportunistic spectrum availability and spectrum coordination errors in CRSN. In Fig. 4.8, desired number of source nodes is revealed using random source node replacement and SERT for selection of new source nodes instead of lost source nodes. As the percentage of lost sensor nodes in the event region increases, the number of activated sensor nodes increases as well to compensate for lost nodes. SERT provides SNR based source selection, and hence, it provides the same amount of distortion level for less amount of activated source sensors with respect to the random source node replacement case. The difference between the number of source nodes between SERT and random replacement scheme varies from around 5 to 10. As the percentage of the lost nodes decreases, achieving distortion constraint requires involvement of more source nodes due to remaining low SNR nodes in the event region, and hence, performance of the non-adaptive scheme comes closer to SERT.

CHAPTER 5

ADAPTIVE SPECTRUM SHARING IN DISTRIBUTED SENSING WITH COGNITIVE RADIO SENSOR AND ACTOR NODES

In this chapter, a new Spectrum Hole Assignment for Reliable Estimation (SHARE) scheme is introduced for real-time distributed sensing with cognitive radio sensor and actor nodes. SHARE is a unified spectrum sharing scheme for both local estimation via sensors connected to an actor node and reaching consensus among actor nodes via communication of local sensing information. SHARE was first presented in [22]. In Section 5.2 related work is presented. In Section 5.3, distributed sensing architecture composed of cognitive radio sensor and actor nodes is elaborated. Impact of cognitive radio utilization in distributed sensing is modelled in Section 5.4. Distortion-aware minimized spectrum access is revealed in Section 5.5. Opportunistic consensus is analyzed in Section 5.6. SHARE scheme is proposed in Section 5.7. Simulation results are presented in Section 5.8 to elaborate performance of SHARE.

5.1 Motivation

Wireless sensor networks (WSN) comprise large number of tiny sensor nodes to enable the remote monitoring of a wide variety of cyber physical systems [13]. Furthermore, with integration of actuator nodes, WSN is not only used for monitoring but also it can be deployed for controlling of physical systems, where actuator nodes can respond immediately against events and interact with the environment [14]. To achieve this operation, energy-efficient collection and timely coordination of sensing results must be addressed along with spectrum efficiency due to limited unlicensed bands [10].

Cognitive radio sensor networks (CRSN) are proposed to mitigate spectrum scarcity specifically in dense deployed sensor networks and enable distributed sensing over temporally unoccupied portions of the licensed spectrum [8]. Incorporation of cognitive radio (CR) into distributed sensing requires sharing of spectrum opportunities among CRSN nodes while addressing event specific sensing requirements, as well as inherited collaborative and energy-constrained nature of sensor networks. Furthermore, cognitive radio actor nodes can collect observations of CRSN nodes and cooperate to reach a global estimate, i.e., consensus [82]. Reaching consensus in a decision, i.e., estimation, interval requires efficient and adaptive sharing of spectrum opportunities among cognitive radio sensor and actor nodes, such that desired amount of samples can be collected from sensors with minimum spectrum access and actors can reach a consensus during an estimation interval.

Due to limited battery sizes, energy efficiency has been the main consideration for communication algorithm design for CRSN. Energy-efficient channel management is studied in [52]. Residual energy aware channel assignment is investigated in [69]. Energy-efficient spectrum sensing algorithm for CRSN is proposed in [77]. However, these works mainly lack in incorporating collaborative nature of sensor networks, and application specific reliability, i.e., estimation distortion and interval, requirements are disregarded. Furthermore, spectrum sharing problem for cognitive radio networks (CRN) are investigated in [56, 117, 118, 51, 43]. Main drawback of these schemes is missing consideration of detection and monitoring requirements of sensor networks. In our design, we specifically target to exploit collaborative effort of sensor nodes on the same event and achieve reliability opportunistically while reaching consensus among actor nodes in an estimation interval.

In this chapter, first, we characterize required spectrum opportunity to attain desired estimation distortion level while minimum amount of channels are accessed in an estimation interval based on spectrum mobility parameters, i.e., licensed user activity, interference, spectrum sensing and handoff durations, as well as real-time distributed sensing parameters, i.e., observation noise, delay-bound on reaching consensus, and energy consumption limitation per estimation interval. Then, we study required duration for reaching consensus among actor nodes after collection of samples from sensors and generating local estimate based on the interruption probability due to licensed user interference. Two regimes are identified: One in which sufficient spectrum opportunity exists and consensus can be achieved among actor nodes, and one in which actor nodes try to minimize the disagreement as much as they

can support, i.e., provide opportunistic consensus, due to limited spectrum availability. The regime of operation depends on the licensed user activity on channels, and the early regime is desirable but achievable only for sparse licensed user existence on the spectrum. It is concluded that in certain environments under sparse spectrum occupancy by licensed users, spectrum access duration of sensor nodes can be adaptively reduced to enable convergence to consensus for actors in an estimation interval. To this end, we propose spectrum hole access for reliable estimation (SHARE) scheme that can adapt assignment of sensor nodes to spectrum holes is proposed. SHARE minimizes spectrum access of sensor nodes and assigns them to unoccupied spectrum portions in time and frequency domains efficiently while providing sufficient duration to actor nodes for reaching consensus. Contribution of this work can be outlined as follows

1. *Distortion-aware Minimized Spectrum Access*: Local estimation distortion at actor node is modelled with respect to sensing signal-to-noise ratio (SNR), energy constraint per estimation interval, reporting rate and channel error rate. Minimum number of channels to be accessed for collection of required number of samples from sensor nodes in a given spectrum access duration to achieve target distortion level is revealed.

2. *Opportunistic Consensus*: Impact of interruptions due to licensed user arrivals, misdetection of licensed users, and wireless channel errors on reaching consensus is formulated. Prolongation in the consensus convergence time is studied under opportunistic spectrum access (OSA).

3. *Spectrum Hole Assignment for Reliable Estimation*: SHARE algorithm is developed using distortion-aware minimized spectrum access framework to enable achievement of consensus in an estimation interval. SHARE adapts spectrum access of sensor nodes in accordance with spectrum opportunities so that consensus can be reached while minimum amount of channels accessed are accessed by sensors during local estimation phase.

5.2 Related Work

In [52], a channel management scheme is proposed via modelling spectrum handoff as partially observable markov decision process. Energy efficiency of sensor nodes is the main de-

sign consideration. Cluster head node distribute spectrum decision its member sensor nodes. Although energy efficiency is important for spectrum decision in CRSN, reliable estimation and coordination requirements of cluster heads is not addressed.

In [69], a channel assignment protocol is proposed in which higher residual energy having nodes are given priority for spectrum access to maximize network life time. However, event detection and tracking requires achievement of a certain distortion level for reliability, and hence, network life-time is not the only concern in CRSN. Furthermore, such channel assignment approach may yield undesirable estimation performance due to collection of information from sensors irrespective of observation quality, i.e., sensing signal-to-noise ratio.

In contrast, SHARE is based on a distortion minimization model and provides reliable event estimation with minimum spectrum access. SHARE also seeks to achieve the required global estimate using consensus algorithm and has an online licensed user activity and interference tracking component.

On the other hand, spectrum sharing solutions in other CRN mainly focus on throughput maximization and are proposed to efficiently utilize the scarce spectrum opportunities. In [56], spectrum sharing for multi-hop cognitive radio networks is studied. In [117, 118, 51, 43] spectrum sharing schemes for multiple input multiple output systems have been proposed. The primary reason for their inapplicability in CRSN is their notion of rate maximization. Furthermore, reliable estimation of event features, collaborative nature of CRSN nodes, coordination requirements of CR actor nodes and spectrum efficiency must be addressed while designing spectrum management algorithms for large scale distributed sensing networks. Hence, there is a need for a novel spectrum access mechanism in CRSN that emphasizes on collective reliability, spectrum efficiency and simplicity.

5.3 Network Setup

Here, we explain details of proposed distributed sensing architecture that is composed of networked sensor and actuator nodes communicating among each other via cognitive radio links to perform remote monitoring and actuation tasks. Collected samples s by sensor nodes m on event signal θ are aimed to be delivered actor nodes k during reporting interval τ_r over assigned channel c during spectrum access duration τ_a to satisfy local reliability requirement

D_o of distributed event observation at actor nodes. Reliability measure for local estimation of actor nodes is defined in terms of distortion D (mean square-error) of the estimated event signal over a τ_a. Then, local estimate $\hat{\theta}$ generated by actor nodes are communicated with neighbor actor nodes to reach a network-wide global estimate, i.e., consensus, Θ.

Sensor nodes occupy a single CR transceiver with capability of adjusting its operating frequency to any channel c in designated spectrum band by actor node, i.e., channel set C_k of actor node k. Channels are shared between selected sensor nodes participating in event delivery by actor. Sensor node behaviour in a channel c consists of data transmission τ_t, spectrum sensing τ_s and spectrum handoff τ_h periods. Sensors access spectrum in an opportunistic manner, such that spectrum access is granted when channel is detected to be vacant, and samples are reported. We assume each sensor node is assigned to a specific channel for periodic spectrum sensing by actor node, such that in spectrum sensing intervals τ_s all sensor nodes perform spectrum sensing to detect spectrum holes, i.e., vacant channels. With detection of licensed user at accessed channel, sensor node accessing that channel performs spectrum handoff and traverses channels provided by actor node to find a spectrum opportunity. Spectrum handoff duration τ_h includes consecutive channel switching τ_{cs} and spectrum sensing τ_s at switched channel operations until a vacant channel is found, i.e., duration between the instant where event reporting stopped due to licensed user detection and the instant when communication is resumed in a vacant channel. To achieve desired distortion level D_o in an estimation interval τ_e, sensors are assigned to channels by their corresponding actor node k, such that they complete their transmission in spectrum access interval τ_{a}, which is less than tau_e, to address delays due to cognitive cycle functionality durations in τ_e. Channels assigned by an actor node k, i.e., $c \in C_k$, are taken to be homogeneous in terms of licensed user activity and interference.

Energy constraints Ω for sensor nodes that limits the energy can be spent for event reporting in an estimation interval are taken to be non-equal due to heterogeneous event arrivals in the field and remaining energy of sensor nodes. This energy variation brings limitation to event reporting duration τ_r of sensor nodes, and hence, causes heterogeneities for number of samples reported by each sensor.

To reach consensus, actors broadcast their state to neighbors after local estimation phase until consensus is reached. This is repeated for every estimation interval. While reaching a

consensus trivial for small scale actor networks, for a large scale actor network computing the global estimate Θ based on local estimates $\hat{\theta}_k$ requires multiple iterations and packet exchanges among actors. Inter-actor communication is exposed to licensed user interference due to arrival of licensed user during transmission or mis-detection of licensed user presence during spectrum sensing period. In case of transmission errors iteration is stopped and this failed step is repeated via automatic repeat request. The exchange of information among actors is performed via a slotted and collision-free medium access control (MAC) scheme. Consensus convergence time τ_c is determined as the multiplication of number of required iterations Υ to reach consensus and iteration duration τ_i, i.e., $\tau_c = \Upsilon \cdot \tau_i$.

5.4 Impact of Spectrum Mobility

Incorporation of cognitive radio capability into sensor and actor nodes enables distributed sensing and actuation over licensed bands to mitigate crowded spectrum problem. However, to realize reliable distributed sensing in local level at actor nodes and reach a network-wide consensus at global level among actor nodes, intermittent communications due to opportunistic spectrum access and interruptions due to licensed user interference must be addressed. To this end, in this section, the instantaneous throughput based on spectrum sensing and spectrum handoff functionalities is found, and channel error rate with licensed user interference is determined.

5.4.1 Instantaneous Throughput

Here, the experienced instantaneous throughput T_k while accessing licensed spectrum bands opportunistically for sensors connected to actor node k is obtained. First, we derive the mean data communication duration $\mathrm{E}\{\tau_{\mathrm{data}}^{(k)}\}$ before licensed user arrival in channels C_k assigned by actor node k. Under exponential inter-arrival and inter-departure durations assumption for licensed user traffic [92, 29, 30, 66], average data communication duration $\mathrm{E}\{\tau_{\mathrm{data}}^{(k)}\}$, i.e., average duration from starting communication in channel C_k until a licensed user is detected is found as

$$\mathrm{E}\{\tau_{\mathrm{data}}^{(k)}\} = \mathrm{E}\{I_k\}\tau_t^{(k)} \tag{5.1}$$

where $\mathrm{E}\{I_k\}$ is the mean number of $(\tau_s^{(k)} + \tau_t^{(k)})$ durations before licensed user arrives at a channel in C_k. To calculate $\mathrm{E}\{I_k\}$, we define the probability of having i intervals without licensed user arrival at the accessed channel as

$$\Pr[I_k = i] = (P_{\text{hole}}^{(k)})^{i-1}(1 - P_{\text{hole}}^{(k)}) \tag{5.2}$$

where $P_{\text{hole}}^{(k)}$ is vacancy probability of a channel in C_k. Mean of I_k can be found as

$$\mathrm{E}\{I_k\} = \sum_{i=1}^{\infty} i \cdot \Pr[I_k = i] = \frac{1}{1 - P_{\text{hole}}^{(k)}}. \tag{5.3}$$

To find the mean of spectrum handoff duration $\mathrm{E}\{\tau_h^{(k)}\}$, i.e., the mean of total channel switching and spectrum sensing durations until data transmission can be started in a vacant channel, we define probability of finding a vacant channel via l consecutive handoffs $\Pr[L_k = l]$ as

$$\Pr[L_k = l] = P_{\text{hole}}^{(k)}(1 - P_{\text{hole}}^{(k)})^{l-1} \tag{5.4}$$

where we assume licensed user arrivals at different channels of C_k are independent from each other. When a licensed user communication is detected at any of accessed channels sensor nodes accessing that channel traverses channels provided by actor k to find a vacant channel, where licensed user detected channel corresponds to $c = 0$. Time spent while performing l consecutive handoffs can be found as

$$\tau_h^{(k)}(l) = l \cdot (\tau_{\text{cs}} + \tau_s^{(k)}) \tag{5.5}$$

where τ_{cs} is channel switching time when moving between channels. As a result, $\mathrm{E}\{\tau_h^{(k)}\}$ can be obtained as

$$\begin{aligned} \mathrm{E}\{\tau_h^{(k)}\} &= \sum_{l=1}^{\infty} \tau_h^{(k)}(l)\Pr[L_k = l] \\ &= \sum_{l=1}^{\infty} l \cdot (\tau_{\text{cs}} + \tau_s^{(k)})P_{\text{hole}}^{(k)}(1 - P_{\text{hole}}^{(k)})^{l-1} \\ &= (\tau_{\text{cs}} + \tau_s^{(k)})\frac{1}{P_{\text{hole}}} \end{aligned} \tag{5.6}$$

Instantaneous throughput T_k in channels of actor node k is found as the ratio of average data transmission duration $(\mathrm{E}\{\tau_{\text{data}}^{(k)}\})$ to average channel time $(\mathrm{E}\{\tau_h^{(k)}\} + \mathrm{E}\{I_k\}(\tau_s^{(k)} + \tau_t^{(k)}))$, where channel time is the time spent from start of communication at a channel to starting

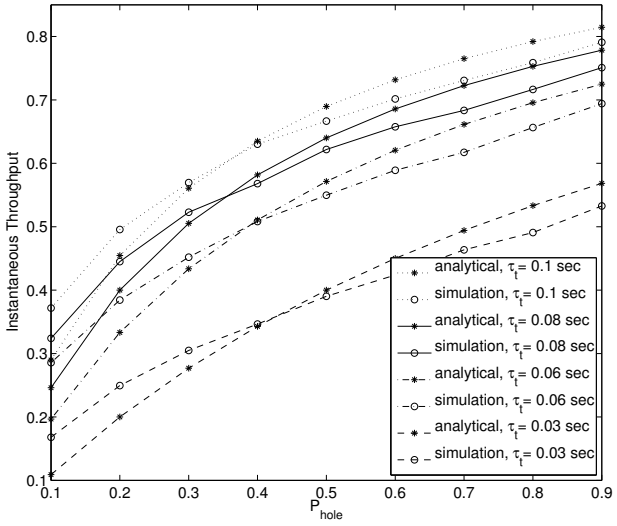

Figure 5.1: Comparision of calculated and achieved instantaneous throughput due to opportunistic spectrum access for $\tau_t = 0.1, \tau_t = 0.08, \tau_t = 0.06, \tau_t = 0.03$ sec.

communication at another channel after licensed user detection. Using (5.1), (5.3), and (5.6), T_k can be obtained as

$$T_k = \frac{E\{\tau_{\text{data}}^{(k)}\}}{\mathrm{E}\{\tau_h^{(k)}\} + \mathrm{E}\{I_k\}(\tau_s^{(k)} + \tau_t^{(k)})} \tag{5.7}$$
$$= \frac{\frac{1}{1-P_{\text{hole}}^{(k)}}\tau_t^{(k)}}{\left(\tau_{\text{cs}} + \tau_s^{(k)}\right)\frac{1}{P_{\text{hole}}^{(k)}} + \left(\tau_t^{(k)} + \tau_s^{(k)}\right)\frac{1}{1-P_{\text{hole}}^{(c)}}}$$

Performance of proposed instantaneous throughput determination model is shown in Fig. 5.1. Analytically calculated instantaneous throughput is shown to be closely following achieved one in simulations. τ_s and τ_{cs} is set to 0.02 and 0.005 sec, respectively. P_{hole} is varied from 0.1 to 0.9. Calculated instantaneous throughputs for $\tau_t = 0.1$, 0.08, 0.06, and 0.03 sec overshoot the achieved ones after a critical value of P_{hole}, e.g., after $P_{\text{hole}} = 0.3$ calculated instantaneous throughput exceeds the achieved one for $\tau_t = 0.08$ sec., and similar relationship between simulated and analytic results is observed for other τ_t values, as well. Therefore, in our design of SHARE algorithm, we introduce safety factor κ to reduce calculated throughput by a little amount to compensate for possible overshoots.

We use developed framework to evaluate instantaneous throughput T_k for channels C_k of actor node k due to opportunistic spectrum access and calculate the mean of the spectrum

access duration μ_k in an event estimation interval for sensor nodes connected to actor node k, i.e., $m \in \mathcal{M}_k$, as $\mu_k = T_k \tau_e$.

5.4.2 Packet Error Rate

Each sensor communicates with its actor node over orthogonal channels that experience independent shadowing and zero-mean AWGN. We use the log-normal channel for received power calculations, which is experimentally shown as the accurate model for low power communication in sensor networks [123]. In this model, the received power at a receiver at distance d from a transmitter is given by

$$P_r(d) = P_t - \mathrm{PL}(d_0) - 10\eta \log_{10}(\frac{d}{d_0}) + X_\sigma, \tag{5.8}$$

where P_t is the transmit power in dBm, $\mathrm{PL}(d_0)$ is the path loss at the reference distance d_0 in dB, η is the path loss exponent, and X_σ is the shadow fading component with $X_\sigma \sim \mathcal{N}(0, \sigma)$. We denote the communication signal-to-noise ratio (SNR) at the actor with and without licensed user interference as Ψ_w, and Ψ_l, respectively. SNR at the receiver without licensed user interference Ψ_w is given by $\Psi_w = P_r(d) - P_n$ in dB, where P_n is the communication noise power in dBm. On the other hand, SINR at the receiver due to licensed user activity is given by $\Psi_l = P_r(d) - P_n - P_l^{(k)}$ in dB, where $P_l^{(k)}$ is the interference caused by licensed user activity at actor node k. To obtain bit error rate P_b to use in analytical derivations, the non-coherent frequency shift keying (FSK) modulation scheme is selected. The bit error rate of this scheme is given by [71]

$$P_b = \frac{1}{2} \exp(-(E_b/N_0)/2), \quad E_b/N_0 = \Psi \frac{B_N}{R} \tag{5.9}$$

where B_N is the noise bandwidth, and R is the data rate. Finally, packet error rate (P_p) for packet length l_p becomes

$$P_p = 1 - (1 - P_b)^{l_p} \tag{5.10}$$

To determine average packet error rate $P_p^*(k)$ incorporating licensed user interference due to opportunistic spectrum access, we propose an error model based on false-alarm P_f and detection P_d probabilities, and licensed user state transition, i.e., birth β_k and death α_k rates. False-alarm, i.e., detection of licensed user communication when licensed user is actually not communicating, probability is represented by P_f and detection probability when licensed user is communicating P_d. Licensed user activity modelled using two state discrete Markov

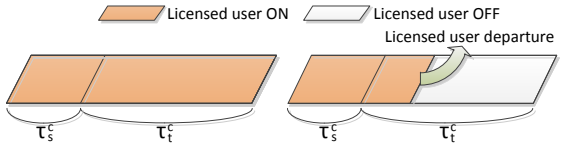

(a) (b)

Figure 5.2: Licensed user interference patterns when mis-detection occurs, no state change in (a) and state transition occurs in (b).

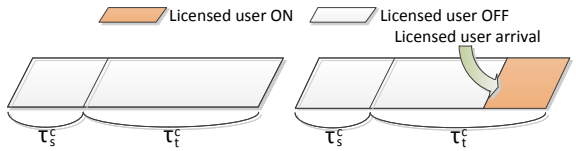

(a) (b)

Figure 5.3: Licensed user interference patterns when licensed user is initially OFF while *spectrum sensing*, no state change in (a) and state transition occurs in (b).

chain model with ON and OFF states [92, 29, 30, 66]. Licensed user being active $(1 - P_{\text{hole}}^{(k)})$ and being inactive $P_{\text{hole}}^{(k)}$ probabilities are equal to $\beta_c/(\beta_c + \alpha_c)$ and $\alpha_c/(\beta_c + \alpha_c)$, respectively. Before finding P_p^*, we describe two different cases in which licensed user interference occurs as follows

1. Although licensed user is active, it may not be detected, i.e., mis-detection can occur, with probability $(1-P_{\text{hole}}^{(k)})(1-P_d)$. In this case, nodes continue to communicate, though there is ongoing licensed user communication. Hence, they get exposed to licensed user interference, which is illustrated in Fig. 5.2.

2. A spectrum band can be identified as vacant and employed by sensor nodes with probability $P_{\text{hole}}^{(k)}(1 - P_f)$. However, licensed users may start communication during the nodes' transmission period. Thereby, until the next spectrum sensing period, sensor nodes are unaware of the licensed user presence and continue to communicate under licensed user interference, which is illustrated in Fig. 5.3.

Licensed user may change its state during $\tau_t^{(k)}$, or it can keep its state along whole $\tau_t^{(k)}$ duration. Having $\tau_t^{(k)}$ is relatively small with respect to average active and inactive durations of licensed user, e.g., $1/\alpha_k$ and $1/\beta_k$, respectively, is a more realistic assumption than having large $\tau_t^{(k)}$ that is longer than licensed user transmission duration. Thus, we assume $\tau_t^{(k)}$ is smaller than both $1/\alpha_k$ and $1/\beta_k$.

Interference due to mis-detection exhibits two different patterns according to $\tau_t^{(k)}$ as in Fig. 5.2 (a) and (b). It can be through whole $\tau_t^{(k)}$ period as in Fig. 5.2 (a) or licensed user state may change to inactive from active as in Fig. 5.2 (b). The probability that the licensed user is transmitting during the entire $\tau_t^{(k)}$ can be obtained as $e^{-\alpha_k \tau_t^{(k)}}$, and the probability that licensed user goes inactive state from active during $\tau_t^{(k)}$ can be found as $1 - e^{-\alpha_k \tau_t^{(k)}}$. If the licensed user state does not change during the $\tau_t^{(k)}$, the licensed user interference persists over the entire transmission period and in which error rate is $P_p^l(k)$. However, if state transition between active and inactive states occurs during $\tau_t^{(k)}$, average error rate converges to $(1 - P_{\text{hole}})P_p^l(k) + P_{\text{hole}}P_p^w(k)$. Thus, average packet error rate for the mis-detection case $P_p^1(k)$ can be expressed as

$$P_p^1(k) = (1 - P_d)\frac{\beta_k}{\alpha_k + \beta_k} \cdot \left((1 - e^{-\alpha_k \tau_t^{(k)}}) \frac{\beta_k P_p^l(k) + \alpha_k P_p^w(k)}{\alpha_k + \beta_k} + e^{-\alpha_k \tau_t^{(k)}} P_p^l(k) \right) \tag{5.11}$$

Similarly, if licensed user is inactive and there is no false-alarm, interference only happens when licensed user state transition occurs during $\tau_t^{(k)}$, as illustrated in Fig. 5.3 (b). Average packet error rate converges to again approximately to $(1 - P_{\text{hole}}^{(k)})P_p^l(k) + P_{\text{hole}}^{(k)}P_p^w(k)$ with probability $1 - e^{-\beta_k \tau_t^{(k)}}$. Average packet error rate in this case $P_p^2(k)$ becomes

$$P_p^2(k) = (1 - P_f)\frac{\alpha_k}{\alpha_k + \beta_k} \cdot \left((1 - e^{-\beta_k \tau_t^{(k)}}) \frac{\beta_k P_p^l(k) + \alpha_k P_p^w(k)}{\alpha_k + \beta_k} + e^{-\beta_k \tau_t^{(k)}} P_p^w(k) \right) \tag{5.12}$$

Then, to find overall packet error rate $P_p^*(k)$ in opportunistic spectrum access incorporating licensed user interference, we add and normalize P_p^1 and P_p^2 as

$$P_p^*(k) = \frac{P_p^1(k) + P_p^2(k)}{\frac{\beta_k(1-P_d)+\alpha_k(1-P_f)}{\alpha_k+\beta_k}} \tag{5.13}$$

Performance of proposed analytical packet error rate calculation scheme is presented in Fig. 5.4. For received power calculations, transmission power P_t is set to -5 dBm, noise

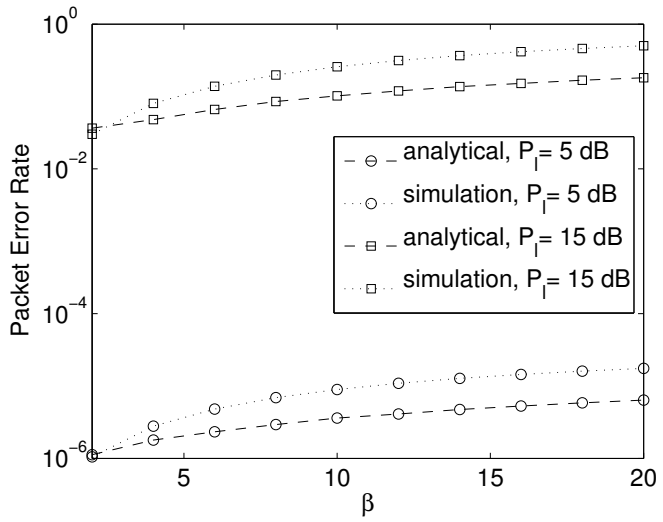

Figure 5.4: Comparison of analytically calculated packet error rate and simulation results with respect to licensed user arrival rate β for SNR values under licensed user interference of P_l = 5 and 15 dB.

power P_n is set to -90 dBm, path loss exponent η is set to 3, shadowing standard deviance σ is set to 3.8, distance is taken to be 5 m, reference distance d_0 is taken to be 1 m, reference path loss $PL(d_0)$ is taken as -40 dB, and B_N/R ratio is taken to be unity. Value of τ_t is taken to be 0.05 sec, P_d is equal to 0.9, P_f is equal to 0.1, and α is equal to 10. Simulations are repeated 1000 times and results are averaged. It is shown in Fig. 5.4, the analytic formulation follows the simulation values closely. While packet error rate is in the order of 10^{-5} when the licensed user interference P_l is 5 dB, packet error rate becomes in the order of 10^{-2} when P_l increases to 15 dB. Values of P_p obtained from analytic calculation stay below of simulation results, which is desirable for energy-efficient scaling of number of collected packets from sensor nodes. Since analytical packet error rate will be slightly less than the actual packet error rate, total number of required packets will be updated conservatively by inverse of calculated analytical packet error rate.

We incorporate the developed analytical packet error rate framework together with derived instantaneous throughput to analyze reliability at local estimation of actor nodes and opportunistic consensus convergence among actor nodes in the next sections.

5.5 Distortion-aware Minimized Spectrum Access

In this section, first, distributed estimation model at actor nodes is presented, and minimized spectrum access under distortion constraints is formulated. It is shown that by accessing spectrum opportunities with sparse licensed user activity, distributed estimation distortion can be achieved without penalizing estimation interval and spectrum efficiency. Then, achieved reliability and experienced spectrum access duration in an estimation interval are related via formulation of event observation distortion with respect to quality, i.e., sensing signal-to-noise ratio (SNR), of samples reported from different channels.

5.5.1 Reliable Local Distributed Sensing

Reporting source nodes and reporting durations are adjusted according to sensing signal-to-noise ratio (SNR) Λ_m values of sensor observations and energy consumption constraint per estimation interval Ω_e of sensor nodes to achieve an estimation distortion below desired threshold value D_o. Then, minimized spectrum access is formulated.

For estimation of event signal from received samples from source nodes, actors use the best linear unbiased estimator (BLUE) [78] for local estimation to make estimate not depending on a specific sensing noise distribution apart from power of noise. Therefore, we do not assume any specific distribution for sensed signal and noise. Observation $s_m(t)$ is the distorted version of event signal $\theta(t)$ by observation noise $\eta_m(t)$ and dispersion loss in signal power $\gamma_m(t)$ through sensor m due to distance between sensor and event source, i.e., $s_m(t) = \gamma_m(t) \cdot \theta(t) + \eta_m(t)$, at sensor m and time t. Each sensor sends measured signal $s_m(t)$ to actor, where θ is estimated locally from the received version of $s_m(t)$. We take both $\theta_m(t)$ and $\eta_m(t)$ are i.i.d. over time. We also assume that $\theta_m(t)$, and $\eta_m(t)$ have zero mean and has a power of σ_θ^2 and ξ_m^2, respectively. Sensors communicate with actor via opportunistic spectrum access. Actor generates a local estimate of the event at the end of each event estimation interval. Under independence over time and space assumption, indices are ignored for all variables. This delay bounded distributed sensing scheme can also bee seen as real-time, since it put timeliness constraint on event reports. Received sample vector by actor at the end of each event estimation interval τ_e, i.e., $\mathbf{r}$, is combination of sensing noise and sensed signal as $\mathbf{r} = \boldsymbol{\gamma} \cdot \boldsymbol{\theta} + \boldsymbol{\eta}$, where $\mathbf{r} = [r_1, \cdots, r_{M_s}]^T$, $\boldsymbol{\gamma} = [\gamma_1, \cdots, \gamma_{M_s}]^T$, and $\eta = [\eta_1, \cdots, \eta_{M_s}]^T$, where

M_s is the number of source nodes selected by actor node. Estimate of event signal using BLUE is formulated as follows [78]

$$\hat{\theta} = \left[\boldsymbol{\gamma}^T \mathbf{R}^{-1} \boldsymbol{\gamma}\right]^{-1} \boldsymbol{\gamma}^T \mathbf{R}^{-1} \mathbf{r} \tag{5.14}$$

Sample covariance matrix $\mathbf{R_s}$ for received samples at actor is a M_s dimensional rectangular diagonal matrix whose diagonal entries are ξ_m^2, and other entries are 0. Hence, the mean square error for BLUE can be determined as [78]

$$\begin{aligned} D = \left[\boldsymbol{\gamma}^T \mathbf{R_s}^{-1} \boldsymbol{\gamma}\right]^{-1} &= \left(\sum_{m=1}^{M_s} (1 - P_p^*) S_p \frac{8 l_p}{\tau_r^{(m)} \nu_m} \frac{\gamma_m^2}{\xi_m^2} \right)^{-1} \\ &= \sigma_\theta^2 \frac{8 l_p}{(1 - P_p^*) S_p} \left(\sum_{m=1}^{M_s} \tau_r^{(m)} \nu_m \Lambda_m \right)^{-1} \end{aligned} \tag{5.15}$$

where Λ_m is the sensing SNR ($\frac{\gamma_m^2 \sigma_\theta^2}{\xi_m^2}$) for samples of node m, S_p is number of samples in a packet, and P_b^* is the bit error rate. We assume during an estimation period, Λ_m is constant for a sensor m. To achieve a distortion D below distortion constraint D_o, sufficient number of samples should be received from each for each reliable estimation interval τ_e.

To achieve desired event estimation distortion at actor, distortion minimization for real-time distributed sensing is formulated as follows

$$\begin{aligned} \textbf{min} \quad & M_s \\ \textbf{s.t.} \quad & \sigma_\theta^2 \frac{8 l_p}{(1 - P_p^*) S_p} \left(\sum_{m=1}^{M_s} \tau_r^{(m)} \nu_m \Lambda_m \right)^{-1} \leq D_o \\ & \tau_r^{(m)} \leq \Omega_e^{(m)} / \Omega_p \cdot l_p / \nu_m \end{aligned} \tag{5.16}$$

where Ω_p is the consumed energy for single packet transmission, D_o is the distortion threshold, and $\Omega_e^{(m)}$ is energy limit of node m for an estimation interval.

Minimum number of source nodes satisfying distortion constraint can be reached via ordering sensors in the descending sensing SNR (Λ_m) order, i.e., $m = 1$ is the largest SNR sensor node, and using in (5.15) with maximum allowed $\tau_r^{(m)}$ until distortion constraint is satisfied. According to this formulation, source nodes will be determined, and their reporting duration is going to be used for assignment to a spectrum hole.

5.5.2 Minimized Spectrum Access

Here, we introduce efficiency notion in access to detected spectrum opportunities. Sensor nodes detects spectrum holes via collaborating with actor and access them until licensed user arrives. Determination of accessed licensed band is performed by actor node that schedules opportunistic access to licensed channels. Here, we focus on sharing of given vacant channels among source nodes. These channels are shared by sensors with consideration of minimum total number of channels accessed in an estimation interval, such that minimum amount of spectrum opportunities, i.e., vacant channels, are consumed in sensor-to-actor event reporting.

To efficiently share available spectrum opportunity between sensor nodes while achieving distortion constraint, we formulate an optimization problem for minimized spectrum access. We group M_s reporting durations $\tau_r^{(m)}$ of source nodes into Y distinct values $\tau_r^{(y)}$ due to , where $Y \leq M_s$. Value of ζ_y indicates the demand for each distinct reporting duration $\tau_r^{(y)}$. Sensors can be scheduled at a channel in different orders during an event estimation interval, which yields various sensor placement patterns of reporting durations $\tau_r^{(y)}$ on a channel. $\mathbf{G}$ matrix contains X different channel scheduling patterns in its columns. We define π_x to indicate how many times the xth sensor placement pattern is used . Accordingly, minimized spectrum access problem is formulated as

$$\begin{aligned} \textbf{min} \quad & \sum_x \pi_x \\ \textbf{s.t.} \quad & \sum_x \pi_x G_{y,x} \geq \zeta_y, \;\; y = 1 \ldots Y, \;\; G_{y,x} \in \mathbb{N} \\ & \pi_x \geq 0, \quad \pi_x \in \mathbb{N} \end{aligned} \tag{5.17}$$

where π_x is a non-negative integer variable that indicates number of accessed channels with time sharing pattern vector $\mathbf{g_x}$, i.e., xth column of matrix $\mathbf{G}$, $G_{y,x}$ is a non-negative integer number that represents the number of yth distinct reporting duration $\tau_r^{(y)}$ of sensor nodes in xth channel sharing pattern.

Minimized spectrum access problem stated in (5.17) is solved using mixed integer programming (MIP) after relaxing integer constraint on π_x. Then, the MIP solution is rounded up to find a solution having objective value within $Y - 1$ of the optimal objective value. The delayed pattern generation technique developed by Gilmore and Gomory [44, 45] is used to solve this problem instead trying all possible time sharing patterns of a channel as columns of

matrix $\mathbf{G}$. Each actor node k solves this optimization problem to schedule its selected source nodes for spectrum access. As initial basic feasible solution for this problem, $\mathbf{G}$ is initially set to be composed of column vectors where $G_{y,x} = \mu_k/\tau_r^{(y)}$ for $y = x$, and 0 otherwise. We obtain an initial feasible solution using obtained initial $\mathbf{G_B}$ as a column matrix. $\tau_r^{(y)}$ represents the yth distinct reporting duration. Reduced cost is 0 for any basic time sharing pattern, which can be obtained as

$$\mathbf{1}^T - \boldsymbol{\phi}^T \mathbf{G_B} = 0 \tag{5.18}$$

where ϕ is associated shadow price and is obtained for any feasible solution as a solution of $\mathbf{G}_B^T \boldsymbol{\phi} = \mathbf{1}$. For generation of new channel sharing patterns, negative reduced cost, i.e., $\mathbf{1}^T - \boldsymbol{\phi}^T \mathbf{G_B} < 0$, indicates the existence of a channel sharing pattern which will improve the MIP solution, i.e., reduce the number of total accessed channels. Existence of new time sharing patterns for channels to replace the existing ones is found via solution of following sub-problem

$$\begin{aligned} \textbf{max} \quad & \sum_y \phi_y z_y \\ \textbf{s.t.} \quad & \sum_y \tau_r^{(y)} z_y \leq \mu_k \\ & z_y \geq 0,\ z_y \in \mathbb{N} \end{aligned} \tag{5.19}$$

where $\mathbf{z}$ represents alternative channel sharing patterns, and μ_k is the average opportunistic channel access duration in a τ_e for C_k. If the defined sub-problem has an optimal solution $\boldsymbol{\phi}^T \mathbf{z} > 1$, then, the regarding reduced cost will be less than 0, i.e., $1 - \boldsymbol{\phi}^T \mathbf{z} < 0$, and hence, we can put this channel sharing pattern $\mathbf{z}$ into the basis $\mathbf{G}$ of the main problem.

When the MIP solution is found, it is modified to round the solution down to integer values, then, the values of π_x for patterns in final basis $\mathbf{G}$ are increased by unit amounts to determine integer solution that is closest to the solution via MIP. For the consecutive solution of the main and the sub-problem CPLEX [2] is used as a linear programming library. Minimum number of total accessed channels is found via solution of this optimization problem, and only selected set of sensors by actor are given access to spectrum holes addressing distortion requirements, i.e., to achieve $D \leq D_0$, of event estimation at actor.

Employed distributed sensing operation can be summarized briefly as follows: Based on mean spectrum access duration per decision interval (μ_k) and reporting duration of each individual sensor per decision interval ($\tau_r^{m_c}$), spectrum is shared by actor at start of each event

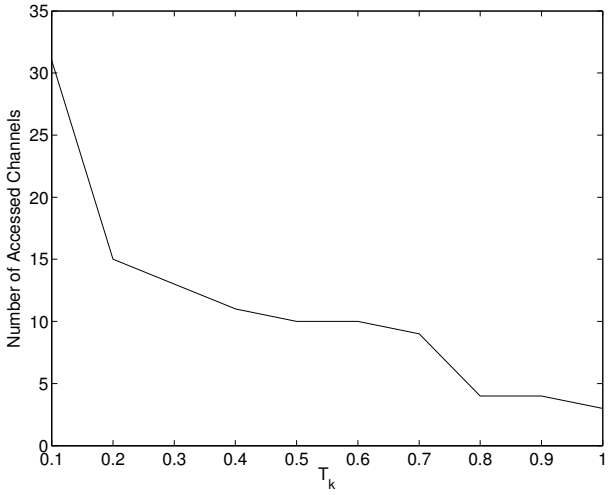

Figure 5.5: Required number of channels with respect to instantaneous throughput T_k for $\tau_e = 1$ sec and distortion constraint D_o of -50 dB.

decision interval τ_e to satisfy desired reliability level D_o. During real-time network operation, actors and sensors can collaboratively gather statistical information on channel accessibility and licensed user traffic using proposed licensed user tracking strategy in Section 5.7.1.

We now provide some numerical results to elaborate required number of channels with respect to available spectrum opportunity and sensor network parameters. Required number of accessed channels to provide reliability under distributed sensing network constraints is investigated. We examine the change in the required number of channels for event estimation interval τ_e = of 1 sec. Transmission current I_t is taken 17.4 mA, byte transmission time τ_{byte} is taken 32 μsec, supply voltage is taken 3.3 V, packet size l_p is taken 64 bytes, samples per packet S_p is set to 10, and transmission rate ν is set to 25 Kbps. Energy consumption constraint per estimation interval $\Omega_e^{(m)}$ is picked up from a uniform random variable between the interval of $[0, 5.7]$ mW. Distortion constraint D_o is set to -50 dB. To investigate effect of spectrum mobility and opportunistic communication, T_k is varied from 0.1 to 1, and mean spectrum access durations μ_k is calculated accordingly for solution of optimization problem. Formulated optimization problem in (5.17) for reliable spectrum sharing with minimum spectrum access in an estimation interval is found using CPLEX library [2].

For required number of channels, it has been shown in Fig. 5.5 that as the instantaneous throughput decreases, required number of channels to schedule sensors increases decreases

however, this decrease becomes marginal after a certain point, e.g., $T_k = 0.8$. This fact also suggest that decrease of spectrum access duration τ_a for sensor-to-actor communication to provide sufficient time opportunity to reach consensus among actor nodes is possible without penalizing spectrum efficiency and heavily increasing required number of channels under sparse licensed user activity, i.e., sufficient instantaneous throughput T_k, relative to estimation interval τ_e.

To reach consensus while satisfying local event estimation requirements at actor, estimation interval should be partitioned. Addressing the required duration to reach consensus, remaining duration in an estimation interval when consensus convergence is subtracted must be used to schedule sensors to channels. Minimization of required number of channels for sensor scheduling is discussed in this section.

5.5.3 Spectrum Access Duration and Sensor Scheduling Order

In this section, event observation distortion at an actor node is discretized into contribution of each channel D_c, i.e., total distortion is expressed as the addition of samples belonging to different channels, addressing the reduction in the reported samples over a channel by the spectrum access duration τ_a during estimation interval τ_e. Sensor nodes can move among spectrum holes via spectrum handoff as a licensed user arrives at current accessed channel. However, sensor nodes' communication is interrupted by periodic spectrum sensing as well as spectrum handoff triggered by licensed user arrival. Therefore, effect of opportunistic spectrum availability on event sensing reliability is investigated analytically according to proposed distributed sensing distortion model.

To this end, we define $\mathcal{M}_k^{(c)}$ as the source sensors of actor k assigned to cth channel for sharing during τ_a. D for proposed distributed sensing scheme can be expressed as

$$D = \left(\sum_c D_c^{-1} \right)^{-1} \tag{5.20}$$

where D_c is the distortion resulted by observations of sensors at channel c. It is dependent on the accessible duration τ_a of a channel assigned by actor k during an estimation interval and required reporting duration of sensors $\tau_r^{(m)}$ sharing the same channel. τ_as are independent and identically distributed (i.i.d.) random variables with mean μ_k representing data communication duration in an estimation interval for channels of actor node. D_c is the distortion

achieved when spectrum access duration τ_a in an estimation interval is allowing ωth sensor starting from $m = 1$ to share that channel for event reporting, and it can be expressed as

$$D_c = \Big[\sum_{m=1}^{\omega-1} D_m^{-1} + D_\omega^{-1} \Big(\frac{\tau_a - \sum_{m=1}^{\omega-1} \tau_r^{(m)}}{\tau_r^{(\omega)}} \Big) \Big]^{-1}, \quad \text{for} \quad \sum_{m=1}^{\omega-1} \tau_r^{(m)} \leq \tau_a \leq \sum_{m=1}^{\omega} \tau_r^{(m)}, \; m \in \mathcal{M}_k, \; \omega \in \mathcal{M}_k \tag{5.21}$$

where ω is the last sensor node that was reporting using the channel c at the instant of licensed user arrival, and D_m is distortion solely depending on samples from sensor m, which can be obtained using formulation in Section 5.5.1 as

$$D_m = \sigma_\theta^2 \frac{8 l_p}{(1 - P_b^*) S_p} \left(\tau_r^{(m)} \nu_m \Lambda_m \right)^{-1} \tag{5.22}$$

Furthermore, it is deduced that D_c is equal to $(\sum_{m=1}^{|\mathcal{M}_k^{(c)}|} D_m^{-1})^{-1}$ for $\tau_a \geq \sum_{m=1}^{|\mathcal{M}_k^{(c)}|} \tau_r^{(m)}$. When $\tau_a \geq \sum_{m=1}^{|\mathcal{M}_k^{(c)}|} \tau_r^{(m)}$, sensors assigned to channel c are able to find an opportunity to completely transmit their observations to actor during the estimation interval, and desired D_c will be achieved. However, when $\tau_a \leq \mu_k$, reporting of sensors assigned to a channel are limited by spectrum access duration ($\tau_a \leq \sum_{m=1}^{|\mathcal{M}_k^{(c)}|} \tau_r^{(m)}$), and contribution to total estimation distortion D_c is calculated using (5.21) via replacing τ_a with its realization. Latest reporting sensor ω at accessed channels can be determined via $\sum_{m=1}^{\omega-1} \tau_r^{(m)} \leq \tau_a \leq \sum_{m=1}^{\omega} \tau_r^{(m)}$, and its unfinished reporting duration can be found as $\tau_a - \sum_{m=1}^{\omega-1} \tau_r^{(m)}$.

Each channel's contribution to distortion of total estimation at actor varies based on sensing SNR Λ_m of assigned sensors to a channel. Therefore, another important issue is the scheduling order of source nodes assigned to same channel. Addressing the interruptions due to opportunistic communication, and hence, random τ_a duration in an estimation interval τ_e, scheduling spectrum access of source nodes with respect to their observation SNR Λ_m in descending order, i.e., highest SNR having node ($m = 1$) accesses first at designated channel, is found favourable. Next, we study the consensus reaching duration among actor nodes.

5.6 Opportunistic Consensus

In this section, we address spectrum access of actor nodes acting on the same event for reaching consensus [82]. In addition to local event sensing via collected samples from sensor

nodes, actor nodes communicate their local estimate information with other actors to mitigate disagreement and reach a global agreed state. We, first, present an overview of used consensus model, and then, investigate consensus convergence duration with respect to different algebraic connectivity of actor network for various licensed user arrival β and interference P_l values.

5.6.1 Overview of Consensus Model

We use a cognitive radio actor network composed of K actor nodes. Actor k can communicate with actor l if l is a neighbor of k on a graph $G = (V, E)$, where V denotes the set of vertices, i.e., actor nodes, and $E \subseteq V \times V$ denotes set of the edges between vertices, i.e., links between actor nodes. The *adjacency* matrix $\mathbf{A}$ of the graph G is composed of binary-valued entries $a_{k,l}$ that indicates existence of a link between actor k and l. Value of $a_{k,l}$ is equal to 1 if actor k and l are connected, and $a_{k,l} = 0$ if there is no link between actor k and l. We assume the links E are bidirectional, and hence, the graph G is undirected. Furthermore, $\mathbf{A}$ is a symmetric matrix with 0 diagonal entries, and since $\sum_{k \neq l} a_{k,l} = \sum_{l \neq k} a_{l,k}$, the undirected graph G is called balanced. The *degree* matrix $\mathbf{D}$ of G is a diagonal matrix with entries $d_{k,k} = |\mathcal{N}_k|$ and zero off-diagonal elements, where $|\mathcal{N}_k| = \sum_{k \neq l} a_{k,l}$ is the number of nodes in the neighborhood set $\mathcal{N}_k$ of actor k. Let $\mathbf{L}$ be the *Laplacian* matrix of the graph G, which is defined as $\mathbf{L} := \mathbf{D} - \mathbf{A}$. Entries $l_{k,l}$ of $\mathbf{L}$ are as

$$l_{k,l} = l_{l,k} = \begin{cases} |\mathcal{N}_k| & \text{if } k = l \\ -a_{k,l} & \text{if } k \neq l \end{cases} \tag{5.23}$$

Aim of consensus algorithm is to make each actor node to reach a globally optimal estimate $\hat{\theta}^*$ from a set of measurements, i.e., local estimates $\hat{\theta}_k$ of actor nodes in our system model. This is achieved via communication of local estimates among nearby actors without utilization of a fusion center. By definition of $\mathbf{L}$ sum of all columns or rows is equal to $\mathbf{0}$, which implies that $\mathbf{L}$ has an eigenvalue of 0. Accordingly, associated eigenvector is $\mathbf{1}$ since $\mathbf{L1} = \mathbf{0}$, or $\mathbf{1}^{\mathrm{T}}\mathbf{L} = \mathbf{0}^{\mathrm{T}}$. Therefore, reached final estimate is of the form $\alpha\mathbf{1}$, and consensus value α is equal to average of local estimates of actors. If G is a connected balanced and undirected graph, a consensus is asymptotically reached with

$$\Theta = \sum_{k} \hat{\Theta}_k(0)/K \tag{5.24}$$

Since minimization of the difference between states of actors is the aim of consensus algorithm, the *disagreement*, i.e., error, function is defined as

$$J(\hat{\Theta}) = \frac{1}{2}\hat{\mathbf{\Theta}}^{\mathrm{T}}\mathbf{L}\hat{\mathbf{\Theta}} = \frac{1}{4}\sum_{k=1}^{K}\sum_{l=1}^{L} a_{k,l}(\hat{\Theta}_k - \hat{\Theta}_l)^2 \tag{5.25}$$

Using steepest descent technique the minimum of $J(\Theta)$ can be achieved in discrete time as

$$\hat{\Theta}_k(t+1) = \hat{\Theta}_k(t) + \vartheta \sum_{l\in\mathcal{N}_k} a_{k,l}(\hat{\Theta}_k(t) - \hat{\Theta}_l(t)) \tag{5.26}$$

where ϑ is the step-size. In matrix form, dynamics of the actor network can be expressed as

$$\hat{\mathbf{\Theta}}(t+1) = \mathbf{P}\hat{\mathbf{\Theta}}(t) \tag{5.27}$$

where $\mathbf{I}$ is the identity matrix, and $\mathbf{P} = \mathbf{I} - \vartheta\mathbf{L}$. Value of ϑ is selected appropriately to ensure all eigenvalues of $\mathbf{P}$ are less than 1. The consensus algorithm is initialized with local estimates of actor nodes, i.e., $\hat{\Theta}_k(0) = \hat{\theta}_k$.

In the next section, the described inter-actor distributed estimation framework is used for assessing consensus convergence duration under opportunistic spectrum access.

5.6.2 Algebraic Connectivity and Consensus Convergence

While the performance of consensus algorithm is characterized by its convergence rate, i.e., time elapsed to reach consensus, convergence speed is lower bounded by the lowest non-zero eigenvalue of $\mathbf{P}$, i.e., λ_2, which is also called *algebraic connectivity* of the graph. Consensus is reached exponentially in discrete-time for connected graphs [82] such that

$$\frac{\|\hat{\mathbf{\Theta}}(t) - \mathbf{\Theta}\|}{\|\hat{\mathbf{\Theta}}(0) - \mathbf{\Theta}\|} \leq \mathrm{O}(e^{-(1-\vartheta\lambda_2(\mathbf{L}))\tau_c}) \tag{5.28}$$

We state the reaching consensus condition as $\frac{\|\boldsymbol{\theta}(t)-\boldsymbol{\theta}^*\|}{\|\boldsymbol{\theta}(0)-\boldsymbol{\theta}^*\|} \leq \varepsilon$. Therefore, the time elapses until convergence τ_c can be defined as the time needed to smallest eigenvalue of the dynamical system can be reduced by a factor $\varepsilon \ll 1$. A step of iteration fails if licensed user arrives or in case of mis-detection during communication of local estimate. Then, a new vacant channel is moved and failed step is repeated there. Failed step is detected after the end of iteration, hence, iteration is re-started. Instead of trying to know when exactly pu arrived during iteration. To mitigate disagreement for a unit amount $1/(1-P_p)\cdot 1/(1-\vartheta\lambda_2(\mathbf{L}))$ iterations are needed, and hence, τ_c is found as

$$\tau_{\mathrm{c}} = \frac{1}{1-P_p}\frac{\log(\varepsilon)}{1-\vartheta\lambda_2(\mathbf{L})}\mathrm{E}\{\tau_i\} \tag{5.29}$$

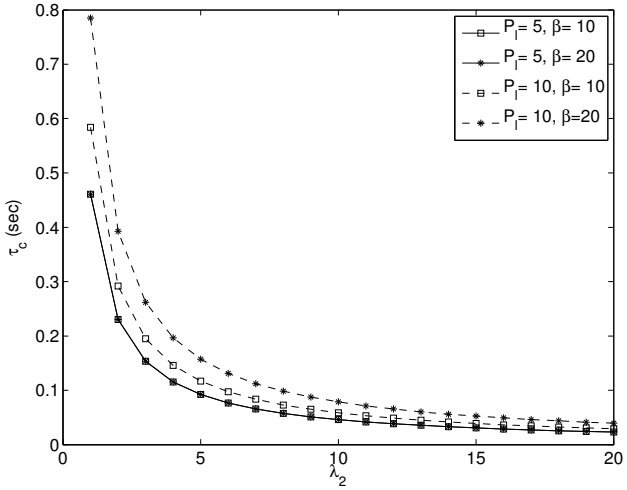

Figure 5.6: Consensus .duration with respect to algebraic connectivity for various P_l and β values.

where τ_i is the time required for a single iteration, i.e., duration in which all actor nodes communicate their local state once with their neighbor actors. We elaborate calculation of mean of τ_i in Section 5.7.2.

Numerical results are provided to elaborate the consensus convergence duration with respect to algebraic connectivity $\lambda_2(\mathbf{L})$ and available spectrum opportunity in terms of licensed user interference and channels errors. The prolongation of consensus convergence duration with respect to various algebraic connectivity of actor graph G, i.e., from 1 to 20, is discussed. Value of ε is set to -40 dB. Value of $\mathrm{E}\{\tau_i\}$ is set to 0.2 sec. To investigate effect of spectrum mobility, effect of licensed user interference P_l is assessed for 5 and 10 dB, and effect of birth rate of licensed user β is assessed for 10 and 20.

For consensus convergence duration τ_c, it has been shown in Fig. 5.5 that as the algebraic connectivity λ_2 increases, effect of spectrum mobility, i.e., P_l and β, decreases. Effect of increasing λ_2 becomes marginal after a certain point, e.g., τ_c reduces to its half value when λ_2 increases from 1 to 2, however, when λ_2 is increased from 9 to 10, this increase does not imply any significant reduction of τ_c. For $P_l = 5$ dB, τ_c follows the same pattern for $\beta = 10$ and 20. It is deduced that for low licensed user interference, β value does not effect the τ_c. However, for $P_l = 10$ dB, experienced τ_c increases with β. Sufficient time opportunity to reach consensus among actor nodes should be provided to reach consensus before end of the

estimation interval. Therefore, we incorporate analytically formulated consensus duration to limit spectrum access duration for local estimation of actors, i.e., τ_a. In the next section, we give details of SHARE algorithm.

5.7 SHARE: Spectrum Hole Assignment for Reliable Estimation

Here, we elaborate SHARE algorithm for overall sensor-to-actor and inter-actor communications. With event detection, each sensor node sends its sensing SNR and reporting duration based on energy limitation per decision interval to its actor node. Then, sensors are assigned to the channels by actor the connected actor node according to formulated distortion-aware minimized spectrum access (DMSA) component of SHARE. Objective of SHARE for local estimation is to minimize unused duration of channels in the accessed spectrum, i.e., maximizing efficiency of spectrum sharing. In addition to DMSA, to mitigate effect unable to find a sufficient spectrum opportunity instantaneously, i.e., experiencing τ_a less then the desired one during estimation interval due to randomness in licensed user activity, spectrum access of sensors assigned to channels is ordered according to sensing SNR in the descending order. On the other hand, for inter-actor communication, SHARE aims to provide sufficient duration for consensus convergence and incorporates an estimation interval partitioning scheme to enable reaching consensus among actors. Details of estimation interval partitioning scheme is presented in 5.7.2. Next, we describe the distributed online spectrum assessment (DOSA) component in SHARE to gather accurate statistics about licensed user activity to empower analytical founding in real-time network operation.

5.7.1 Distributed Online Spectrum Assessment

In this section, we introduce DOSA algorithm. DOSA is build upon diffusion LMS protocol [75]. At the end of each spectrum sensing interval i, each sensor node and its connected actor node distributes its state vector $\chi_m(i)$, i.e., spectrum accessibility ratio (SAR) $\chi_m^{(c)}(i)$ estimations for each sensed channel c to neighbor nodes. SAR means the accessibility to a channel by secondary users. At the end of each spectrum sensing interval, nodes update their state with neighbor nodes' states, i.e., estimates spectrum accessibility individually for transmission interval i. However, final spectrum decision is given by the actor node. DOSA algorithm

incorporates diffusion LMS algorithm. Mean-square convergence analysis for diffusion LMS is presented in [75]. However, we examine performance and robustness for SAR and NIL estimation against various learning rates via simulations in Section 5.8.1.

State vector $\boldsymbol{\chi}_m(i)$ is $|C_k|$ x 1 dimensional and contains estimations $\chi_m^{(c)}(i)$ for at instant i as

$$\boldsymbol{\chi}_m(i) \triangleq [\chi_m^{(1)}(i), \chi_m^{(2)}(i), \cdots, \chi_m^{(|C_k|-1)}(i), \chi_m^{|C_k|}(i)]^T \tag{5.30}$$

State vectors$\boldsymbol{\chi}_m(i)$ are collected from every neighbor node m and actor node k and used for calculation of error in local measurements $d_m^{(c)}(i)$ due to miss-detection and varying wireless environment. Combination strategy for these collected SAR states is provided as well as determination of tracked value $\boldsymbol{\chi}_m(i+1)$.

For SAR estimation, each sensor combines its state with neighbor nodes $\mathcal{N}_m$ in a uniform manner as

$$c_m = \frac{1}{|\mathcal{N}_m|} \tag{5.31}$$

Measured spectrum sensing result data for SAR is modeled as

$$d_m^{(c)}(i) = u_c(i) \oplus z_m^{(c)}(i) \tag{5.32}$$

where $d_{k,\mathrm{SAR}}^{l}(m)$ is the measured binary valued licensed user detection result, $u_c(i)$ is a binary random variable indicating licensed user presence, i.e., ON, or absence, i.e., OFF, at channel c during spectrum sensing interval i, and $z_m^{(c)}(i)$ is a binary number indicating miss-detection and false alarm for node m. For each channel c steps of SAR estimation is explained next.

After each spectrum sensing period, nodes distribute their observations to neighbor nodes, and update their estimate of SAR. This process can be seen as a diffusion LMS state update scheme [75]. Firstly, local state $\boldsymbol{\chi}_m(i)$ is combined with received states $\boldsymbol{\chi}_n(i)$ of neighbor nodes as

$$\overline{\boldsymbol{\chi}}_m(i) = \sum_{\substack{n=1 \\ n \neq m}}^{|\mathcal{N}_m|} c_m \boldsymbol{\chi}_n(i) \tag{5.33}$$

Calculated $\overline{\boldsymbol{\chi}}_m(i)$ is introduced into diffusion LMS filter

$$\mathbf{e}_m(i) = \mathbf{d}_m(i) - \overline{\boldsymbol{\chi}}_m(i) \tag{5.34}$$

$$\boldsymbol{\chi}_m(i+1) = \overline{\boldsymbol{\chi}}_m(i) + \kappa \cdot \mathbf{e}_m(i) \tag{5.35}$$

where κ is the learning rate between 0 and 1, and $\chi_m(i+1)$ is the predicted value of SAR. Estimated SAR at actor node is used for prediction of spectrum access duration τ_a opportunity in an estimation interval via formulated instantaneous throughput in Section 5.4.1. Estimation interval partitioning for consensus convergence is elaborated in the next section.

5.7.2 Estimation Interval Partitioning For Consensus

Estimation interval must be partitioned adaptively addressing varying spectrum parameters with spectrum mobility. Objective of SHARE is to provide sufficient duration for communication of local states among actor nodes after completion of local estimation. We first describe MAC for inter-actor communication and formulate mean iteration duration $\mathrm{E}\{i\}$. Then, estimation interval partitioning is introduced.

Actor nodes employ a ρ-persistent carrier sense multiple access (CSMA) mechanism for MAC such that they access channel during slot intervals with a probability of ρ if channel is no other actor node is sensed to be transmitting. Expected number of actor nodes that will transmit when channel becomes idle is given by $|\mathcal{N}_k|\rho$. If $|\mathcal{N}_k|\rho > 1$, then a collision is expected to occur. To prevent collisions and resultant retransmissions, ρ should be chosen accordingly, i.e., $\rho < 1/|\mathcal{N}_k|$. For this scheme, successful transmission probability of actor node k can be found as

$$\varsigma_k = \rho(1-\rho)^{|\mathcal{N}_k|-1} \tag{5.36}$$

Using ς_k, mean number of channel access trials φ_k before gaining access to channel is found as

$$\mathrm{E}\{\varphi_k\} = \sum_{l=0}^{\infty} l\varsigma_k(1-\varsigma_k)^{l-1} \tag{5.37}$$

Finally, mean duration of an iteration can be found as

$$\mathrm{E}\{\tau_i\} = \sum_{k=1}^{K} \tau_{\mathrm{slot}}\mathrm{E}\{\varphi_k\} \tag{5.38}$$

where τ_{slot} is the channel access duration of an actor node while broadcasting its local state to neighbor actors. Found $\mathrm{E}\{\tau_i\}$ is incorporated into (5.29), to find τ_c.

Spectrum access duration for sensor nodes is reduced to allow convergence of consensus algorithm. To this end, although, higher available spectrum access τ_a duration is possible, τ_a is reduced at the expense of increased number of required channels during local estimation.

Reduced spectrum access duration τ_a^* is determined as

$$\tau_a^* = \min_k \{\mu_k\} - \tau_c \tag{5.39}$$

where $\tau_a^* \geq \max_m \tau_r^{(m)}$. Using developed DOSA scheme, α and β values are found, and T_k values are determined and updated according to spectrum opportunities. We now provide performance assessment of SHARE scheme.

5.8 Performance Evaluation

In this section, we provide simulation results for SHARE. First, tracking performance of proposed DOSA scheme is assessed. DOSA is compared with a local spectrum assessment scheme employed at an actor node, and its superiority in spectrum opportunity tracking is presented. Then, overall performance of SHARE for consensus is presented. Specifically, consensus reaching rate nodes and disagreement among actor nodes at the end of an estimation interval is presented with respect to algebraic connectivity of the graph for different instantaneous throughput values. Furthermore, scaling of number of accessed channels with respect to algebraic connectivity is also investigated for different instantaneous throughput values.

5.8.1 Spectrum Opportunity Tracking

For tracking performance evaluation of DOSA algorithm, we use a spatially varying mean arrival rate for licensed users. Mean arrival rate is a Gaussian random variable with variance=0.01 and mean is set to 0.5 and 1.2 for performance comparison. Number of cooperating agents is set to 20, and performance is also compared with local tracking instead of cooperative. Learning rate κ is varied from 10^{-4} to $2 \cdot 10^{-2}$.

In Fig. 5.7, tracking performance of DOSA is presented. Diffusion LMS provides a performance gain about 7 dB for for both mean values of 0.5 and 1.2 compared to local LMS approach. It is also shown that for lower licensed user mean arrival rate from, i.e., for 0.5 compared to 1.2, DOSA achieves less MSE in SAR estimation.

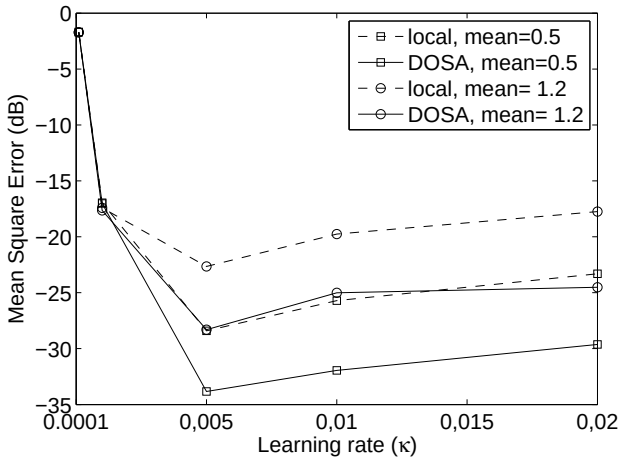

Figure 5.7: Performance of DOSA compared to local tracking for different mean licensed user arrival with respect to learning rate.

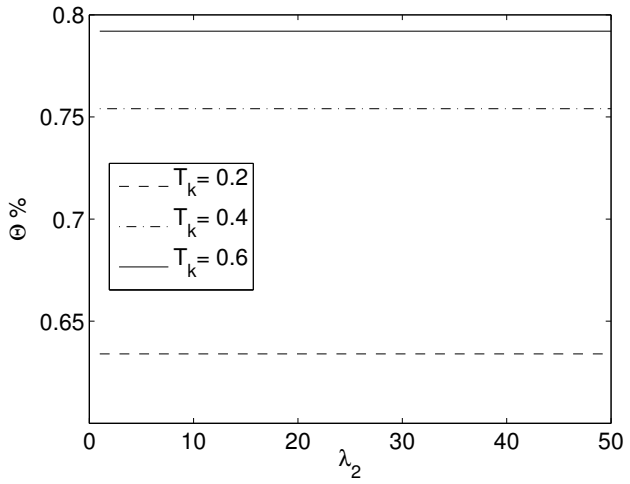

Figure 5.8: Consensus reaching rate of actor nodes.

5.8.2 Adaptive Spectrum Sharing for Consensus

In the previous sections, we developed the minimized spectrum access, inter-actor consensus, and distributed licensed user activity tracking schemes. In this section, we present simulation results on the performance of proposed sensing framework.

In Fig. 5.8, consensus reaching performance of SHARE is presented with respect to algebraic connectivity for different T_k values. P_l is set to 15 dB. It is shown that for different

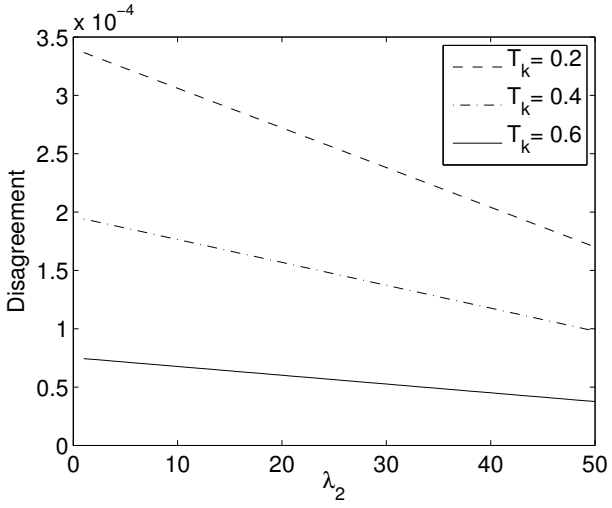

Figure 5.9: Consensus disagreement of actor nodes.

λ_2 values, consensus is reached is reached irrespective of algebraic connectivity. SHARE achieves higher consensus reaching rate performance with high instantaneous throughput values, i.e., consensus reaching rate decreases with decreasing $\min\{T_k\}$ = from 0.6 to 0.2. Reducing spectrum access duration of sensor nodes in local estimation, provides this performance gain in channels having high licensed user activity spectrum bands. Proposed estimation interval partitioning scheme strictly reduces spectrum access interval in accordance with sparse spectrum availability and high licensed user interference. Reduction of local estimation duration is benefited in high licensed user interference scenarios, and for low instantaneous throughput case, higher duration for consensus convergence is left.

In Fig. 5.9, disagreement among actors at the end of estimation interval is presented. With increasing algebraic connectivity λ_2, left duration for consensus decreases. Therefore, higher number of incomplete consensus phases yields higher disagreement than desired disagreement ε, which is set to 10^{-4}. Since the predicted τ_c decreases with increased λ_2, spectrum access interval for local estimation increases, as well. Due to randomness in licensed user activity, this reduction in τ_c results in increase of disagreement among actor nodes. However, as it is shown in Fig. 5.9, disagreement is still very close to and in the order of the objective value.

CHAPTER 6

DEDICATED RADIO UTILIZATION FOR SPECTRUM HANDOFF AND EFFICIENCY IN COGNITIVE RADIO NETWORKS

In this chapter, impact of dedicated radio utilization is investigated for communication of spectrum handoff information. Achievable efficiency gains and trade-offs are revealed for transmission delay, spectrum and energy efficiency, and distributed event sensing distortion. The dedicated radio utilization for spectrum handoff and efficiency in cognitive radio networks was analyzed in [25]. Section 6.2 summarizes the related work in the field of intermittent communications. SFT duration for with and without CCI cases is formulated in Section 6.3. In Section 6.4, spectrum efficiency analysis is performed. Energy efficiency analysis is presented in Section 6.5. Distributed event sensing distortion analysis is presented in Section 6.6. Performance evaluations are provided in Section 6.7.

6.1 Motivation

Dynamic spectrum access (DSA) techniques for wireless communications have emerged to mitigate inefficient spectrum utilization. Cognitive radio capable nodes can tune their communication parameters autonomously to adapt and communicate over unoccupied frequency bands in the spectrum.

Apart from salient improved spectrum utilization and communication capacity promises, cognitive radio inherently brings the burden of intermittent communication to wireless networks. Since spectrum access is paused during spectrum handoff functionality, communica-

tion is interrupted instantly with licensed user, i.e., primary user (PU), arrival. Even when sufficient spectrum opportunity for communication exists, communication is still interrupted by periodic spectrum sensing functionality for PU detection. Furthermore, in case of limited spectrum availability, spectrum handoff functionality does not stand for a single channel switching, i.e., frequency tuning to a new channel. In such scenarios, consecutive channel switching and spectrum sensing periods take place until spectrum handoff is completed at a vacant channel, which imposes severe frame transmission delay, spectrum and energy inefficiencies. Therefore, analysis and understanding of the delay due to intermittent communications with its effects on efficiency in cognitive radio networks (CRN) are essential for devising communication algorithms.

Since multiple parties are involved in the communication process, cognitive radio nodes are required to distribute spectrum sensing results and negotiate with each other on spectrum decision over a common medium, i.e., spectrum coordination is needed [72, 32, 73]. Spectrum coordination can be performed over the existing cognitive radio interface [32, 17, 65, 122], or a dedicated interface, i.e., common control interface (CCI), can be integrated to nodes for the spectrum coordination purpose [73, 63, 95]. The existence of CCI is a distinctive factor for efficiency in CRN. Without CCI nodes are required to wait until current frame transmission to finish for spectrum coordination. On the other hand, if a spectrum coordination scheme exploiting CCI is employed, then spectrum coordination can be performed simultaneously with frame transmission. Thus, transmission can be ceased before the whole frame is transmitted by PU detection information from spectrum coordination functionality. Decreased delay and energy consumption, and increased spectrum efficiency are tempting benefits of CCI, nevertheless incorporation of CCI for spectrum coordination increases the cost of a CRN node. Therefore, efficiency improvements provided by incorporation of CCI into cognitive radio nodes must be thoroughly assessed according to spectrum conditions and cognitive radio parameters, such as PU activity, spectrum sensing, and frame transmission duration. Such assessments are useful to analyze achievable payoffs and associated efficiency gains in opportunistic communication among cognitive radio nodes resulting from CCI utilization in CRN.

In this chapter, we present an analytical framework to assess the efficiency gains via CCI utilization for spectrum handoff in CRN. The developed framework enables comparison of achievable delay, spectrum utilization, and energy consumption with and without incorporation of CCI into CRN nodes. Furthermore, achieved distributed event sensing distortion via

CCI utilization is analyzed for cognitive radio sensor networks (CRSN). To this end, successful frame transmission (SFT) duration is formulated for a CRN node pair and closed form expressions incorporating any given channel sequence under heterogeneous PU activity, wireless error rate, spectrum sensing and frame transmission periods are derived for spectrum handoff with and without CCI cases. The developed framework can also be used under any propagation model. Furthermore, the SFT duration analyses are extended to formulate spectrum and energy efficiency for both with and without CCI cases. SFT duration analyses are also used to analyze event estimation distortion in CRSN with and without CCI employment. Finally, performance evaluations regarding CCI employment in CRN are presented. Achievable frame transmission delay, spectrum and energy efficiency, and distributed event sensing distortion gains are investigated for various spectrum conditions and cognitive radio parameters to identify regimes that yield CCI favourable in CRN.

6.2 Related Work

Here, we describe the existing works in the literature on the spectrum handoff performance in CRN and point out our work's significance. In [107], authors examine delay of multiple spectrum handoffs on the data communication duration. A preemptive resume priority (PRP) M/G/1 queueing system is proposed to model multiple handoff delay. Extended data delivery duration due to interruptions caused by PU arrival is modelled to assist the progress in designing admission control strategies for secondary networks according to specific latency requirements. Instead of using CCC for coordination, a frequency hopping-based spectrum handoff scheme is proposed in [91]. The authors study delay caused by spectrum handoff process in ad hoc CRN under homogeneous PU activity at each channel. A three dimensional discrete-time Markov chain is proposed to capture behaviour of spectrum handoffs and assess performance of cognitive radio users according to communication requirements. In [108], a PRP M/G/1 queueing network model is also proposed to reveal spectrum utilization of connection-oriented spectrum handoffs. Extended data delivery time is derived, and latency performance is analyzed. In [99], authors investigate prioritized secondary user traffic. They consider a general setting in which the PU transmissions can happen at any time instant. Centralized and distributed schemes are considered to manage the prioritized secondary user traffic that use different handoff mechanisms. The proposed DSA schemes are analyzed using

a continuous time Markov chain. The mean handoff delay, for different priority secondary users is derived. In [109], the effects of interruptions due to multiple spectrum handoffs on connection-based channel usage is investigated based on a PRP M/G/1 queueing model. In [116], spectrum handoff process is analysed. The average number of spectrum handoffs is derived to assess spectrum handoff performance.

In these works, CCI is either discarded because of introduced additional cost or included in the system model to ease synchronization for spectrum handoff. Apart from the existing works on spectrum handoff delay calculation, we rather focus on impact of CCI utilization for spectrum handoff on frame transmission duration, spectrum utilization, and energy consumption. We reveal the achievable improvements for frame transmission delay, spectrum and energy efficiency via CCI employment in CRN and compare it to without CCI case. None of the existing works develop such an approach to investigate potentials of CCI. Therefore, our work fills the empty space in the literature for cost and benefit, i.e., trade-off, analysis of CCI in CRN.

6.3 Successful Frame Transmission Duration Analysis

In this section, we formulate successful frame transmission (SFT) durations for spectrum coordination with and without common control interface (CCI) and derive their probability density functions (p.d.f.s). SFT durations are prolonged by PU arrivals. Without CCI, PU communication can only be detected after completion of current frame transmission, while SU can be informed by neighbour nodes at the instant of frame transmission for PU communication with CCI. We, first present the system model, then continue with the formulation of the spectrum access (SA) delay, which accounts for the duration until an SU node gets a spectrum opportunity to transmit its frame. During this duration the SU node performs spectrum sensing to detect PU communication and channel switching to find a new vacant channel, i.e., performs spectrum handoff.

6.3.1 System Model

In CRN, unlicensed users, i.e., secondary users (SUs), coexist with primary users (PUs). SU has a cognitive radio interface, which supports channel switching and spectrum sensing

Table 6.1: Illustration of Spectrum Access Delay for a Channel List Composed of 3 Channels

# of Visited Channels	Cumulative Spectrum Access Delay	Probability
1	τ_s	$P_+^{(1)}$
2	$\tau_{\text{is}}^{(1)}+\tau_s$	$P_-^{(1)}\cdot P_+^{(2)}$
3	$\tau_{\text{is}}^{(1)}+\tau_{\text{is}}^{(2)}+\tau_s$	$P_-^{(1)}\cdot P_-^{(2)}\cdot P_+^{(3)}$
4	$\tau_{\text{is}}^{(1)}+\tau_{\text{is}}^{(2)}+\tau_{\text{is}}^{(3)}+\tau_s$	$P_-^{(1)}\cdot P_-^{(2)}\cdot P_-^{(3)}\cdot P_+^{(1)}$
5	$\tau_{\text{is}}^{(1)}+\tau_{\text{is}}^{(2)}+\tau_{\text{is}}^{(3)}+\tau_{\text{is}}^{(1)}+\tau_s$	$P_-^{(1)}\cdot P_-^{(2)}\cdot P_-^{(3)}\cdot P_-^{(1)}\cdot P_+^{(2)}$
...	...	...

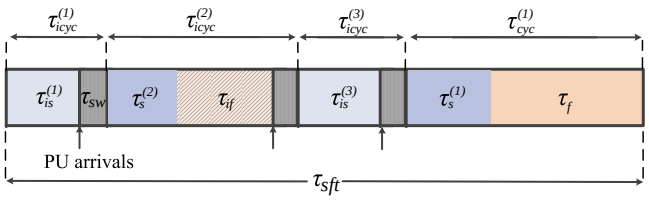

Figure 6.1: Illustration of spectrum access delay τ_{sft}.

functionalities. SU performs periodic spectrum sensing to detect PU presence. When an SU performs spectrum sensing on a channel c, it cannot transmit data. Upon detection of PU communication, SUs perform spectrum handoff. During spectrum handoff, SU moves to the next channel in its pre-determined circular channel list, and then spectrum sensing is performed at this channel. If PU communication is not detected at switched channel, SU resumes its communication in this channel, otherwise spectrum handoff is performed consecutively until a vacant channel is found for communication.

The traversed channel list during spectrum handoff may be provided by a centralized spectrum sharing mechanism to CRN nodes, or it may also be constructed by means of cooperative spectrum sensing, as well as each node may be required to decide individually on which channel is to be sensed next [11]. Formation of the optimal channel list is beyond the scope of this work, and the effect of channel list on our analysis is normalized using the same channel list for both spectrum handoff with and without CCI cases.

We assume that PU activity pattern for each channel follow an i.i.d. ON/OFF random process [92, 29, 30, 66]. The ON period represent the duration while the channel is occupied by

a PU. The OFF period stands for PU absence at the channel. Inter-arrival and inter-departure times of PU with an arrival rate of λ_c and departure rate of β_c on a specific channel c are exponentially distributed with a mean of $\frac{1}{\lambda_c}$ and $\frac{1}{\beta_c}$, respectively.

6.3.2 SFT Duration without CCI

Here, we analytically model the experienced delay for the waiting time until a spectrum opportunity is detected in a predetermined circular list of channels. This delay comprises the consecutive spectrum sensing periods, i.e., repetitive spectrum handoff durations that elapses until a vacant channel is detected. Required spectrum sensing durations are not identical for all channels and vary based on the channel signal-to-noise ratio (SNR) and PU arrival λ_c and departure β_c rates [66]. To reflect this randomness in the spectrum parameters, we assume that the required spectrum sensing intervals ($\tau_s^{(c)}$) for different channels are outcomes of a uniform random variable. We drop channel index c from spectrum sensing interval and take spectrum sensing intervals for every channel c in channel list at different access instants as an independent and identically distributed (i.i.d.) random variable τ_s, distributed as

$$f_{\tau_s}(\tau) = \begin{cases} \frac{1}{\tau_s^{\max} - \tau_s^{\min}}, & \tau_s^{\min} \leq \tau \leq \tau_s^{\max} \\ 0, & \text{otherwise} \end{cases} \tag{6.1}$$

where $\tau_s^{\max}$ and $\tau_s^{\min}$ are the maximum and minimum values of spectrum sensing duration.

To determine the p.d.f. of SA delay τ_{sa}, we define the random variable $\tau_{\text{is}}^{(c)}$ for the duration of an interrupted spectrum sensing period in channel c. If a PU transmission occurs before the completion of the sensing period τ_s, SU stops spectrum sensing and performs channel switching and restarts spectrum sensing in a new channel. This operation is repeated until a PU arrival does not occur until completion of spectrum sensing interval. Frame transmission commence right after detection of the vacant channel. In accordance with the PU behaviour model described in Section 6.3.1 and using definition of exponential random variable, the conditional cumulative distribution function (c.d.f.) of the SA delay $\tau_{\text{is}}^{(c)}$ is given by

$$F_{\tau_{\text{is}}^{(c)}}(\tau|\tau_s) = \frac{P(t \leq \tau \cap t \leq \tau_s)}{P(t \leq \tau_s)} = \frac{P(t \leq \tau)}{P(t \leq \tau_s)} = \frac{1 - e^{-\lambda_c \tau}}{1 - e^{-\lambda_c \tau_s}}, \quad 0 < \tau \leq \tau_s \tag{6.2}$$

where λ_c represents the PU arrival rate in channel c. By taking the derivative of (6.2) with respect to τ, we find the conditional p.d.f. of $\tau_{\text{is}}^{(c)}$ as

$$f_{\tau_{\text{is}}^{(c)}}(\tau|\tau_s) = \frac{\lambda_c e^{-\lambda_c \tau}}{1 - e^{-\lambda_c \tau_s}}, \quad 0 < \tau \leq \tau_s \tag{6.3}$$

Then, by removing conditioning using the p.d.f. of τ_s given in (6.1), the p.d.f. of $\tau_{\text{is}}^{(c)}$ is obtained for $0 < \tau \leq \tau_s^{\min}$ as

$$f_{\tau_{\text{is}}^{(c)}}(\tau) = \int_{\tau_s^{\min}}^{\tau_s^{\max}} \frac{\lambda_c e^{-\lambda_c \tau}}{1 - e^{-\lambda_c \tau_s}} \frac{1}{\tau_s^{\max} - \tau_s^{\min}} \mathrm{d}\tau_s = \frac{e^{-\lambda_c \tau}}{\tau_s^{\max} - \tau_s^{\min}} \ln\left(\frac{e^{\lambda_c \tau_s^{\max}} - 1}{e^{\lambda_c \tau_s^{\min}} - 1}\right) \tag{6.4}$$

and for $\tau_s^{\min} \leq \tau \leq \tau_s^{\max}$ as

$$f_{\tau_{\text{is}}^{(c)}}(\tau) = \int_{\tau}^{\tau_s^{\max}} \frac{(\lambda_c e^{-\lambda_c \tau})}{(1 - e^{-\lambda_c \tau_s})(\tau_s^{\max} - \tau_s^{\min})} \mathrm{d}\tau_s = \frac{e^{-\lambda_c \tau}}{\tau_s^{\max} - \tau_s^{\min}} \ln\left(\frac{e^{\lambda_c \tau_s^{\max}} - 1}{e^{\lambda_c \tau} - 1}\right) \tag{6.5}$$

Finally, $f_{\tau_{\text{is}}^{(c)}}$ can be expressed by

$$f_{\tau_{\text{is}}^{(c)}}(\tau) = \begin{cases} \frac{e^{-\lambda_c \tau}}{\tau_s^{\max} - \tau_s^{\min}} \ln\left(\frac{e^{\lambda_c \tau_s^{\max}} - 1}{e^{\lambda_c \tau_s^{\min}} - 1}\right), & 0 \leq \tau \leq \tau_s^{\min} \\ \frac{e^{-\lambda_c \tau}}{\tau_s^{\max} - \tau_s^{\min}} \ln\left(\frac{e^{\lambda_c \tau_s^{\max}} - 1}{e^{\lambda_c \tau} - 1}\right), & \tau_s^{\min} < \tau \leq \tau_s^{\max} \\ 0, & \text{otherwise} \end{cases} \tag{6.6}$$

Table 6.1 illustrates the SA delay τ_{sa} in case of repetitive spectrum handoffs, where $P_+^{(c)}$ represents the probability of finding channel c vacant, and $P_-^{(c)}$ is the probability of occupancy of channel c by a PU. Channel switching delay τ_{sw} due to software-based hardware reconfiguration is counted in spectrum sensing duration τ_s. According to this model, $P_+^{(c)}$ during a spectrum sensing interval τ_s is found as

$$P_+^{(c)} = \int_{\tau_s^{\min}}^{\tau_s^{\max}} e^{-\lambda_c \tau_s} \frac{1}{\tau_s^{\max} - \tau_s^{\min}} \mathrm{d}\tau_s = \frac{e^{-\lambda_c \tau_s^{\min}} - e^{-\lambda_c \tau_s^{\max}}}{\lambda_c (\tau_s^{\max} - \tau_s^{\min})} \tag{6.7}$$

$P_-^{(c)}$ is obtained as $1 - P_-^{(c)}$. τ_s and $\tau_{\text{is}}^{(c)}$, are mutually independent random variables.

SA delay τ_{sa} is shown to be the sum of independent τ_{is} random variables in Table 6.1, and its p.d.f. is found by the convolution of the p.d.f.s of added random variables as

$$\begin{aligned} f_{\tau_{\text{sa}}}(\tau) = & \left[1 + \left(\prod_{c=1}^{C} P_-^{(c)}\right) f_{\tau_{\text{sa}}^{\text{tr(C)}}}(\tau) + \left(\prod_{c=1}^{C} P_-^{(c)}\right)^2 \left(f_{\tau_{\text{sa}}^{\text{tr(C)}}} * f_{\tau_{\text{sa}}^{\text{tr(C)}}}\right)(\tau) + \cdots\right] \\ & \cdot \left[\sum_{c=1}^{C} \left(\prod_{l=1}^{c-1} P_-^{(l)}\right) P_+^{(c)} \left(f_{\tau_{\text{sa}}^{\text{tr(c-1)}}} * f_{\tau_s}\right)(\tau)\right] \end{aligned} \tag{6.8}$$

where $\left(f_{\tau_{\text{sa}}^{\text{tr(c-1)}}} * f_{\tau_s}\right)(\tau)$ is the conditional p.d.f. of SA delay given that channel c is vacant. $f_{\tau_{\text{sa}}^{\text{tr(c-1)}}}(\tau)$ is the p.d.f. of the total duration spent for seeking a vacant channel until spectrum sensing starts at channel c, which is equal to $f_{\tau_{\text{is}}^{(1)}} * f_{\tau_{\text{is}}^{(2)}} * \cdots * f_{\tau_{\text{is}}^{(c-1)}}$. For ease of analysis, convolutions can be turned into a multiplication by taking the Laplace transform of the expression. In the resulting Laplace domain expression, since $\left|\prod_{c=1}^{C} (P_-^{(c)} f_{\tau_{\text{is}}^{(c)}}(s))\right| < 1$, $\mathcal{F}_{\tau_{\text{sa}}}(s)$ can

be found via geometric series interpretation on infinite series as

$$\mathcal{F}_{\tau_{\mathrm{sa}}}(s) = \frac{\sum_{c=1}^{C}(\prod_{l=1}^{c-1} P_{-}^{(l)})P_{+}^{(c)}\left(\prod_{k=1}^{c-1}\mathcal{F}_{\tau_{\mathrm{is}}^{(\mathrm{k})}}(\tau)\right)\mathcal{F}_{\tau_{\mathrm{s}}}(s)}{1-\prod_{c=1}^{C}\left(P_{-}^{(c)}\mathcal{F}_{\tau_{\mathrm{is}}^{(\mathrm{c})}}(s)\right)}, \tag{6.9}$$

where $\mathcal{F}_{\tau_{\mathrm{sa}}}(s)$ is the Laplace transform of $f_{\tau_{\mathrm{sa}}}(\tau)$, $\mathcal{F}_{\tau_{\mathrm{s}}}(s)$ is the Laplace transform of $f_{\tau_{\mathrm{s}}}(\tau)$, and $\mathcal{F}_{\tau_{\mathrm{is}}^{(\mathrm{c})}}(s)$ is the Laplace transform of $f_{\tau_{\mathrm{is}}^{(\mathrm{c})}}(\tau)$. It is assumed that $P_{-}^{(0)} = 1$ and $f_{\tau_{\mathrm{is}}^{(0)}}(s) = 1$.

To extend our SA delay analysis to SFT duration for the without CCI case, we define distribution of random variable $\tau_{\mathrm{sft}}^{\mathrm{sa}}$ for having k frame transmission trials before having a successful frame transmission using definition of exponential random variable as $f_{\tau_{\mathrm{sft}}^{\mathrm{sa}}}(k) = k(\mathrm{E}\{\tau_{\mathrm{sa}}\} + \tau_f)e^{-\lambda_k\tau_f}\prod_{c=1}^{k-1}(1-e^{-\lambda_c\tau_f})$, and the mean of SFT duration without CCI is obtained as $\mathrm{E}\{\tau_{\mathrm{sft}}^{\mathrm{sa}}\} = \sum_{k=1}^{\infty} k(\mathrm{E}\{\tau_{\mathrm{sa}}\} + \tau_f)e^{-\lambda_k\tau_f}\prod_{c=1}^{k-1}(1-e^{-\lambda_c\tau_f})$, where k is the number of frame transmissions until successfully delivering a single frame, and τ_f is the deterministic duration for transmission of a single frame.

6.3.3 SFT Duration with CCI

Here, we analytically model the SFT duration with CCI case τ_{sft} and derive its p.d.f.. This duration comprises the consecutive spectrum sensing and frame transmission periods. We call the duration of $\tau_s^{(c)} + \tau_f$ as the cognitive cycle duration $\tau_{\mathrm{cyc}}^{(c)}$. Each cognitive cycle $\tau_{\mathrm{cyc}}^{(c)}$ starts with a spectrum sensing interval $\tau_{\mathrm{s}}^{(c)}$ to seek a spectrum opportunity in a pre-defined circular channel list, and when an opportunity is found, the frame transmission interval τ_f starts. If PU arrival does not occur during the frame transmission period, the frame is said to be successfully transmitted, otherwise it is discarded and re-transmitted with next spectrum opportunity. Apart from without CCI case, not only spectrum sensing is ceased with PU detection but also frame transmission is cancelled via spectrum coordination over dedicated radio, i.e., CCI.

Since $\tau_{\mathrm{s}}^{(c)}$ is an i.i.d. random variable and τ_f is deterministic, $\tau_{\mathrm{cyc}}^{(c)}$ is also an i.i.d. random variable for each channel at each access instant, and hence, channel index c is dropped from

it. Using (6.1), p.d.f. of $\tau_{\text{cyc}}^{(c)}$ is found as

$$f_{\tau_{\text{cyc}}}(\tau) = \begin{cases} \frac{1}{\tau_{\text{cyc}}^{\max} - \tau_{\text{cyc}}^{\min}}, & \tau_{\text{cyc}}^{\min} \leq \tau \leq \tau_{\text{cyc}}^{\max} \\ 0, & \text{otherwise} \end{cases} \tag{6.10}$$

where $\tau_{\text{cyc}}^{\max}$ and $\tau_{\text{cyc}}^{\min}$ are equal to $\tau_s^{\max} + \tau_f$, and $\tau_s^{\min} + \tau_f$, respectively.

To determine the distribution of τ_{sft}, we define the random variable $\tau_{\text{icyc}}^{(c)}$ for interrupted cognitive cycle durations. The probability of finding channel c in an ON, i.e., busy, and OFF, i.e., hole, state are $P_{\text{b}}^{(c)} = \frac{\lambda_c}{\lambda_c + \beta_c}$, and $P_{\text{h}}^{(c)} = \frac{\beta_c}{\lambda_c + \beta_c}$, respectively. Similar to derivation of $\tau_{\text{is}}^{(c)}$ in Section 6.3.2, τ_{icyc} is found to be distributed by

$$f_{\tau_{\text{icyc}}^{(c)}}(\tau) = \begin{cases} \frac{e^{-\lambda_c \tau}}{\tau_{\text{cyc}}^{\max} - \tau_{\text{cyc}}^{\min}} \ln\left(\frac{e^{\lambda_c \tau_{\text{cyc}}^{\max}} - 1}{e^{\lambda_c \tau_{\text{cyc}}^{\min}} - 1}\right), & 0 < \tau \leq \tau_{\text{cyc}}^{\min} \\ \frac{e^{-\lambda_c \tau}}{\tau_{\text{cyc}}^{\max} - \tau_{\text{cyc}}^{\min}} \ln\left(\frac{e^{\lambda_c \tau_{\text{cyc}}^{\max}} - 1}{e^{\lambda_c \tau} - 1}\right), & \tau_{\text{cyc}}^{\min} \leq \tau \leq \tau_{\text{cyc}}^{\max} \\ 0, & \text{otherwise} \end{cases} \tag{6.11}$$

Fig. 6.1 illustrates the p.d.f. of the SFT duration τ_{sft}, and $f_{\tau_{\text{sft}}}(\tau)$ is found as

$$\begin{aligned} f_{\tau_{\text{sft}}}(\tau) = & \left[1 + \left(\prod_{c=1}^{C} P_b^{(c)}\right) f_{\tau_{\text{sft}}^{\text{tr(C)}}}(\tau) + \left(\prod_{c=1}^{C} P_{\text{b}}^{(c)}\right)^2 \left(f_{\tau_{\text{sft}}^{\text{tr(C)}}} * f_{\tau_{\text{sft}}^{\text{tr(C)}}}\right)(\tau) + \ldots\right] \\ & \cdot \left[\sum_{c=1}^{C} \left(\prod_{l=1}^{c-1} P_b^{(l)}\right) P_h^{(c)} \left(f_{\tau_{\text{sft}}^{\text{tr(c-1)}}} * f_{\tau_{cyc}}\right)(\tau)\right] \end{aligned} \tag{6.12}$$

where $\left(f_{\tau_{\text{sft}}^{\text{tr(c-1)}}} * f_{\tau_{cyc}}\right)(\tau)$ is the conditional p.d.f. of SFT duration given that c^{th} accessed channel is a spectrum hole. $f_{\tau_{\text{sft}}^{\text{tr(c-1)}}}(\tau)$ is the p.d.f. of the total interrupted cognitive cycle durations until cognitive cycle starts at channel c, which equals to $f_{\tau_{\text{icyc}}^{(1)}} * f_{\tau_{\text{icyc}}^{(2)}} * \ldots * f_{\tau_{\text{icyc}}^{(c-1)}}$. Following the derivation of $\mathcal{F}_{\tau_{\text{sa}}}(s)$ in Section 6.3.2, since $\left|\prod_{c=1}^{C}(P_b^{(c)} \mathcal{F}_{\tau_{\text{icyc}}^{(c)}}(s))\right| < 1$, $\mathcal{F}_{\tau_{\text{sft}}}(s)$ can be found via Laplace transform of (6.12) as

$$\mathcal{F}_{\tau_{\text{sft}}}(s) = \frac{\sum_{c=1}^{C} \left(\prod_{l=1}^{c-1} P_b^{(l)}\right) P_h^{(c)} \left(\prod_{k=1}^{c-1} \mathcal{F}_{\tau_{\text{icyc}}^{(k)}}(s)\right) \mathcal{F}_{\tau_{\text{cyc}}}(s)}{1 - \prod_{c=1}^{C} \left(P_b^{(c)} \mathcal{F}_{\tau_{\text{icyc}}^{(c)}}(s)\right)}, \tag{6.13}$$

where $\mathcal{F}_{\tau_{\text{sft}}}(s) = \mathcal{L}\{f_{\tau_{\text{sft}}}(\tau)\}$, $\mathcal{F}_{\tau_{\text{cyc}}}(s) = \mathcal{L}\left\{f_{\tau_{\text{cyc}}}(\tau)\right\}$, and $\mathcal{F}_{\tau_{\text{icyc}}^{(c)}}(s) = \mathcal{L}\left\{f_{\tau_{\text{icyc}}^{(c)}}(\tau)\right\}$. It is assumed that $P_b^{(0)} = 1$ and $f_{\tau_{\text{icyc}}^{(0)}}(s) = 1$.

The obtained closed form expressions for p.d.f.s of SFT durations for both with (τ_{sft}) in Section 6.3.2 and without ($\tau_{\text{sft}}^{\text{sa}}$) CCI in Section 6.3.3 are used to assess gain in delay performance via incorporation of CCI into CRN nodes. Impact of incorporation of CCI on providing delay guarantees in CRN are studied in Section 6.7. Furthermore, the obtained closed form expressions are used to formulate spectrum efficiency, energy efficiency, and distributed event sensing performance analyses in Section 6.4, 6.5, and 6.6, respectively.

6.4 Spectrum Efficiency Analysis

Here, we formulate the spectrum utilization for both with and without CCI cases. Achieved goodput for SFT is used as metric for spectrum efficiency. Assuming that SU always has data to send, transmission starting at $t = 0$ successfully delivers $D(t)$ frames and achieves a goodput of $G(t) = D(t) \cdot R \cdot \tau_f / t$ in a duration of t for a communication rate of R. Steady-state goodput G of such a spectrum utilization is found as

$$G = \lim_{t \to \infty} \frac{\mathrm{E}\{D(t)\} \cdot R \cdot \tau_f}{t} \tag{6.14}$$

where $\mathrm{E}\{D(t)\}$ is the mean of the number of frames transmitted successfully in $[0, t]$ for $t \to \infty$.

The achieved goodput for a SFT, i.e., $D(t) = 1$, in the duration of $\tau_{\text{sft}}^{\text{sa}}(i)$, i.e., in a realization of i.i.d random variable for SFT duration without CCI employment, is $G_{\text{sft}}^{\text{sa}} = R \cdot \tau_f / \tau_{\text{sft}}^{\text{sa}}(i)$. Since each $\tau_{\text{sft}}^{\text{sa}}(i)$ ends with a SFT, the evolution of SFT duration $\tau_{\text{sft}}^{\text{sa}}(i)$ can be taken as a Markov regenerative process [74] with a reward of SFT. From the renewal theorem, the asymptotic goodput for the without CCI case is found as $G_{\text{sft}}^{\text{sa}} = R \cdot \tau_f / \mathrm{E}\{\tau_{\text{sft}}^{\text{sa}}\}$ where $\mathrm{E}\{\tau_{\text{sft}}^{\text{sa}}\}$ is the mean SFT duration without CCI for spectrum handoff derived in Section 6.3.2.

The asymptotic goodput for the with CCI case is expressed by $G_{\text{sft}} = R \cdot \tau_f / \mathrm{E}\{\tau_{\text{sft}}\}$ where $\mathrm{E}\{\tau_{\text{sft}}\}$ is the mean of the SFT duration with CCI for spectrum handoff (6.12) derived in Section 6.3.3. We use $G_{\text{sft}}^{\text{sa}}$ and G_{sft} to elaborate role of CCI on spectrum efficiency in Section 6.7.3.

6.5 Energy Efficiency Analysis

To investigate energy efficiency gain via CCI utilization, we study SFT energy consumption for with and without CCI cases. We use power level of spectrum sensing Υ_s and frame

transmission Υ_f to determine SFT energy consumption. The mean energy consumption for an SFT without CCI is found as $\Omega_{\text{sft}}^{\text{sa}} = \sum_{k=1}^{\infty} k(\text{E}\{\tau_{\text{sft}}^{\text{sa}}\} \cdot \Upsilon_s + \tau_f \cdot \Upsilon_f) \cdot e^{-\lambda_c \tau_f}(1 - e^{-\lambda_c \tau_f})^{k-1}$. Energy efficiency of successful frame transmission without CCI case can be found as $\Gamma_{\text{sft}}^{\text{sa}} = \Upsilon_f \tau_f / \Omega_{\text{sft}}^{\text{sa}}$.

On the other hand, since frame transmission τ_f and spectrum sensing τ_s durations are embedded into τ_{cyc}, for with CCI case, energy consumption analysis reveals mean of maximum power consumption as $\Omega_{\text{sft}} = \text{E}\{\tau_{\text{sft}}\} \cdot \max(P_s, P_t)$. The minimum energy efficiency via incorporation of CCI into CR nodes can be determined by $\Gamma_{\text{sft}} = \Upsilon_f \tau_f / \Omega_{\text{sft}}$. Using Γ_{sft} and $\Gamma_{\text{sft}}^{\text{sa}}$, we elaborate and compare the achievable energy efficiency gains for the with and without CCI utilization scenarios in Section 6.7.4.

6.6 Distributed Event Sensing Distortion Analysis

Here, we address distributed sensing performance in cognitive radio sensor networks (CRSN). Event communication duration in an estimation interval is determined as $\text{E}\{\tau_e^{\text{non}}\} = \lfloor \tau_e / \text{E}\{\tau_{\text{sft}}^{\text{sa}}\} \rfloor \tau_f$ and $\text{E}\{\tau_e^{\text{cci}}\} = \lfloor \tau_e / \text{E}\{\tau_{\text{sft}}\} \rfloor \tau_f$ for without and with CCI cases, respectively. This duration reveals the average amount of time spent for communication of event features with fusion center apart from spectrum sensing and handoff functionalities, as well as retransmissions due to PU arrival and wireless link errors. We use $\text{E}\{\tau_e^{\text{cci}}\}$ and $\text{E}\{\tau_e^{\text{non}}\}$ to calculate received samples from sensor nodes at sink at the end of each estimation interval.

We formulate estimation distortion with respect to event communication duration in an estimation interval under opportunistic spectrum access in CRSN. For estimation distortion analysis, the best linear unbiased estimator (BLUE) [78] is used to assess distortion without any specific assumption or requirement on distribution of sensed signal and sensing noise. Sensor k obtains distorted version $s_k(t)$ of the event signal $\theta(t)$ at time t due to signal attenuation factor $h_k(t)$ and sensing noise $n_s^k(t)$, i.e., $s_k(t) = h_k(t)\theta(t) + n_k^s(t)$. We also assume that $h_k(t)$, $\theta(t)$ and $n_k^s(t)$ are i.i.d. over time. $\hat{\theta}(t)$ is estimated from the received samples from sensor nodes. We also assume that the mean of $\theta(t)$ and $n_k^s(t)$ are zero, and sensing noise $n_k^s(t)$ has a power of σ_k^2. Time indices are dropped in accordance with independence over time assumption. Using formulated event communication duration, number of received samples X from sensor k is found as $X_{\text{non}} = \text{E}\{\tau_e^{\text{non}}\}/\tau_f \cdot S_f$ and $X_{\text{cci}} = \text{E}\{\tau_e^{\text{cci}}\}/\tau_f \cdot S_f$ for without and

with CCI cases, where S_f is the number of samples per frame. Received sample vector $\mathbf{r}_k$ from sensor k is as $\mathbf{r_k} = \mathbf{h_k}\theta + \mathbf{n_k^s}$, where $\mathbf{r_k} = [r_{1,k}, \cdots, r_{X,k}]^{\mathrm{T}}$, $\mathbf{h_k} = [h_{1,k}, \cdots, h_{X,k}]^{\mathrm{T}}$, and $\mathbf{n_k^s} = [n_1^s, \cdots, n_{X,k}^s]^{\mathrm{T}}$. Covariance matrix $\mathbf{R_k}$ for received samples from CRSN node k is a X dimensional rectangular diagonal matrix whose diagonal entries are σ_k^2 for $1 \cdots X$, and other entries are 0. Hence, the mean square error (MSE) for BLUE can be determined as [78]

$$Var\left[\hat{\theta}_k\right] = \left[\mathbf{h_k}^{\mathrm{T}}\mathbf{R_k}^{-1}\mathbf{h_k}\right]^{-1} = \left(\sum_{k=1}^{K}\frac{X_k}{\sigma_k^2}\right)^{-1} \tag{6.15}$$

We use obtained MSE formulation in (6.15) for distortion assessment of distributed sensing over CRSN with and without dedicated radio utilization for spectrum handoff in Section 6.7.5.

6.7 Performance Evaluation

CCI utilization for spectrum handoff is investigated from SFT duration, spectrum efficiency, energy efficiency, and event estimation performance perspectives. Results guide for employment of CCI for various spectrum conditions and cognitive radio parameters. We first give network setup and investigate accuracy presented delay analysis in Section 6.3. Then, achievable gains via CCI utilization for spectrum handoff are examined.

6.7.1 Network Setup

Frame transmission duration τ_f and mean of spectrum sensing duration $\mathrm{E}\{\tau_s\}$ are taken to be 100 ms and 5 ms [113], respectively. PU packet arrival rate λ is varied from 2 to 20 packets/sec. SNR for AWGN channels is assumed to be 20 dB, unless otherwise stated.

6.7.1.1 The Nearest-neighbor Model

We use randomly deployed ad hoc PU and SU networks. From this setting, we deduce distribution of the nearest neighbour distance and the average PU arrival rate induced on a nearest neighbor SU communication link. For tractability, we assume that both PU and SU nodes are distributed according to a stationary homogeneous Poisson Point Process (PPP), with intensities λ_{PU} and λ_{SU} respectively. With the PPP assumption, the probability that an SU node has less than k neighbours in a neighbourhood of radius r is $P(\#$ of neighbours $<$

$k) = \sum_{i=0}^{k-1} e^{-\lambda_{\mathrm{SU}}\pi r^2} \frac{(\lambda_{\mathrm{SU}}\pi r^2)^i}{i!}$. The p.d.f. for the distance to the nearest SU neighbour is then $f_{r_1} = 2\pi\lambda_{\mathrm{SU}} r_1 \cdot e^{-\lambda_{\mathrm{SU}}\pi {r_1}^2}$ [50]. Given the distance r_1 between these two neighbor nodes, and assuming each PU node has an average packet arrival rate of α arrivals/second, the total PU traffic in channel c can be approximated by arrivals in a radius $R_c = 2r_1$ neighborhood of the SU link as $\mathrm{E}\{\lambda_{R_c}\} = \sum_{i=1}^{\infty} \alpha k e^{-\lambda_{\mathrm{PU}}|\pi R_c^2|} \frac{(\lambda_{\mathrm{PU}}\pi R_c^2)^k}{k!} = \alpha(\lambda_{\mathrm{PU}}\pi R_c^2)$.

6.7.1.2 Wireless Channel Model

Potential gains via CCI are investigated for both AWGN and flat fading channels. Ubiquitous Quadrature Amplitude Modulation (4-QAM) is assumed for SU transmissions. The bit error rate (BER) expression for AWGN channel under 4-QAM is $P_b^{\mathrm{awgn}} = \frac{3}{4} Q(\sqrt{4\frac{\overline{E_b}}{N_0}/5})$ where E_b in the energy per bit and noise has flat PSD $N_0/2$ [46]. The BER expression for 4-QAM over a fading channel (P_b^{fade}) is $P_{b,fade} = \frac{2}{\pi}\int_0^{\pi/2} M_\gamma\left(-\frac{9}{2sin^2(\phi)}\right) \mathrm{d}\phi - \frac{1}{\pi}\int_0^{\pi/4} M_\gamma\left(-\frac{9}{2sin^2(\phi)}\right) \mathrm{d}\phi$, where $M_\gamma(s) = (1 - s\overline{\gamma})^{-1}$ and $\overline{\gamma}$ is the SNR [89].

6.7.2 SFT Duration

The SFT durations under the implications of network conditions are denoted by τ_{cci} and $\tau_{\mathrm{n-cci}}$ for with or without CCI, respectively. They incorporate delays due to spectrum unavailability and channel errors. To point out conditions for which the use of CCI is advantageous, we first evaluate the accuracy of the analytical expressions for $\mathrm{E}\{\tau_{\mathrm{sft}}^{\mathrm{sa}}\}$ and $\mathrm{E}\{\tau_{\mathrm{sft}}\}$, derived in Section 6.3 via time-step simulations. Using them, we investigate and compare τ_{cci} and $\tau_{\mathrm{n-cci}}$.

6.7.2.1 Validation of Delay Analyses

For validation, the analytical expressions are constructed in Mathematica and their results are compared with results of a realistic time-step simulation framework in MATLAB. The PU packet departure rate is set to 30, corresponding to the assumption that as an SU switches to a new channel, it always finds the channel initially idle, in conformity with notion of stable channel. The analytical and simulation results for $\mathrm{E}\{\tau_{\mathrm{sft}}^{\mathrm{sa}}\}$ and $\mathrm{E}\{\tau_{\mathrm{sft}}\}$ are given in Fig. 6.2. The error between the analytical and simulation result values are below 5% for all given λ values, increasing slightly as λ's become comparable to the β value.

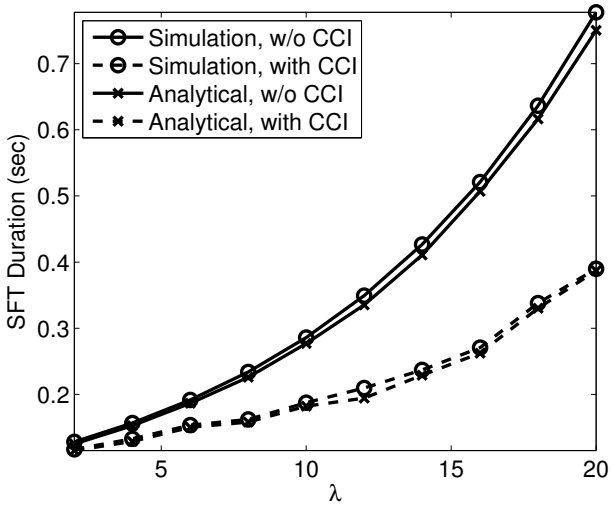

Figure 6.2: Validation of successful frame transmission duration with and without CCI. $\mathrm{E}\{\tau_s\}$ and $\mathrm{E}\{\tau_{cyc}\}$ are uniformly distributed between 2.5 ms to 7.5 ms and 100 ms to 110 ms, respectively.

6.7.2.2 SFT Duration with and without CCI

We first define the SFT durations under the network setup, which are denoted by τ_{cci} and $\tau_{\mathrm{n-cci}}$ for the cases with and without CCI, respectively. Assumption here is that whole τ_{sft} and $\tau_{\mathrm{sft}}^{\mathrm{sa}}$ durations have to be repeated in case of a wireless error in these two scenarios. $\mathrm{E}\{\tau_{\mathrm{cci}}\}$ is given by $\mathrm{E}\{\tau_{\mathrm{cci}}\} = \sum_{k=1}^{\infty} k \cdot \mathrm{E}\{\tau_{\mathrm{sft}}\} \cdot P_{\mathrm{cf}}(1 - P_{\mathrm{cf}})^{k-1}$, where $P_{\mathrm{cf}} = (1 - \mathrm{BER})^{R \cdot \tau_f}$ is the correct transmission probability and BER and R are the bit error rate and transmission rate, respectively. Similarly, $\mathrm{E}\{\tau_{\mathrm{n-cci}}\}$ is $\mathrm{E}\{\tau_{\mathrm{n-cci}}\} = \sum_{k=1}^{\infty} k \cdot \mathrm{E}\{\tau_{\mathrm{sft}}^{\mathrm{sa}}\} \cdot P_{\mathrm{cf}} \cdot (1 - P_{\mathrm{cf}})^{k-1}$.

In Fig. 6.3, the SFT durations with and without CCI are presented, for both AWGN and flat fading channels. As the $\frac{\tau_f}{\mathrm{E}\{\tau_s\}}$ ratio increases, the CCI case becomes highly advantageous. This advantage becomes significant when τ_f is greater than $5 \cdot \mathrm{E}\{\tau_s\}$, and follows an exponential trend. However, gains in SFT duration by employing CCI is still not impressive when PU arrival rate is low. Under fading, the reduction in delay by CCI is higher than the reduction in delay by CCI under AWGN only; hence CCI is even more useful for SFT duration under fading. However, the gains in SFT duration vanish under low PU arrival rate or unconventionally low $\frac{\tau_f}{\mathrm{E}\{\tau_s\}}$ ratio.

Fig. 6.4 illustrates the effect of SU node density on the SFT duration. Two α values

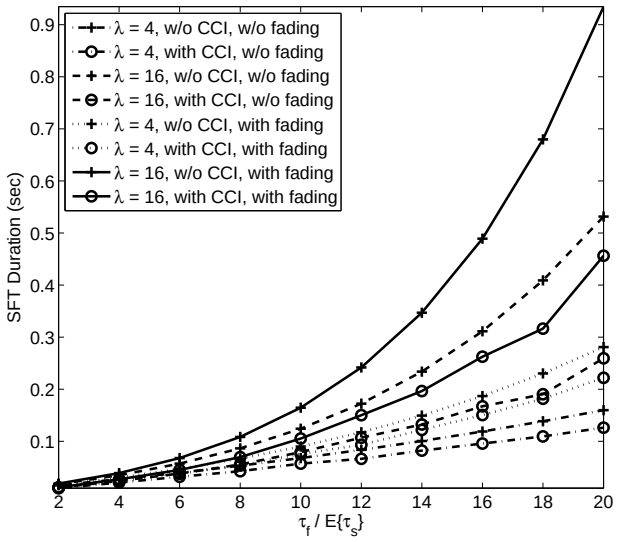

Figure 6.3: Variation of SFT duration by employing CCI, for different PU arrival rates and varying $\frac{\tau_f}{\mathrm{E}\{\tau_s\}}$ ratios. Both AWGN and flat fading channels are considered.

from Section 6.7.1, 1 and 0.25, are taken for the lowest SU node density case ($\lambda_{\mathrm{SU}} = 0.01$); resulting in λ values of 16 and 4. AWGN only channel is assumed, with 15 dB SNR. The SNR and total PU packet arrival rate values for other λ_{SU} values are calculated according to their R_c values. In Fig. 6.4, increasing the λ_{SU} decreases the SFT duration, since SU nodes become closer and links bear less PU traffic. CCI provides same SFT duration as the non-CCI case, at a lower SU density. Still, benefits of CCI vanishes with increasing node density, specifically for the $\lambda = 4$ case where $\lambda_{SU} = 0.015$ acts as a threshold to decide on CCI, whereas the threshold for the higher traffic case is slightly higher. For low λ_{SU} under high PU traffic, incorporation of CCI instead of increasing node density to achieve SFT duration constraint can yield reduced deployment costs.

6.7.3 Spectrum Efficiency

The variation of the goodput with respect to the rate R is given in Fig. 6.5. The gain in goodput by employing a CCI varies according to the PU arrival rate. With the provided framework, it is possible to decide on whether employing a CCI is favorable according to channel and network conditions, i.e., PU arrival rates and mean link distances. In Fig. 6.5, it is observed that with CCI utilization achieved goodput is higher when compared to without CCI cases for

various PU arrival rates.

6.7.4 Energy Efficiency

Here, potentials of CCI utilization for energy efficiency gain are investigated with respect to varying τ_f and for a fixed E$\{\tau_s\}$ of 5 ms. Energy efficiency gain via CCI depends on the τ_s and τ_f durations, as well as power consumption levels in these periods. We use two different spectrum sensing Υ_s and frame transmission Υ_f power level pairs, i.e., $\{\Upsilon_{s_1} = 180\text{mW}, \Upsilon_{f_1} = 320\text{mW}\}$, and $\{\Upsilon_{s_2} = 240\text{mW}, \Upsilon_{f_2} = 200\text{mW}\}$. Energy efficiency gain via CCI utilization is presented in Fig. 6.6.

When τ_f is close to E$\{\tau_s\}$, we see that energy efficiency gains do not differ much between two pairs for transmission and spectrum sensing power levels. Nevertheless, with increasing τ_f, the efficiencies increase on the overall, and the difference between the two scenarios grow steadily in favor of pair 1. Accordingly, when τ_f is small and transmission power is greater than the spectrum sensing power, i.e., for power level pair 2, energy efficiency gain provided by CCI diminishes. In other scenarios, CCI is mostly advantageous.

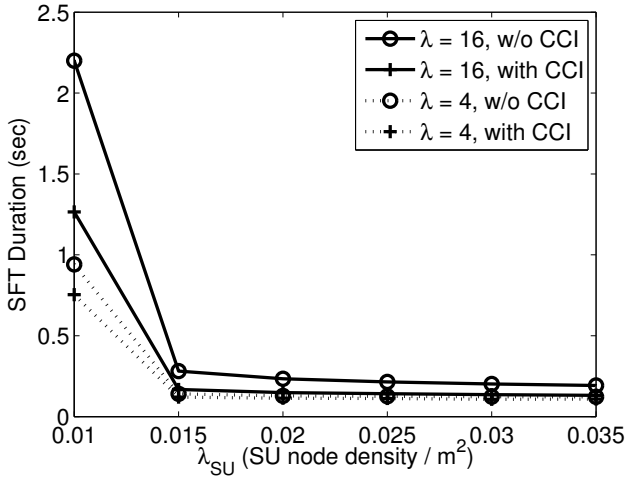

Figure 6.4: Variation of SFT duration, with increasing SU node density, for both with CCI and without CCI cases. E_b/N_0 is assumed to be 15 dB for lowest SU density.

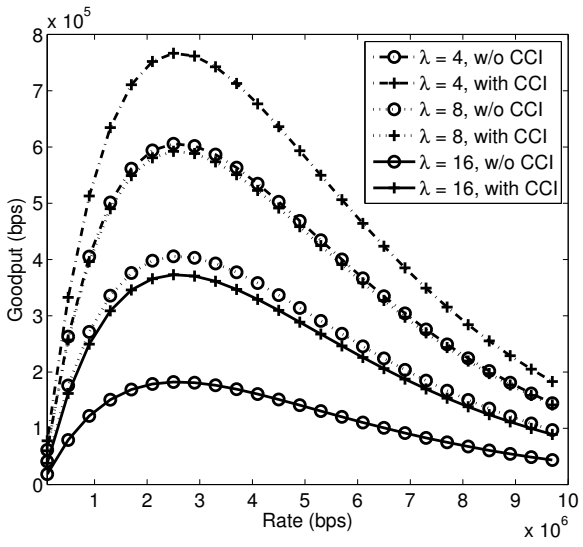

Figure 6.5: Variation of goodput, with increasing rate R for both with and without CCI cases, under different PU arrival rates.

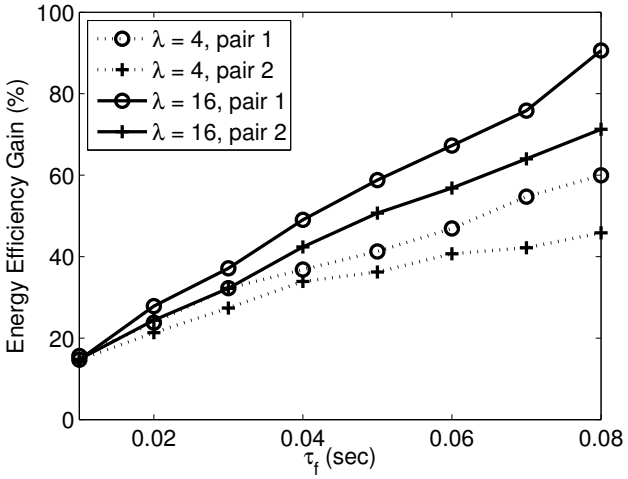

Figure 6.6: Energy efficiency gain via CCI, for Υ_{s_1} = 180 mW, Υ_{f_1} = 320 mW (pair 1) and Υ_{s_2} = 240 mW, Υ_{f_2} = 200 mW (pair 2)

6.7.5 Distributed Event Sensing Performance

Distributed event sensing distortion results are presented in Fig. 6.7. Sensing noise σ_k^2 is taken to be 0.01 for all sensors. Estimation interval τ_e is taken to be 1 sec. Samples per frame S_p is set to 10. Achieved mean square error (MSE) with CCI is expectedly lower than the one achieved without CCI. Thus, CCI employment for CRSN nodes provides MSE gain.

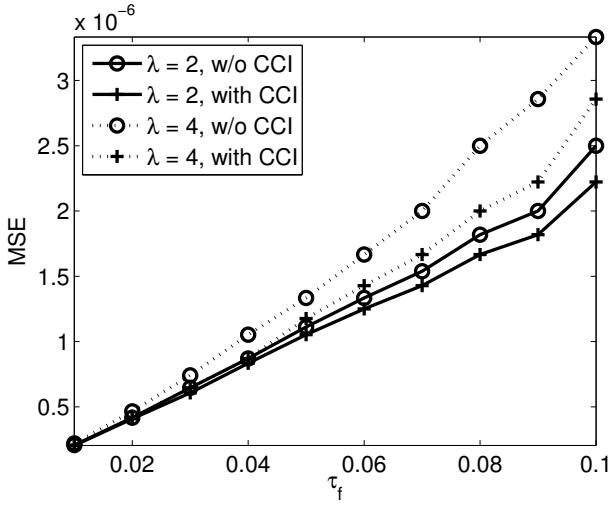

Figure 6.7: Distributed sensing distortion performance with and without CCI, under different PU arrival rates.

Nevertheless, this gain heavily depends on frame duration to spectrum sensing duration ratio and the PU traffic conditions. Since sensor nodes have lower ranges, we consider a lower PU traffic imposed upon those nodes, than their CRN counterparts. Accordingly, the gains in MSE by employing CCI are not that bright, when frame duration is not an order greater than the spectrum sensing duration. The difference between achieved MSE in CRSN nodes with and without CCI increase with increasing PU traffic, but not as drastically as their CRN equivalents.

CHAPTER 7

SPECTRUM-AWARE AND COGNITIVE SENSOR NETWORKS FOR SMART GRID APPLICATIONS

In this chapter, Spectrum-aware and Cognitive Sensor networks (SCSN) for smart grid applications are presented. The objective of this work is to envision potentials of SCSN for reliable and low-cost remote monitoring solutions for smart grid. SCSN for smart grid applications was first presented in [23]. In Section 7.2, the potential applications of SCSN in smart grid are briefly discussed. The spectrum management functionalities in SCSN are presented in Section 7.3. The specific technical challenges and open research directions for the communication layers of SCSN are summarized, and reliable transport performance in SCSN for various smart grid environments is asses via a case study in Section 7.4. Different energy harvesting solutions for SCSN-based smart grid applications are reviewed in Section 7.5.

7.1 Motivation

Smart grid has been conceived as the evolution of electric power systems to enhance efficiency, reliability and safety of the existing power grid. The need for next-generation electricity network has arisen with the increasing demand for electricity, aging grid equipment, advancement of alternative energy resources, and climate changes to provide reliable, safe and economical power delivery [16, 27, 39, 53]. To this end, remote and timely information gathering from smart grid equipment about failures, capacity limitations, and natural accidents is extremely crucial for ensuring proactive and real-time diagnosis of possible blackouts and transient faults in the smart grid. This makes cost-effective remote monitoring and control technologies vital for safe, reliable and efficient power delivery in smart grid [49, 111]. An

illustrative architecture of the smart grid is shown in Fig. 7.1.

Recently, wireless sensor networks (WSN), which are mainly characterized by their collaborative, low-cost, and energy-limited nature, have gained attention for electric power network monitoring instead of wired systems. Reliable and efficient management of smart grid can be accomplished with the installation of wireless sensor nodes on the critical power grid equipment [49, 111]. Gathered information from this equipment can help in responding to changing conditions and malfunctions of the electric grid in a proactive manner. Moreover, obtained information from sensors can be used to diagnose arising problems rapidly, and hence, autonomous and reliable operation can be achieved in smart grid. However, the realization of smart grid literally depends on the communication capabilities of sensor network in harsh and complex electricity network environments that bring out great challenges for reliability and energy efficiency in WSN.

To this end, dynamic and opportunistic spectrum access capabilities of cognitive radio can be benefited to address many of the unique requirements and challenges of smart grid for WSN, i.e., heterogeneous spectrum characteristics changing over time and space, reliability and latency requirements, harsh environmental conditions, and energy constraints of low-power sensor nodes. With its adaptability to existing spectrum utilization and characteristics in the deployment field, spectrum-aware and cognitive sensor networks can enhance the overall network performance and spectrum utilization [8]. Promising advantages of spectrum-aware and cognitive radio equipped sensor nodes in smart grid can be outlined as follows:

- ***Minimization of environmental effects*:** Field tests in [49] show that wireless links in smart grid are exposed to spatio-temporally varying spectrum characteristics due to electromagnetic interference, equipment noise, dynamic topology changes, and fading due to obstructions and hindrances. This leads to both time and location dependent delay and capacity variations of wireless links in smart grid environments. Therefore, to overcome varying link conditions in time and space domains, sensor nodes must be capable of reconfiguring themselves autonomously without hardware modifications. With the ability of dynamic and opportunistic access to spectrum, sensor nodes can mitigate these effects while minimizing energy consumption.

- ***Access to licensed and unused spectrum bands*:** Different services operating in licensed bands of spectrum can be accessed by users in smart grid. Cognitive radio

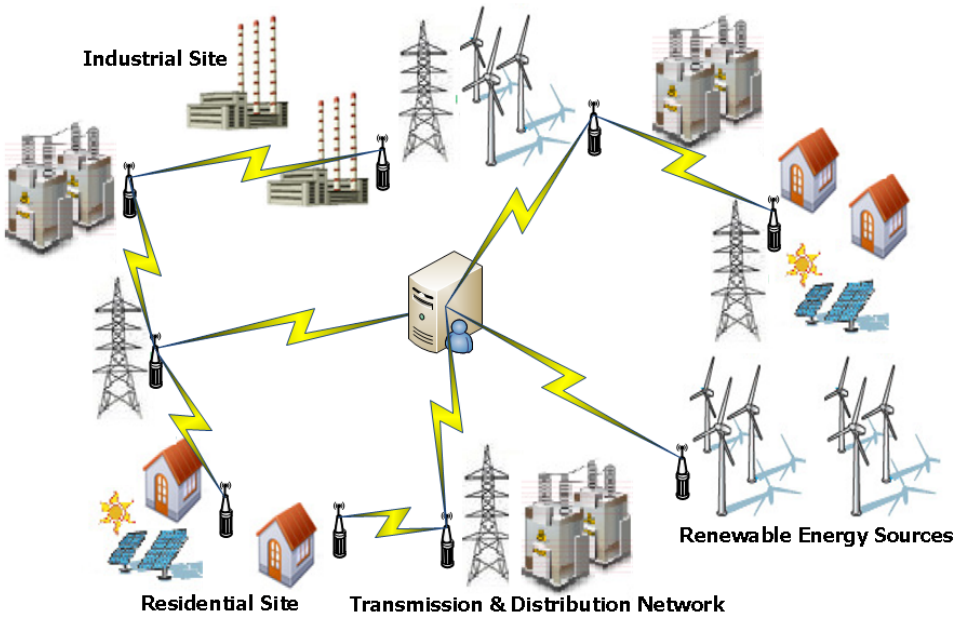

Figure 7.1: An illustrative architecture of smart grid using sensor networks. Smart grid can be defined as a modernized electric power T&D network using robust two-way communications, advanced sensors, and distributed computing technologies to improve efficiency, reliability and safety of power delivery and use.

capability empowers sensor nodes to detect spectrum holes and access them without interfering with licensed users. Therefore, cognitive radio equipped sensor nodes can dynamically access vacant bands based on spectrum opportunities, and achieve higher capacity levels with the same amount of power consumption.

- ***Adaptation to different spectrum utilization patterns*:** Smart grid is distributed over a large geographic area, and different spectrum utilization patterns can be experienced in these areas. Sensor nodes equipped with cognitive radio can continue reporting of sensed phenomenon under different spectrum characteristics. Therefore, cognitive capability does not only increase overall spectrum utilization, but also alleviate adaptation to different spectrum utilization patterns in smart grid as well.

- ***Overlay deployment of multiple sensor networks*:** The existing WSN deployments are based on static spectrum apportionment. Since multiple nodes from different sensor networks try to send its information simultaneously, sensor nodes are subject to interference and collisions. Cognitive radio can provide efficient spectrum sharing between co-existing sensor networks in a fair manner.

Table 7.1: Summary of SCSN Applications for Smart Grid vs. Power Grid Segment

Applications	Power Grid Segment
Wireless Automatic Meter Reading	Consumer Side
Real Time Pricing and Demand Response	Consumer Side
Residential Energy and Load Management	Consumer Side
Line Fault and Power Theft Detection	T&D Side
Outage Detection	T&D Side
Underground Cable System Monitoring	T&D Side
Towers and Poles Monitoring	T&D Side
Animals and Vegetation Control Monitoring	T&D Side
Conductor Temperature and Dynamic Thermal Rating Systems	T&D Side
Traditional Power Plant Monitoring	Generation Side
Wind Farm Monitoring	Generation Side
Solar Farm Monitoring	Generation Side

In general, spectrum-aware and cognitive sensor networks (SCSN) for smart grid can be specified as a distributed wireless network of spectrum-aware sensor nodes, which monitor the critical smart grid equipment and send their information dynamically over available spectrum bands in a multi-hop fashion to meet the application-specific requirements. Albeit the recent interest in power grid monitoring based on WSN, the SCSN for smart grid is a vastly unexplored area. To the best of our knowledge, there exist no comprehensive work on employment of cognitive radio sensor networks for smart grid applications. In addition to study of potential applications and communication algorithm needs of SCSN, in this chapter we also investigate incorporation of energy harvesting techniques for different power grid segments to extend limited life time of sensor nodes. Here, our objective is to envision potentials of SCSN for smart grid applications and discuss the open research issues in this timely and exciting field.

7.2 Potential Applications of SCSN in Smart Grid

WSN has already started to be used in a diverse range of power grid applications from home area networks to power transmission and distribution (T&D) network monitoring [16], [49], [111], [37], [67]. In Table 7.1, an overview of some of these potential applications and their

corresponding power grid segment are given [16],[49], [37], [111], [67]. In general,the electric power systems contain three major subsystems, power generation, T&D, and consumer facilities.

7.2.1 Remote Monitoring for Electric Power Generation Systems

A wide variety of sensors, such as current, voltage, temperature, etc., have been used in conventional electric power generation systems (EPGS). Lately, green energy resources, such as wind power and solar energy, have been gaining popularity in electricity generation, since the green electricity generation techniques meet environmental regulations by producing lower carbon emission in contrast to conventional EPGS. Due to variations and limitations on the availability of solar and wind power, real-time information obtained from green EPGS is crucial for electrical energy storage units.

Recently, employing wireless sensors in EPGS has been an active research field due to the collaborative nature and flexibility of WSN [37]. However, realization of wireless remote monitoring applications in EPGS is challenging due to the crowded spectrum problem in unlicensed bands. Moreover, performance of WSN in smart grid is severely restricted by packet losses, collisions and contention delays due to spatio-temporally varying heterogenous spectrum characteristics [24]. In this regard, the SCSN nodes can access the spectrum opportunistically to improve the overall network performance in terms of reliability and communication latency. In addition to remote monitoring of EPGS equipment, SCSN can also be deployed for monitoring the workspace for the safety of staff.

7.2.2 Remote Monitoring for Electricity T&D Network

Transmission and distribution (T&D) power networks are very critical power grid assets, where an equipment failure can result in electricity blackouts and various accidents. In T&D equipment monitoring, several variables, such as temperature, conductor thermal capacity, faulted circuit indicators, conductor sag, conductor vibration, can be monitored [111]. Since transmission power lines are distributed over a large geographic area, different spectrum utilization patterns are exposed in these areas. Cognitive capability helps to adapt different spectrum patterns in smart grid easily. Substation monitoring and control is also important for the

power grid [111]. The SCSN nodes can overcome challenges due to electromagnetic interference and fading in substations with their spectrum-aware nature. Moreover, the SCSN can achieve higher throughput with its DSA capability, and hence, surveillance of power lines and substations can be achieved with enhanced real-time communication capability of the SCSN, and bandwidth-greedy multimedia applications can be realized, e.g., power grid infrastructure security via video surveillance in smart grid.

7.2.3 Remote Monitoring for Consumer Facilities

Unlike the conventional power grid, effective power demand control of consumer facilities can be achieved in smart grid. With the opportunistic spectrum access capability of SCSN, monitoring of consumer facilities' power consumption can be incorporated into smart grid without interfering with the existing communication infrastructure at the consumer side. Moreover, DSA capability can help to overwhelm environmental interference and fading. Based on gathered information from different users with various power consumption characteristics, such as industrial and home users, predictive and robust electrical power load balancing strategies can be developed. [49].

As part of the end-user facilities, advanced metering infrastructures (AMI) can also be efficiently realized with the use of the SCSN. The SCSN can contribute to AMI technology for self-configuration and easy deployment in co-existing wireless networks at different customer premises. With the spectrum-aware communication capability, AMI meters and equipment can be easily deployed at the remote sides to achieve seamless and reliable communication between utility control center and AMI. The SCSN nodes designed with consideration of energy and price limitations in remote monitoring can be the main components for efficient realization of wireless AMI.

7.3 Spectrum Management Requirements and Challenges of SCSN

Minimization of environmental effects, adaptation to different spectrum utilization patterns, and overlay deployment of multiple sensor networks are some of the promising advantages of SCSN in smart grid. However, the realization of SCSN for smart grid mainly requires efficient spectrum management functionalities to dynamically manage the spectrum access

of sensor nodes in harsh smart grid environments. Requirements and research challenges for main four spectrum management functionalities in cognitive radio, i.e., spectrum sensing, spectrum decision, spectrum sharing, and spectrum mobility, are explored below for SCSN.

7.3.1 Spectrum Sensing

To take advantage of spectrum sensing in the SCSN, an efficient solution is needed considering both sensor network resource limitations and DSA network challenges. Considering high numbers of sensor nodes in large-scale smart grid systems and low-cost requirements, it may not be feasible to equip sensor nodes with multiple radios and highly capable processors. Therefore, sophisticated spectrum sensing algorithms cannot be used. Spectrum sensing should be performed with limited node hardware, possibly using single radio. Assuming that deployed sensor nodes in smart grid environments have single radio due to their scalability and low-cost requirements, sensing durations should be minimized as much as possible with the consideration of possible transmission activities and energy efficiency. There are various spectrum sensing methods, such as energy detection, feature detection, matched filter, and interference temperature [9]. Incorporating of one (or hybrid) of these techniques, detection of dynamically changing noise components in smart grid, and modelling of their interference with respect to time and space can be achieved.

Overall, the benefits of DSA, such as lower packet collisions due to the capability of switching to the best available channel, less contention delay and more bandwidth, come with the additional energy consumption caused by spectrum sensing and distribution of these sensing results. The trade off between energy efficiency and sensing accuracy is should be addressed and a detailed analysis of cost vs. benefits for a specific smart grid environment should be performed.

7.3.2 Spectrum Decision

With the DSA capability, sensor networks have ability to change their operating spectrum band when they decide that communication can be done in an another band with increased efficiency and QoS. Selecting one radio frequency as network-wide cannot yield the expected performance gain due to spatio-temporally varying spectrum characteristics. For example,

power grid equipment may work periodically, since they may not be required to always work, and hence, their RF interference can also vary with time. In addition, some licensed band users, such as TV and cellular phones, may exist around, especially in consumer sites.

Parameter selection is crucial for efficiency of spectrum decision. These parameters include but not limited to spectrum sensing duration to data transmission ratio, transmission power, expected duration to spend in a channel without spectrum handoff, predictive capacity and delay, energy-efficiency and error rate. For underlay approaches and existing smart grid equipment RF interference, the trade-off between spectrum handoff and adaptation to ongoing channel must be investigated. Overall, this yields an optimization problem as to handoff or not to handoff based on channel conditions.

In distributed coordination approaches for spectrum decision, sensor nodes sense the radio spectrum and communicate their spectrum sensing and decision results to their neighbors in order to overcome the spectrum decision problems caused by the limited knowledge of spectrum availability and network topology [9]. Overall, energy efficient and scalable methods of spectrum decision mechanisms are yet to be investigated in order to efficiently realize the proposed SCSN for smart grid.

7.3.3 Spectrum Sharing

The transmissions in smart grid environments should be coordinated by spectrum sharing functionality to prevent packet collisions and multi-user colliding in crowded radio spectrum environments of the smart grid [9]. Importantly, different applications in smart grid may co-exist, and to satisfy their reliability and latency requirements, QoS-aware spectrum sharing schemes are essential for the proposed SCSN. To achieve this objective and thus to overcome dynamically varying spectrum characteristics, the temporal and spatial reuse of spectrum must be benefited. In general, spectrum sharing functionality is closely related to Medium Access Control (MAC) layer functionality and thus, it can be incorporated into the MAC layer. Some of the main challenges against efficient spectrum sharing schemes include time-synchronization, distributed power allocation and spectrum utilization, and topology discovery. Overall, an effective spectrum sharing scheme helps to meet QoS requirements of smart grid applications by allocating network resources adaptively.

7.3.4 Spectrum Mobility

In SCSN for smart grid, spectrum handoff (or mobility) can be triggered by excessive interference caused by smart grid equipment. In case of excessive RF interference and noise, ongoing communication should be carried onto an another channel selected by spectrum decision algorithm. To have effective spectrum mobility functionality, the trade-offs between communication parameters must be well understood. Moreover, since spectrum mobility brings interruptions to ongoing communication, the schemes to prevent buffer overflows and minimize communication delay should be developed in order to allow reliable and real-time remote monitoring in SCSN. Based on changes in spectrum characteristics in time and space domains, spectrum handoff can be performed heterogeneously, and hence, this will yield heterogeneous link conditions on the way to sink node. Since smart grid is spread over a large geographic area, spectrum mobility functionality is also critical for adapting to different spectrum regulations.

7.4 SCSN Communication Protocol Suite

Efficient operation of the proposed SCSN is tightly-coupled by the running communication protocol suite. In addition to dynamic spectrum access, dense deployment, event driven nature and energy efficiency concerns of the SCSN, harsh environmental conditions and variable link capacity arises in smart grid environments. In this section, the SCSN specific challenges for communication layers are briefly investigated due to space limitations, and then, adaptive reliability control in SCSN is addressed.

7.4.1 Physical Layer

To overcome spatio-temporally varying spectrum characteristics and fading, SCSN node's physical layer must be configurable in terms of operating frequency, modulation, channel coding, transmission power and spectrum sensing duration. This configuration should be based on spectrum sensing and decision results. Due to resource-limited nature and low-cost requirement of sensor nodes, implementing RF front-end for SCSN node is a challenging task. Importantly, SCSN physical layer must be capable of providing statistical information

about channel conditions to upper layers for empowering spectrum-awareness. Therefore, effective, energy-efficient, and yet practical cognitive radio for sensor nodes is essential for the realization of SCSN. Existing fundamental open research issues for the realization of physical layer of SCSN can be outlined as follows:

- In order to overwhelm temporally and spatially varying environmental RF interference in smart grid, adaptive power allocation schemes are essential. Interference problem due to dense deployment in sensor networks should also be considered. Designed solution must maximize energy usage efficiency.
- Adaptive modulation should be employed to maximize network life time and map application-specific QoS requirements to configurable parameters of the physical layer. SCSN node's physical layer must be configurable without hardware modification. Thus, software-defined radios ensuring efficient DSA are needed for SCSN.
- Cooperative transmission schemes must be investigated to benefit from sender diversity in SCSN. Cooperative relaying can help to realize energy-efficient communication in such a harsh RF interference environment as SCSN.
- Statistical methods are required to help channel information gathering in physical layer. Considering limited processing capabilities and low-cost requirements of sensor nodes, practical signal processing algorithms should be developed to enable effective spectrum management, and spectrum awareness at upper layers.

7.4.2 Data Link Layer

Efficient medium access control (MAC), and error control are the main functionalities of the data link layer. In the proposed SCSN, these objectives must be achieved in an energy-efficient manner with consideration of dynamic spectrum management challenges. We investigate MAC and error control in SCSN separately as follows:

7.4.2.1 Medium Access Control

Resource limitations, dense deployment, and application-specific QoS requirements of sensor networks are exacerbated by spatially and temporally varying channel conditions in smart

grid. Furthermore, event estimation, spectrum sensing, and channel identification requirements should be considered jointly to determine sleep schedules to reduce energy consumption in the network.

Additional challenges that MAC layer in SCSN must handle to empower DSA are outlined as follows:

- Solutions with minimum control overhead and no additional hardware requirements, such as an additional transceiver, should be developed.
- Joint consideration of spectrum sensing and duty cycling is required to balance the trade-off between energy efficiency and spectrum efficiency.
- Novel spectrum-aware MAC protocol should be developed. It must jointly consider spatial correlation of sensed phenomenon, energy efficiency requirement of sensor nodes, and contention due to dense deployment.

7.4.2.2 Error Control

With its multiple channel access ability, and dynamically varying spectrum conditions, a fixed FEC scheme may not yield optimal results for every channel. Hence, the error correction mechanism must consider this trade-off and adaptive FEC schemes or hybrid ARQ mechanisms can be employed. Enabling spectrum-aware energy-efficient error control mechanisms can be made possible with the consideration of the following additional challenges.

- Cooperative schemes based on ARQ can be developed to help lost packets recovery. Nodes receiving the transmitted information can keep this information for a while although they are not the destination node, and can re-transmit based on loss prediction or ARQ. Moreover, cooperative relaying schemes may be employed by relay nodes to increase probability of successful packet forwarding. However, efficient synchronization of sensor nodes is required in this case.
- Repetitive ARQs due to harsh smart grid environmental interference can block packet forwarding and can cause congestion due to excessively incoming packets. Added redundancy by FEC employment must be spectrum-aware and predictive such that it must

adapt spatially and temporally varying environmental interferences, and must rapidly react to spectrum handoffs.

- Cost vs. benefit analysis of employing FEC, ARQ, hybrid, and cooperative schemes should be well investigated with consideration of spectrum handoff and licensed user activity to provide energy conservation maximization.

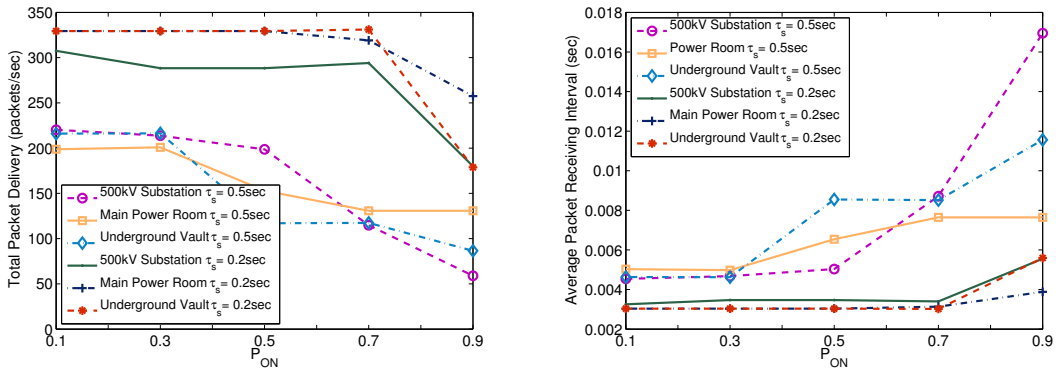

(a) (b)

Figure 7.2: Variation of (a) packet delivery and (b) packet receiving interval with respect to licensed user ON probability (P_{ON}).

7.4.3 Routing Layer

DSA capability provides interference minimizing opportunity in route selection through the sink node. Moreover, spectrum sensing durations are limiting factor for the throughput of sensor nodes. Moreover, in order to detect variations in the environmental interference, spectrum sensing durations also vary depending on spatially varying characteristics of RF interference sources on the path to sink. Open research issues in SCSN for routing layer are stated below.

- Multi-path routing can be employed to benefit from path diversity for interference mitigation.
- Cooperative routing schemes, such as diffusion-based cooperative routing protocols, can be developed to increase energy efficiency on packet forwarding.
- Depending on spatial variation of environmental interference, different channels can be benefited for forwarding on the event-to-sink path. To this end, spectrum-aware

multi-channel routing algorithm can be developed that is maximizing spectrum usage efficiency while minimizing exposed event-to-sink delay.

- Moreover, spectrum decision mechanism should be in contact with routing layer, i.e., spectrum decisions must be performed after investigation of trade-off between spectrum handoff and adaptation of routing layer to concurrent operating channel.

7.4.4 Transport Layer

Reliability and congestion control become an extremely challenging task with integration of cognitive radio and sensor networks [20, 24]. In SCSN, congestion control algorithms must be aware of cognitive-cycle, and should perform load balancing in a distributed manner. Spatially and temporally varying lossy links makes rate control a very challenging task, and requires careful design for congestion avoidance. Moreover, control packet exchanges must be minimized and congestion control mechanism must be proactive to help energy harvesting. Furthermore, in SCSN, environmental RF interference further amplifies the challenges emerging from union of those. Open research directions for reliability and congestion control in SCSN are summarized as follows.

- Statistical rate control schemes must be developed to provide reliable event transport under varying spectrum characteristics and spectrum sensing durations. Obviously, rate control algorithm must not aim to maximize rate and reach maximum bandwidth utilization, instead it must aim to maximize reliability.

- Furthermore, real-time requirements of time-critical applications should be considered, as well as maximizing reliability, real-time transport protocols must minimize delay. This requires additional information at source nodes to determine event to sink path characteristics, and apply rate control to minimize delay while satisfying reliability.

7.4.5 A Case Study of Reliable Transport in Different Smart Grid Environments

We have performed simulation experiments to reveal the reliability performance of cognitive radio equipped sensor nodes in smart grid [24]. Wireless channel model and parameters that

are determined in our previous study via field-test experiments in different spectrum environments of power grid, e.g., 500kV substation, main power room and underground network transformer vaults [49], are used in simulations. Experimentally determined log-normal channel parameters for different power system environments are given in Table 3.2. 200 nodes and a sink are placed randomly in a 100m x 100m field. 10 source nodes are randomly selected within an event area of radius 15m, and transmit power (P_t) is set to 10 dBm. Sensor nodes activity pattern with time consists of data transmission (τ_t), spectrum sensing (τ_s) and spectrum handoff (τ_h) intervals. As licensed user communication is detected, accessed channel is vacated and spectrum handoff is performed. For smart grid environment, licensed user activity can be perceived as wireless channel conditions that restricts communication of sensor nodes. TFRC [41] is used as transport protocol in the simulation experiment, and packet size is limited to 100 bytes. 10 channels are created for each power grid spectrum environment, e.g., 500kV substation, main power room and underground network transformer vault, given in Table 3.2.

In Fig. 7.2 (a) and (b), to gain more insight regarding the challenges of reliable transport in SCSN, comparative performance evaluations in terms of packet delivery rate and average packet receiving interval are presented, respectively. Increase in the spectrum sensing duration caused a downswing in the packet delivery performance about 30% for each environment. Moreover, with the increasing P_{ON} packet delivery performance decays. Average packet receiving interval increases four times with increasing licensed user activity. Extended simulations and their detailed discussions for delay-sensitive and multimedia communications can be found in [24].

7.5 Energy Harvesting in SCSN

While communicating sensor node's power consumption is on the order of a few milliwatts, it reduces to a few microwatts in sleeping periods. In addition to transmission distance, power consumption of SCSN nodes alter based on the spectrum conditions and different factors, such as employed frequency band, environmental noise, licensed user interference limitations, and spectrum sharing policies with other unlicensed networks. Since battery maintenance and wiring for densely deployed sensor network in smart grid is not a feasible solution, extending battery lifetime is a significant challenge. Meanwhile, mains power might be available in

Table 7.2: Summary of Existing Energy Harvesting Techniques for SCSN

Energy Harvesting Technique	***Effect***	**Energy *Source***
Magnetic Induction	Electromagnetic	Current passing lines
Modulated Backscattering	Wave backscattering	RF source
Piezoelectric	Piezoelectric materials	Vibrations
Pyroelectric	Pyroelectric materials	Heat
Thermoelectric	Seebeck effect	Heat
Solar	Photovoltaic effect	Sun
Electrostatic	Mechanical	Vibrations

some of the WSN-based smart grid applications, such as in residential energy management. However, sensor nodes, which are deployed in a high voltage smart grid environments, will still need appropriate power sources. Recently, a few energy harvesting techniques have been introduced [79]. Energy harvesting can enhance the performance of the SCSN with the self-charging, i.e., self-healing, capability. Unattended energy in the environment, such as, solar, mechanical, thermal, and magnetic, can be scavenged to energize sensor nodes. Possible energy harvesting techniques for SCSN are summarized in Table 7.2, and explained below:

- ***Magnetic induction*:** Generated magnetic field by the AC current carrying power lines can be used to induce electric current, and hence, power for sensor nodes. Sensors nearby power lines can benefit from magnetic flux linkage opportunity, and harvested energy can be used for battery recharging purposes.

- ***Modulated backscattering*:** Recently, modulated backscattering is proposed for sensor networks, in which radiated wave is backscattered by source node, and modulated accordingly [7]. With modulated backscattering, only receiver node is required to consume power, since source node only modulates the received signal. If receiver node has battery charging opportunity, such as a node that has energy harvesting opportunity and capability by magnetic induction, network lifetime can be greatly extended by the employment of modulated backscattering at source node.

- ***Other energy harvesting opportunities*:** Apart from magnetic induction and modulated backscattering, there exists piezoelectric, pyroelectric, thermoelectric, solar, and elec-

trostatic energy harvesting techniques that can also be employed in SCSN for smart grid. While solar harvesting techniques can only applicable to sensors placed on outdoor equipment, pyroelectric and thermoelectric are applicable to sensors placed on both outdoor and indoor equipments. Piezoelectric and electrostatic harvesting techniques exploit mechanical strain deformation and vibration motion to acquire electrical energy, respectively.

CHAPTER 8

SPECTRUM-AWARE UNDERWATER NETWORKS: COGNITIVE ACOUSTIC COMMUNICATIONS

In this chapter, Spectrum-aware Underwater Networks (SUN) to address harsh underwater acoustic spectrum conditions. The objective of this work is to reveal achievable capacity gains via cognitive acoustic communications. SUN was first presented in [26]. In Section 8.2, we define underlying underwater communication channel model. Then, we investigate spectrum scarcity in SUN via inspecting the relationship between capacity and frequency for different bandwidths in Section 8.3. Afterwards, we move to analysis of capacity gain in SUN for DSA and OSA separately, in Section 8.4 and Section 8.5, respectively, with respect to various depth, distance, shipping and wind speed values.

8.1 Motivation

Frequency dependent severe path loss and noise confine underwater acoustic communications (UAC) to frequencies below a few hundred kHz [36, 94]. Thus, UAC capacity is inherently limited by scarce underwater acoustic spectrum. Underwater acoustic spectrum exhibits spatiotemporally varying characteristic, e.g., path loss may change based on depth and season of the year while noise can be further amplified by human activities and waves. Moreover, sharing available scarce acoustic spectrum with other existing UAC systems, such as autonomous underwater vehicles (AUV), underwater fleet and underwater acoustic sensor networks (UASN) deployed for underwater exploration tasks, can further decrease limited communication capacity. Nearby active sonars as well pose a significant challenge for UAC. Especially, frequencies used by low frequency ultrasonic sonars fall in the range of frequen-

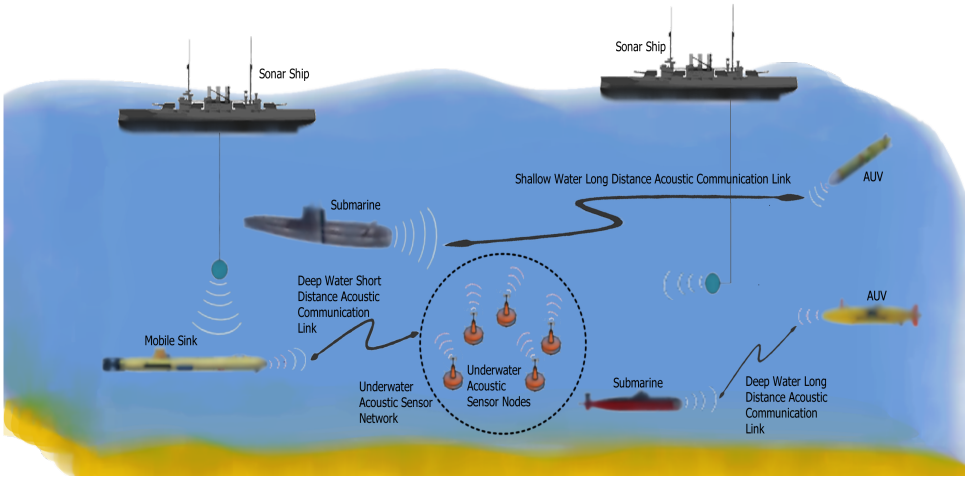

Figure 8.1: Example UAC system consisting of sonar ships, AUVs, submarines, UASN, and a mobile sink.

cies that are used for underwater communications, and this can cause interference to UAC systems. This highly challenging and unique characteristics of underwater acoustic spectrum points out the need for spectrum-aware communications in underwater networks.

Cognitive radio (CR) is an emerging technology to overcome spectrum scarcity by enabling unlicensed users to access licensed bands via dynamic and opportunistic spectrum access (DSA and OSA) and improve overall spectrum utilization in terrestrial wireless communications [10]. Similarly, UAC networks can exploit cognitive acoustic communications (CAC). UAC capacity can be increased, and spectrum scarcity can be mitigated via DSA and OSA, i.e., dynamic spectrum sharing. CAC can be employed to overcome effects of spatiotemporally changing path loss and noise on underwater acoustic channel capacity. Furthermore, capacity limitation due to interference caused by co-existing low frequency ultrasonic sonars and existing other UAC systems can be mitigated as well. CAC unifies DSA and OSA to empower spectrum-aware acoustic communications in underwater networks. A UAC network with CAC capability can benefit from the following potential advantages:

- **DSA** can help to alleviate extreme path loss and noise via tuning to suitable unused frequency band in the spectrum. Nodes can tune higher capacity spectrum bands and adapt spatiotemporally changing characteristics to achieve enough capacity. Active UAC systems, and noise sources, such as shipping, waves, and low frequency ultrasonic sonars, can be detected via sensing of underwater acoustic spectrum, i.e., *spectrum*

sensing, and decision for appropriate band to be tuned in can be taken, i.e., *spectrum decision*. Then, nodes can adapt their hydrophones to selected band, i.e., *spectrum handoff*. This operational sequence is called *cognitive cycle* [10], and it is inherited from CR to increase achievable capacity in UAC networks.

- **OSA** enables UAC network nodes to benefit from instantaneous communication opportunities in underwater acoustic spectrum. OSA capable nodes can identify suitable portions of the underwater acoustic spectrum for communication and capture their vacant periods via *spectrum sensing*. Then, nodes can adapt their transmission schedule to minimize effects of noise sources and path loss on communication capacity and not to interfere with existing other UAC systems and active sonars. Especially, mobile underwater nodes such as AUV can benefit from OSA to adapt spatiotemporally varying spectrum characteristics.

These advantages of CAC lead to a new networking paradigm, *Spectrum-aware Underwater Networks* (SUN). SUN can access any portion of the spectrum and adjust its transmission schedule via CAC to ease effects of spatiotemporally varying path loss, noise, co-existing UAC systems, and ultrasonic sonars. In order to illustrate mixture of different UAC systems, an arbitrary topology is presented in Fig. 8.1. While UASN is deployed for acquiring samples from ocean, submarines and AUVs travel around in the communication range, and a nearby ship runs its sonar as well.

Recently, some research efforts have been presented in literature to adopt cognitive radio oriented approaches to UAC networks. Channel allocation methods are proposed to improve achieved capacity in the UAC network and provide fairness between users [19, 18]. Techniques for bandwidth management in underwater networks are also investigated from a cognitive radio approach [96]. Learning from experiential interactions and tuning communication algorithms accordingly is addressed to overcome obstacles of underwater spectrum [114]. An algorithm for acoustic channel parameter estimation and mapping is developed based on concept of cognitive radio [5]. Incorporating spectrum sensing facility of cognitive radio networks, distributed spectrum coordination protocol is designed for channel allocation in one hop UAC networks [98]. Furthermore, applications of software-defined radio technology for UAC are discussed in [60]. On the other hand, development efforts for software-defined underwater acoustic modem are presented in [81, 61, 68]. However, although these software-

based solutions ease reconfiguration of physical layer parameters, they do not aim to provide dynamic and autonomous adaptation of communication parameters, i.e., these software-based solutions are not specifically designed to enable DSA and OSA, in UAC.

In this chapter, we propose SUN, which is empowered with CAC inspired from wireless spectrum sharing via cognitive radio in terrestrial communications. First, we investigate the limited and heterogeneous spectrum problem in UAC. Then, we explore and give a clear understanding of the achievable capacity gain in SUN with respect to non-CAC underwater networks. Effects of spectrum management and accessibility delay, i.e., spectrum sensing, decision, coordination and opportunity duration, on communication capacity are investigated under extremely challenging channel conditions of SUN. Relation between the capacity gain and the accessed portion of the spectrum is pointed out for both DSA and OSA schemes, separately.

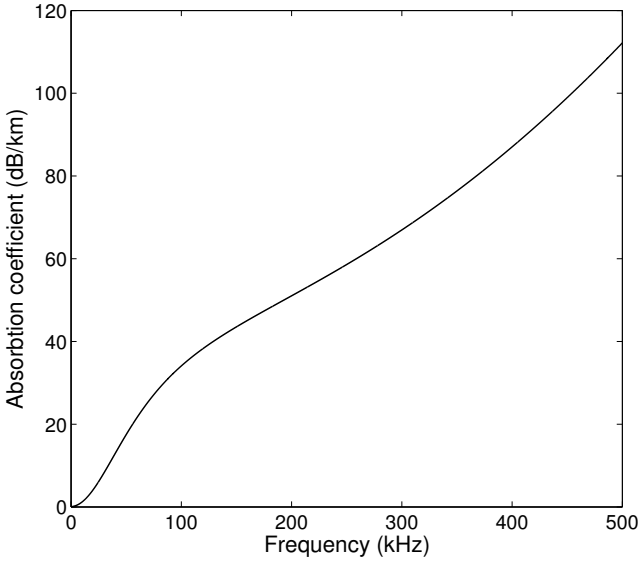

Figure 8.2: Variation of absorption coefficient with respect to frequency.

8.2 Underwater Acoustic Communication Channel Model

SUN nodes can tune their transmission parameters via CAC capability without replacing any hardware. If the noise is Gaussian and channel is time-invariant for some duration, then the

channel response function is found to be flat. Therefore, noise $N(f_i)$ can be approximated for a narrow bandwidth Δf centered at f_i as white. Then, capacity $C(d)$ in bps can be obtained as

$$C(d) = \sum_i \Delta f \cdot \log_2 \left[\frac{S(f_i, d)}{PL(f_i, d) \cdot N(f_i)} \right] \tag{8.1}$$

where $S(f, d)$ is power spectral density (p.s.d.) of the transmitted acoustic signal in W/Hz, and $PL(f, d)$ is path loss in dB. $PL(f, d)$ for acoustic signals in underwater environments is obtained by Urick propagation model [101]

$$PL(f, d) = k \cdot 10 \log_{10}(d) + \frac{d}{1000} \cdot \alpha(f) \tag{8.2}$$

where k is the geometric spreading factor, f is frequency in kHz, d is distance in meters, and α is the absorption coefficient in dB/km. k is taken as 1 for shallow underwater communications due to its cylindrical (horizontal) spreading property and 2 for deep underwater communications due to its spherical (omni-directional) spreading property [36]. Calculation of $\alpha(f)$ is given in [101]. $\alpha(f)$ is plotted versus frequency in Fig. 8.2. Especially after 100 kHz, $\alpha(f)$ increases sharply and confines UAC spectrum to a few hundred kHz. In evaluations, transmission power is set to 250 $\mathrm{dB}_{re\ \mu Pa}$/Hz. Depth is assumed 10 m for shallow water and 1000 m for deep water.

Noise in underwater acoustic channel is separated into four sources, namely, turbulence (n_t), human activity (shipping) (n_s), wind (waves) (n_w), and thermal noise (n_{th}). These four noise components are formulated in $\mathrm{dB}_{re\ \mu Pa}$/Hz incorporating effect of shipping activity factor (s) that varies between 0 and 1, and wind speed (w) in m/s [34].

8.3 Spectrum Scarcity in Underwater Acoustic Communications

Here, we investigate and elaborate spectrum confinement in UAC. In Fig. 8.2, absorption coefficient $\alpha(f)$ is plotted with respect to carrier frequency f_0. As the carrier frequency increases, $\alpha(f)$ increases enormously. Since, path loss is proportional to loss due to medium absorption determined by $\alpha(f)$, sharp increase in $\alpha(f)$ makes communication over a few hundred kHz hard to realize as a result of excessive path loss. Additionally, ambient noise for underwater communications rely upon frequency and environmental factors, i.e., shipping and wind. Ambient noise has a p.s.d. that resembles a V shaped curve that reaches its minimum value around a few tens of kHz based on shipping and wind factors [94]. When ambient

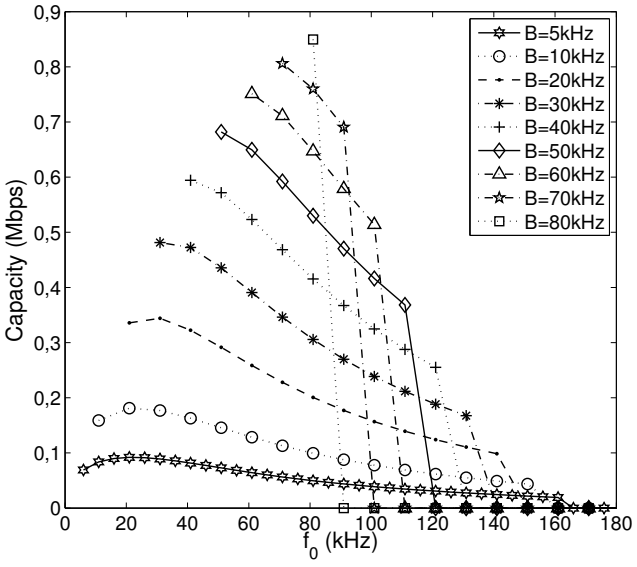

Figure 8.3: Variation of capacity with respect to center frequency for $d = 5$ km, $s = 1$, and $w = 10$ m/s.

noise is combined with the extreme absorption loss proportional to distance and frequency, underwater acoustic nodes are confined to operate with a f_0 below a few hundred kHz.

In Fig. 8.3, capacity with respect to f_0 is presented for different bandwidths, and distance is taken to be 5 km, shipping factor s is set 1, and wind speed w is assumed to be 10 m/s. From viewpoint of a basic application, frequencies above 180 kHz become infeasible for UAC. Furthermore, due to increasing path loss with f_0, capacity decreases dramatically with increasing f_0 for same bandwidth. For example, from $f_0 = 50$ kHz to 110 kHz, one third of the capacity diminishes for $B = 20$ kHz, while for $B = 50$ kHz, one half of the capacity diminishes in the same f_0 range. Therefore, nodes that are operating at higher f_0 than others, i.e. if they are closer to higher end of available spectrum, are likely to suffer from fixed channel allocation scheme due to capacity variation illustrated in Fig. 8.3.

Heterogeneity in underwater acoustic spectrum points out necessity of spectrum awareness, and hence, it is promising to adopt DSA and OSA approaches for cognitive radio oriented UAC. SUN nodes must have the capability of CAC, i.e., sharing acoustic spectrum adaptively via tuning their acoustic transducers to dynamically changing environment based on application needs, such as UASN event reporting, AUV coordination, inter-submarine video conferencing, and distributed sonar imaging. Hence, SUN is essential to improve commu-

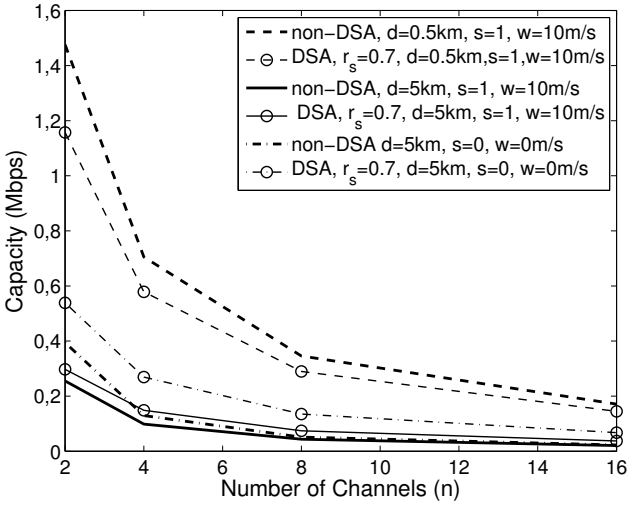

Figure 8.4: Capacity of DSA-enabled SUN with respect to number of channels in deep water (1 km).

nication capacity via CAC. In the following sections, we investigate and detail performance of DSA and OSA with respect to various environmental conditions, spectrum management delay and spectrum accessibility duration in SUN.

8.4 Dynamic Spectrum Access for Underwater Acoustic Networks

In this section, we analyze the effect of DSA on communication capacity in SUN. 0-160 kHz band is divided to C equal bandwidth channels, e.g., there are 8 channels with 20 kHz bandwidth for $n = 8$. Duration spent for spectrum management functionalities, i.e., spectrum management delay, is expressed by τ_s. In order to analyze effect of different τ_s values, we alter instantaneous throughput r_s, i.e., ratio of the communication duration (τ_c) to total spent duration including spectrum management delay ($\tau_c + \tau_s$), which equals to $r_s = \tau_c/(\tau_c + \tau_s)$.

DSA scheme is compared with the capacity of fixed spectrum assignment at the highest available f_0 with same B, e.g., fixed access to $140 - 160$ kHz band for $n = 8$. For DSA scheme, nodes sequentially change their f_0 and access each channel in the spectrum with equal probability. Here we calculate achieved capacity for DSA scheme via multiplying average capacity of these heterogeneous n channels with instantaneous throughput r_s. In Fig. 8.4 and 8.5, comparison of achievable capacities via non-DSA and DSA schemes with equal and

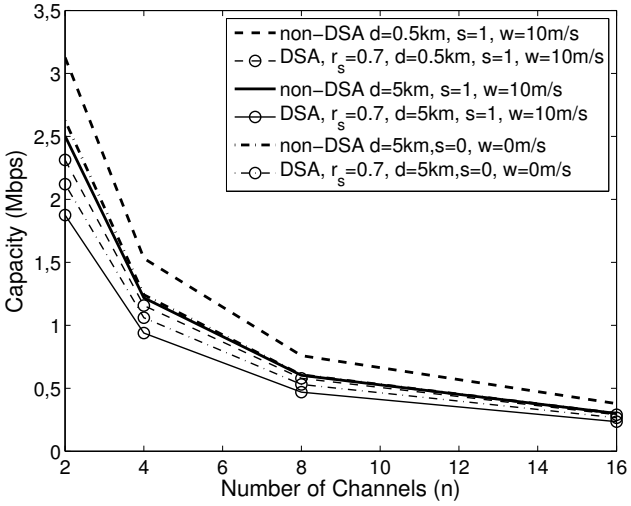

Figure 8.5: Capacity of DSA-enabled SUN with respect to number of channels in shallow water (0.01 km).

non-equal channel access probabilities are presented for different depth, d, s, w, n, and r_s values.

8.4.1 Deep Water

Simulation results for deep water environment are presented in Fig. 8.4. DSA provides access to lower f_0 channels with same B. For 5 km distance, achievable capacity for $r_s = 0.7$ stays above the one for non-DSA scheme, while capacity of non-DSA scheme reaches higher value than the one for $r_s = 0.7$ when communication range is decreased from 5 km to 0.5 km. The effect of spectrum management delay becomes dominant as the communication range decreases, thus, communication capacity gain decreases for lower r_s. For $d = 5$ km, $s = 0$ and no wind ($w = 0$), non-DSA scheme stays behind of DSA scheme in Fig. 8.4. Furthermore, non-DSA scheme for that environmental setting achieves less capacity than DSA scheme for $d = 5$ km, $s = 1$, and $w = 10$ m/s case. Although, noise due to shipping and wind, DSA scheme performs better than non-DSA scheme with no shipping and wind. Capacity gain provided by DSA is smaller for $d = 5$ km, $s = 1$, and $w = 10$ m/s case with respect to the one for $d = 5$ km, $s = 0$, and $w = 0$ m/s case, hence, s and w affect capacity gain via DSA adversely.

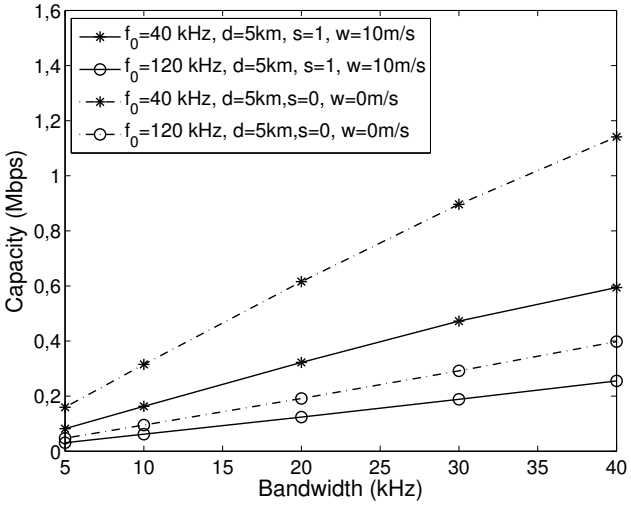

Figure 8.6: Capacity of OSA-enabled SUN with respect to bandwidth in deep water (1 km).

In SUN, accessed spectrum channels can be dynamically altered based on communication range to increase capacity, since noise is not the same for each spectrum band. Therefore, communication capacity gain can be achieved via accessing better conditioned spectrum bands dynamically in underwater acoustic spectrum. Furthermore, dividing spectrum into higher number of channels (n) is also depicted in Fig. 8.4. Increasing number of channels causes degradation of B per channel. However, higher number of channels allow to operate higher number of communication systems concurrently. Therefore, underwater acoustic spectrum must be fine grained to allow different underwater acoustic systems with heterogeneous capacity requirements.

8.4.2 Shallow Water

In Fig. 8.5, performance of DSA scheme with $r_s = 0.3$ is given for different distances, s, and w values in shallow water. As in deep water case, capacity monotonically decreases while spectrum is further divided into smaller channels. Although, achieved capacity is higher than deep water case at overall, for $r_s = 0.7$ DSA does not provide capacity gain in shallow water, i.e., a higher r_s value is required to achieve capacity increase. For $r_s = 0.7$, DSA schemes stay behind of non-DSA scheme in each environment setting. This reveals the fact that capacity gain via CAC reduces with decreasing depth as well as decreasing distance for the same value

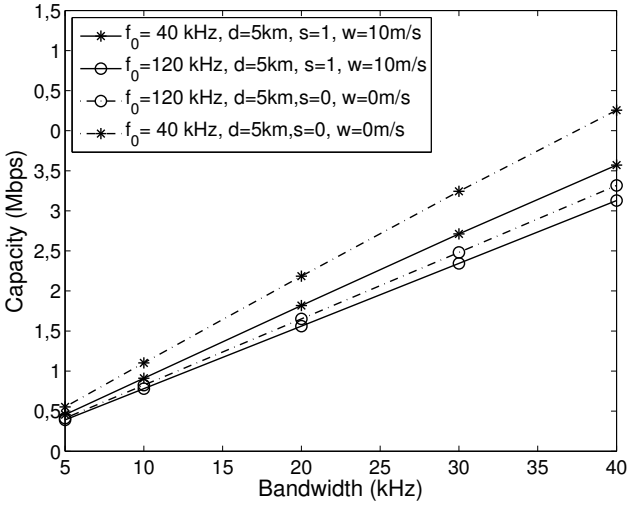

Figure 8.7: Capacity of OSA-enabled SUN with respect to bandwidth in shallow water (0.01 km).

of r_s.

In shallow water, communication capacity exhibits less variation with respect to altering distance, shipping, and wind than in deep water. However, obtained gain via CAC is lower with respect to deep water case. When compared with deep water case, a higher r_s value is needed to benefit from CAC and reach higher capacity values in shallow water.

8.5 Opportunistic Spectrum Access For Underwater Acoustic Networks

CAC is formed by unification of OSA and DSA. Apart from DSA, OSA can provide access to higher capacity portions of underwater acoustic spectrum in an opportunistic manner such that effects of spatiotemporally varying noise and path loss on communication are minimized. Here, we analyze the relation between bandwidth, center frequency, and underwater communication parameters, i.e., distance, shipping, and wind. For OSA, spectrum accessibility ratio r_a is defined as the probability of having access to that channel at any time during communication. r_a is taken as $1/2$ for accessed channels in evaluations.

8.5.1 Deep Water

In Fig. 8.6, capacity available to OSA users increases linearly as the opportunistically accessed bandwidth increases. For $d = 5$ km regardless of shipping activity and wind, achieved capacity is favourable for $f_0 = 40$ kHz case against $f_0 = 120$ kHz case. This result points out the fact that achieved capacity in OSA is higher while accessing lower f_0 channels than higher f_0 channels with same bandwidth. Nodes operating at higher f_0 portions of the spectrum can be moved opportunistically to increase communication capacity. While moving from $f_0 = 120$ kHz channels to $f_0 = 40$ kHz channels with same bandwidth, achieved capacity increases at 5 km distance for $s = 0$ and $w = 0$ m/s case is higher when compared to $s = 1$ and $w = 10$ m/s case.

Adverse effects of frequency dependent noise and path loss on communication capacity can be mitigated via opportunistically accessing the higher capacity portions of acoustic spectrum. Limitations on capacity due to small r_a can be mitigated as well via dynamically moving to higher capacity portions of the spectrum, i.e., lower f_0 channels of spectrum. Small r_a cases with lower f_0 can achieve higher capacity levels than higher r_a cases with higher f_0 for same B, due to acute path loss and ambient noise proportional to frequency.

8.5.2 Shallow Water

Achieved capacity evaluation regarding to shallow water are presented in Fig. 8.7. In shallow water, achieved capacity via OSA for different settings becomes closer with respect to deep water case. Since path loss decreases compared to deep water, received signal power for same distance is higher for shallow water. Therefore, communication capacity becomes less vulnerable to noise for the same frequency range, i.e., f_0 and B, in shallow water compared to deep water case. For example, only a small difference in achievable capacities via OSA is observed for $f_0 = 120$ kHz with the removal of shipping and wind when $d = 5$ km. However, when achieved capacity difference between $f_0 = 40$ and $f_0 = 120$ kHz is considered, it is greater for $d = 5$ km, $s = 0$, and $w = 0$ m/s than the one for $d = 5$ km, $s = 1$, and $w = 10$ m/s although the significant path loss decrease in the later one. This result reveals once again the importance of the accessed spectrum band in accordance with the environmental settings in SUN.

In shallow water, increasing bandwidth results in increased achieved capacity for same f_0, while it decreases if f_0 is increased for same B. Capacity difference between low and high f_0 is smaller compared to deep water case, and this difference grows as the bandwidth of the channel increases. This relatively small variation in capacity provides flexibility in f_0 selection while accessing with same bandwidth and r_a.

CHAPTER 9

CONCLUSIONS AND FUTURE RESEARCH DIRECTIONS

In this thesis, design and analysis of communication techniques are performed to enable reliable and energy-efficient distributed sensing in cognitive radio sensor networks (CRSN). The following six areas have been investigated under this research and each of them is described in the following subsections:

1. Reliability and Congestion Control in Cognitive Radio Sensor Networks

2. Delay-sensitive and Multimedia Communication in Cognitive Radio Sensor Networks

3. Spectrum-aware and Energy-adaptive Reliable Transport in Cognitive Radio Sensor Networks

4. Adaptive Spectrum Sharing in Distributed Sensing with Cognitive Radio Sensor Networks

5. Dedicated Radio Utilization for Spectrum Handoff and Efficiency in Cognitive Radio Networks

6. Spectrum-aware and Cognitive Sensor Networks for Smart Grid Applications

7. Spectrum-aware Underwater Networks: Cognitive Acoustic Communications

9.1 Research Contributions

9.1.1 Reliability and Congestion Control in Cognitive Radio Sensor Networks

CRSN challenges for reliable data delivery are explored, and it is shown by simulation experiments that the existing transport layer protocols for WSN and cognitive radio ad hoc networks are not suitable for CRSN in Chapter 2. Furthermore, open research issues for CRSN transport layer are stated. Clearly, there is a need for energy-efficient novel rate control, error recovery and congestion avoidance mechanisms which take challenges of CRSN into account. New CRSN transport protocols must consider communication impairments due to spectrum sensing and mobility such as excessive delays and packet losses incurred by cognitive cycle. Due to strict coupling of DSA challenges and transport layer, cross-layer paradigm seems promising in order to address CRSN challenges.

9.1.2 Delay-sensitive and Multimedia Communication in Cognitive Radio Sensor Networks

CRSN challenges for multimedia and delay-sensitive data transport are explored, and emerging challenges are shown by simulation experiments in different spectrum environments in Chapter 3. Furthermore, open research issues for the realization of energy-efficient and real-time transport in CRSN are presented. Clearly, there is a need for energy-efficient and delay-sensitive rate control mechanisms which take unique challenges of real-time communication in CRSN into account. In this regard, novel CRSN transport protocols for multimedia and delay-sensitive applications must consider communication impairments due to spectrum sensing and mobility, such as excessive delays and packet losses incurred by cognitive cycle. Overall, the performance evaluations provide valuable insights about real-time transport in CRSN and guide design decisions and tradeoffs for CRSN applications in smart electric power grid. Future work includes development of adaptive and spectrum-aware transport layer solutions and investigating the impact of different heterogeneous resources, such as transmission power, network bandwidth and processing power, on overall network performance and optimal placement of these resources in the network.

9.1.3 Spectrum-aware and Energy-adaptive Reliable Event Transport in Cognitive Radio Sensor Networks

To address emerging challenges with the incorporation of cognitive radio capability into the sensor network, Spectrum-aware and Energy-adaptive Reliable Transport (SERT) protocol is presented for CRSN in Chapter 4. SERT dynamically adjusts its parameters to match heterogeneous spectrum conditions of CRSN and performs energy-adaptive source node selection under an opportunistically available spectrum. In this respect, SERT jointly addresses reliable and energy-efficient event transport objectives in CRSN via tuning itself to adapt to the heterogeneous licensed spectrum and providing the required reliability level through the devised network life-time. To the best of our knowledge, this is the first research effort focusing on event transport for heterogeneous and opportunistically available spectrum environments of CRSN. Performance evaluations show that SERT provides high performance in terms of reliability and selection of source nodes.

9.1.4 Adaptive Spectrum Sharing in Distributed Sensing with Cognitive Radio Sensor and Actor Nodes

Minimized spectrum access and reaching consensus with cognitive radio and actor nodes is discussed in Chapter 5. Furthermore, spectrum hole assignment for reliable estimation (SHARE) scheme is proposed to enable consensus convergence of actor nodes with minimum spectrum access in local estimation by sensor nodes. Effects of licensed user in terms of both interruption and interference are modelled, and implications on design and performance are highlighted. SHARE is shown to be satisfying consensus convergence requirements especially in dense licensed user activity and high interference scenarios.

9.1.5 Dedicated Radio Utilization for Spectrum Handoff and Efficiency in Cognitive Radio Networks

The effects of employing a dedicated radio for spectrum coordination, i.e. common control interface (CCI), in cognitive radio networks (CRN) are analyzed in Chapter 6. Firstly, we built an analytical framework to characterize the time elapsed until a frame is successfully transmitted (namely successful frame transmission duration), both with and without CCI.

We extended our work also to cover the effects of CCI employment on energy efficiency and spectrum utilization. In numerical results, considering a simple random ad hoc network setting, guidelines regarding the employment of CCI were extracted. Accordingly, CCI is mostly beneficial when i) frame duration is an order larger than sensing duration, ii) power consumption level in frame transmission is not small compared to that in spectrum sensing, iii) there is significant PU arrival rate in the deployment region of the CRN. CCI is also more beneficial for fading conditions than it is for non-fading conditions. Since CCI would be costly to implement, additional detailed analyses can be made with the proposed framework prior to network design.

9.1.6 Spectrum-aware and Cognitive Sensor Networks for Smart Grid Applications

Recent field tests show that, reliable communication in smart grid is a challenging task for WSN-based smart grid applications due to electromagnetic interference, equipment noise, dynamic topology changes, and fading. Spectrum-aware and cognitive sensor networks (SCSN) is introduced to provide reliable and efficient communication for remote monitoring applications in smart grid in Chapter 7. First, SCSN-based applications explored for power generation systems, T&D networks, and consumer facilities. Then, the challenges and requirements of spectrum management functionalities, i.e., spectrum sensing, spectrum decision, spectrum sharing, and spectrum mobility, are discussed from the perspective of SCSN. The communication protocol suite is discussed from the perspective of SCSN, while putting emphasis on open research directions. A case study is presented to uncover the reliable transport performance in SCSN for various smart grid environments. Lastly, different energy harvesting techniques for SCSN-based smart grid applications are reviewed. We have provided a contemporary perspective to the current state of the art in remote monitoring and control of smart grid via SCSN.

9.1.7 Spectrum-aware Underwater Networks: Cognitive Acoustic Communications

Cognitive acoustic communications (CAC) to empower spectrum-aware underwater networks (SUN) inspiring from cognitive radio paradigm in wireless terrestrial communications is proposed in Chapter 8. Spectrum scarcity in UAC due to the uniquely challenging underwater acoustic spectrum is discussed, and the need for spectrum-aware communication techniques

is pointed out. We explore the capacity gain that can be achieved via CAC in SUN by simulation experiments, and investigate advantages and limitations of SUN along with its trade-offs for DSA and OSA, separately. Clearly, SUN can reach higher capacities than traditional fixed spectrum approaches with the help of CAC capability. We aim to provide better recognition for the capabilities of SUN and actuate further research efforts to explore this favourable area.

9.2 Future Research Directions

The investigation of communication algorithms in the context of energy and spectrum efficient distributed sensing in cognitive radio sensor networks provides many research areas in various fields of cognitive radio networking.

9.2.1 Adaptive spectrum sharing for heterogeneous multi-event sensing in CRSN

Cognitive Radio Sensor Networks (CRSN) will converge a wide range of wireless monitoring and tracking applications from smart grid to public protection that exhibit challenging spectrum conditions in terms of opportunistic availability and varying bit error rate. In this thesis, the spectrum hole assignment for reliable estimation (SHARE) scheme is developed to address these heterogeneous spectrum conditions while sharing spectrum among cognitive radio sensor and actor nodes. In addition to that, it may be required to integrate multi-event sensing cognitive radio sensor and actor nodes acting on multiple events. To achieve this, SHARE mechanism must be extended to address the challenges posed by the heterogeneous distributed sensing requirements such as number of collected samples, quality, i.e., signal-to-noise ratio (SNR) of received samples, and delay-bound on estimation for each distinct event. The new solution must also be adaptive to changing spectrum conditions as well as able to address the distributed event sensing requirements.

9.2.2 Co-existence and Integration of CRSN with the Internet

The evolution in cognitive radio technology has enabled the realization of various network architectures for different applications such as infrastructure-based cognitive radio networks, cognitive radio ad hoc networks, cognitive radio mesh networks, and cognitive radio sen-

sor networks. To improve efficiency in the co-existence of these heterogeneous cognitive radio networks and provide useful information any time and anywhere, integration of these networks with the Internet is an important challenge. Co-existence of these networks will require tight integration and interoperability. Therefore, it is crucial to develop location- and spectrum-aware cross-layer communication protocols as well as heterogeneous spectrum management mechanisms for co-existence and integration of cognitive radio sensor networks with other types of cognitive radio networks and Internet.

9.2.3 Passive communications in CRSN

The main research focus for sensor networks has been on energy-efficient communication algorithm design to extend network life-time. However, when the batteries deplete, operations stop. Replacement of batteries are impractical due to random deployment and low cost requirements. To overcome this, modulated backscattering technique is a promising alternative for passive communications to mitigate limited network life-time problem in sensor networks. CRSN can utilize the potential of passive communications to address network life-time problem as well as spectrum scarcity problem. In this respect, intermittent energy and opportunistic spectrum availability should be jointly incorporated into design of communication suite with a focus on reliable event detection and reduced energy consumption.

9.2.4 Topology control and power adaptation in CRSN

Cognitive radio networks are characterized by the spatially and temporally varying spectrum opportunities. Thus, communication in cognitive radio sensor networks necessitates an adaptive topology control approach to efficiently exploit the available spectrum for distributed event sensing. This necessitates design of a power adaptation scheme for cognitive radio sensor networks that focuses on spectrum mobility and spatio-temporal correlation between the sensor observations.

REFERENCES

[1] "EvalVid - A Video Quality Evaluation Tool-set," Available: http://www.tkn.tu-berlin.de/research/evalvid.

[2] "IBM ILOG CPLEX Optimizer," Available: http://www-01.ibm.com/software/integration/optimization/cplex-optimizer/.

[3] "The Network Simulator - (ns-2)," Available: http://www.isi.edu/nsnam/ns/.

[4] "The Network Simulator, - (ns-3)," Available: http://www.nsnam.org

[5] S. Ahmed, and H. Arslan, "Cognitive Intelligence in the Mapping of Underwater Acoustic Communication Environments to Channel Models," in *MTS/IEEE OCEANS 2009,* 26-29 Oct. 2009.

[6] O. B. Akan and I. F. Akyildiz, "Event-to-Sink Reliable Transport in Wireless Sensor Networks," *IEEE/ACM Transactions on Networking,* vol. 13, pp. 1003-1016, Oct. 2005.

[7] O. B. Akan, M. T. Isik, and B. Baykal, "Wireless Passive Sensor Networks," *IEEE Commun. Mag.,* vol. 47, no. 8, pp. 92-99, Aug. 2009.

[8] O. B. Akan, O. B. Karli, and O. Ergul, "Cognitive Radio Sensor Networks," *IEEE Network,* vol. 23, no.4, pp. 34-40, July-August 2009.

[9] I. F. Akyildiz, W. Y. Lee, and K. Chowdhury, "Spectrum Management in Cognitive Radio Ad Hoc Networks," *IEEE Network,* July-August 2009.

[10] I. F. Akyildiz, W. Y. Lee, M. C. Vuran, and S. Mohanty, "NeXt Generation/Dynamic Spectrum Access/Cognitive Radio Wireless Networks: A Survey," *Computer Networks Journal (Elsevier),* vol. 50, no. 13, pp. 2127-2159, Sept. 2006.

[11] I.F. Akyildiz, B. F. Lo, and R. Balakrishnan, "Cooperative Spectrum Sensing in Cognitive Radio Networks: A Survey," *Elsevier Physical Communication,* vol. 4, no. 1, pp. 40-62, March 2011.

[12] I. F. Akyildiz, T. Melodia, and K. R. Chowdhury, "A survey on wireless multimedia sensor networks," *Computer Networks Journal (Elsevier),* vol. 51, no. 4, pp. 921-960, Mar. 2007.

[13] I. F. Akyildiz, W. Su, Y. Sankarasubramaniam, and E. Cayirci, "A survey on Sensor Networks," *IEEE Communications Magazine,* vol. 40, no. 8, pp. 102-114, Aug. 2002.

[14] I. F. Akyildiz, and I. H. Kasimoglu, "Wireless sensor and actor networks: research challenges," *Ad Hoc Networks (Elsevier),* vol .2, no. 4, pp. 351-367, Oct. 2004.

[15] I. F. Akyildiz, W. Y. Lee, and K. Chowdhury, "CRAHNs: Cognitive Radio Ad Hoc Networks," *Ad Hoc Networks Journal (Elsevier),* vol. 7, no. 5, pp. 810-836, Jul. 2009.

[16] S. M. Amin and B. F. Wollenberg, "Toward a Smart Grid," *IEEE Power and Energy Mag.,* vol. 3, no. 5, pp. 34-41, Sep./Oct. 2005.

[17] N. Baldo, A. Asterjadhi, and M. Zorzi, "Dynamic Spectrum Access Using a Network Coded Cognitive Control Channel," *IEEE Transactions on Wireless Communications,* vol. 9, no. 8, pp. 2575-2587, 2010.

[18] N. Baldo, P. Casari, P. Casciaro, and M. Zorzi, "Effective Heuristics for Flexible Spectrum Access in Underwater Acoustic Networks," in *Proc. MTS/IEEE OCEANS 2008,* 15-18 Sept. 2008.

[19] N. Baldo, P. Casari, and M. Zorzi, "Cognitive Spectrum Access for Underwater Acoustic Communications," in *Proc. IEEE ICC Workshops 2008,* pp. 518-523, 19-23 May 2008.

[20] A. O. Bicen, and O. B. Akan, "Reliability and Congestion Control in Cognitive Radio Sensor Networks," *Elsevier Ad Hoc Networks,* vol. 9, no. 7, pp. 1154-1164, Sept. 2011.

[21] A. O. Bicen, and O. B. Akan, "Spectrum-aware and Energy-adaptive Reliable Transport in Cognitive Radio Sensor Networks," *submitted to IEEE Transactions on Wireless Communications,* 2012.

[22] A. O. Bicen, and O. B. Akan, "Adaptive Spectrum Sharing in Distributed Sensing with Cognitive Radio Sensor and Actor Nodes," *submitted to IEEE Journal of Selected Topics in Signal Processing,* 2012.

[23] A. O. Bicen, V. C. Gungor, and O. B. Akan, "Spectrum-aware and Cognitive Sensor Networks for Smart Grid Applications," *IEEE Communications Magazine,* vol. 50, no. 5, pp. 158-165, May 2012.

[24] A. O. Bicen, V. C. Gungor, and O. B. Akan, "Delay-sensitive and Multimedia Communication in Cognitive Radio Sensor Networks," *Elsevier Ad Hoc Networks,* vol. 10, no. 5, pp. 816-830, July 2012.

[25] A. O. Bicen, E. B. Pehlivanoglu, S. Galmes, and O. B. Akan, "Dedicated Radio Utilization for Spectrum Handoff and Efficiency in Cognitive Radio Networks," *submitted to IEEE Transactions on Wireless Communications,* 2012.

[26] A. O. Bicen, A. B. Sahin, and O. B. Akan, "Spectrum-aware Underwater Networks: Cognitive Acoustic Communications," *IEEE Vehicular Technology Magazine,* vol. 7, no. 2, pp. 34-40, June 2012.

[27] A. Bose, "Smart Transmission Grid Applications and Their Supporting Infrastructure," *IEEE Transactions on Smart Grid,* vol. 1, no. 1, pp. 11-19, June 2010.

[28] M. Chen and A. Zakhor, "Rate Control for Streaming Video over Wireless," in *Proc. INFOCOM 2004,* Hongkong, China, Mar. 2004.

[29] Y. Chen, Q. Zhao, and A. Swami, "Joint Design and Separation Principle for Opportunistic Spectrum Access," in *Proc. IEEE Asilomar Conference on Signals, Systems and Computers 2006,* Oct. 2006.

[30] C. Chou, S. Shankar, H. Kim, and K. G. Shin, "What and How much to Gain by Spectrum Agility?", *IEEE JSAC,* vol. 25, no. 3, pp. 576-588, Apr. 2007.

[31] K. R. Chowdhury, I. F. Akyildiz, Cognitive Wireless Mesh Networks with Dynamic Spectrum Access, IEEE Journal on Selected Areas in Communications (JSAC), vol. 26, no. 1, pp. 168-181, Jan. 2008.

[32] K. R. Chowdhury, and I. F. Akyildiz, "OFDM-based Common Control Channel Design for Cognitive Radio Ad Hoc Networks," *IEEE Transactions on Mobile Computing,* vol. 10, no. 2, pp. 228-238, 2011.

[33] K. R. Chowdhury, M. Di Felice, and I. F. Akyildiz, "TP-CRAHN: A Transport Protocol for Cognitive Radio Ad-Hoc Networks," in *Proc. IEEE INFOCOM,* Apr. 2009.

[34] R. Coates, *Underwater Acoustic Systems.* Wiley, 1989.

[35] D. R. Cox, "Renewal Theory." NY: John Wiley & Sons Inc, 1962.

[36] M. C. Domingo, "Overview of channel models for underwater wireless communication networks," *Elsevier Physical Communication,* vol. 1, no. 3, pp. 163-182, Sept. 2008.

[37] M. Erol-Kantarci, H. T. Mouftah, "Wireless Multimedia Sensor and Actor Networks for the Next-Generation Power Grid," *Elsevier Ad Hoc Networks*, vol. 9, no. 4, pp. 542-551, June 2011.

[38] M. Di Felice, K. R. Chowdhury, W. Kim, A. Kassler, and L. Bononi, "End-to-end protocols for Cognitive Radio Ad Hoc Networks: An evaluation study," *Performance Evaluation Journal (Elsevier),* 2010.

[39] H. Farhangi, "The Path of the Smart Grid," *IEEE Power and Energy Mag.,* vol. 8, no. 1, pp. 18-28, Jan.-Feb. 2010.

[40] S. Floyd, and K. Fall, "Promoting the Use of End-to-End Congestion Control in the Internet," *IEEE/ACM Transactions on Networking,* vol. 7, no. 4, pp. 458-472, Aug. 1999.

[41] S. Floyd, M. Handley, J. Padhye, and J. Widmer, "Equation-based Congestion control for unicast applications," in *Proc. ACM SIGCOMM 2000,* pp. 45-58, Aug. 2000.

[42] S. Floyd, M. Handley, J. Padhye, and J. Widmer, "TCP Friendly Rate Control (TFRC): Protocol Specification," in *IETF RFC 5348*, Sept. 2008.

[43] C. Gao, Y. Shi, Y. T. Hou, and S. Kompella, "On the Throughput of MIMO-Empowered Multihop Cognitive Radio Networks," *IEEE Transactions on Mobile Computing,* vol. 10, no. 11, pp. , Nov. 2011.

[44] P. C. Gilmore, and R. E. Gomory, "A linear programming approach to the cutting stock problem", *Operations Research,* vol. 9, no. 6, pp. 848-859, Nov. - Dec. 1961.

[45] P. C. Gilmore, and R. E. Gomory, "A linear programming approach to the cutting stock problem-Part II," *Operations Research,* vol. 11, no. 6, pp. 863-888, Nov. - Dec. 1963.

[46] A. Goldsmith, *Wireless Communications,* U.K., Cambridge Univ. Press, 2004.

[47] V. C. Gungor, O. B. Akan, and I. F. Akyildiz, "A Real-Time and Reliable Transport Protocol for Wireless Sensor and Actor Networks," *IEEE/ACM Transactions on Networking,* vol. 16, no. 2, pp. 359-370, Apr. 2008.

[48] V.C. Gungor, and F. C. Lambert, "A Survey on Communication Networks for Electric System Automation," *Computer Netwroks Journal (Elsevier),* vol. 50, pp. 877-897, May 2006.

[49] V. C. Gungor, B. Lu, G.P. Hancke, "Opportunities and Challenges of Wireless Sensor Networks in Smart Grid - A Case Study of Link Quality Assessments in Power Distribution Systems," *IEEE Transactions on Industrial Electronics,* vol. 57, no. 10, pp. 3557-3564, October 2010.

[50] M. Haenggi , "On distances in uniformly random networks," IEEE Transactions on Information Theory, vol.51, no.10, pp.3584-3586, Oct. 2005.

[51] K. Hamdi, W. Zhang, and K. B. Letaief, "Opportunistic Spectrum Sharing in Cognitive MIMO Wireless Networks," *IEEE Transactions on Wireless Commun.,* vol 8, no. 8, August 2009.

[52] J. A. Han, W. S. Jeon, and D. G. Jeong, "Energy-Efficient Channel Management Scheme for Cognitive Radio Sensor Networks," *IEEE Transactions on Vehicular Tech.,* vol. 60, no. 4, pp. 1905-1910, May 2011.

[53] C. H. Hauser, D. E. Bakken, and A. Bose, "A Failure to Communicate: Next Generation Communication Requirements, Technologies, and Architecture for the Electric Power Grid," *IEEE Power and Energy Magazine,* vol.3, no.2, pp. 47- 55, March-April 2005.

[54] S. Haykin, "Cognitive Radio: Brain-empowered Wireless Communications", *IEEE Journal on Selected Areas in Communications (JSAC)*, Vol. 23, No. 2, pp. 201-220, Feb. 2005.

[55] B. Heile, "Smart Grids for Green Communications," *IEEE Wireless Communications,* vol. 17, no. 3, pp. 4-6, June 2010.

[56] Y. T. Hou, Y. Shi, and H. D. Sherali, "Spectrum Sharing for Multi-Hop Networking with Cognitive Radios," *IEEE Journal of Selected Areas in Communications,* vol. 26, no. 1, pp. 146-155, Jan. 2008.

[57] D. Hu, S. Mao, Y. T. Hou, and J. H. Reed, "Scalable Video Multicast in Cognitive Radio Networks," *IEEE Journal on Selected Areas in Communications (JSAC),* vol. 28, no. 3, pp. 434-444, Apr. 2010.

[58] T. Issariyakul, L. S. Pillutla, V. Krishnamurthy, "Tuning radio resource in an overlay cognitive radio network for TCP: Greed isn't good," *IEEE Communications Magazine,* vol.47, no.7, pp.57-63, July 2009.

[59] D. Johnson, D. Maltz, Y. Hu, and J. Jetcheva, The Dynamic Source Routing Protocol for Mobile Ad Hoc Networks (DSR), IETF Internet draft, Feb. 2002.

[60] E. Jones, "The Application of Software Radio Techniques to Underwater Acoustic Communications," in *MTS/IEEE OCEANS 2007,* 18-21 June 2007.

[61] R. Jurdak, P. Baldi, and C. V. Lopes, "Software-driven sensor networks for short-range shallow water applications," *Elsevier Ad Hoc Networks,* vol. 7, no. 5, pp. 837-848, July 2009.

[62] R. Jurdak, A. G. Ruzelli, and G. M. P. O'Hare, "Radio Sleep Mode Optimization in Wireless Sensor Networks," *IEEE Transactions. on Mobile Computing,* vol.9, no.7, pp. 995-968, Jul. 2010.

[63] Y. R. Kondareddy, and P. Agrawal, "Synchronized MAC Protocol For Multi-hop Cognitive Radio Networks," in Proc. *IEEE ICC 2008,* 2008.

[64] Y. R. Kondareddy, and P. Agrawal, "Effect of Dynamic Spectrum Access on Transport Control Protocol Performance," in *Proc. IEEE GLOBECOM 2009,* Hawaii, USA, Dec. 2009.

[65] L. Le, and E. Hossain, "OSA-MAC: A MAC Protocol for Opportunistic spectrum access in cognitive radio networks," in Proc. *IEEE WCNC 2008,* pp. 142-1430, April 2008.

[66] W. Y. Lee, and I. F. Akyildiz, "Optimal Spectrum Sensing Framework for Cognitive Radio Networks," *IEEE Transactions on Wireless Commununications,* vol. 7, no. 10, pp. 3845-3857, 2008.

[67] R. A. Leon, V. Vittal, G. Manimaran, "Application of Sensor Network for Secure Electric Energy Infrastructure," in *IEEE Transactions on Power Delivery*, vol. 22, no, 2, pp. 1021-1028, 2007.

[68] Y. Li, and H. Huang, "The design and experiment of a software-defined acoustic modem for underwater sensor network," in *Proc. IEEE OCEANS 2010,* May 2010.

[69] X. Li, D. Wang, J. McNair, and J. Chen, "Residual Energy Aware Channel Assignment in Cognitive Radio Sensor Networks," in *Proc. IEEE WCNC 2011.,* 2011.

[70] Z. Liang, S. Feng, D. Zhao, and X. Shen, "Delay Performance Analysis for Supporting Real-Time Traffic in a Cognitive Radio Sensor Network," *IEEE Transactions on Wireless Commun.,* vol. 10, no. 1, pp. 325-335, January 2011.

[71] S. Lin, and D. J. Costello Jr., *Error Control Coding: Fundamentals and Applications. Englewood Cliffs,* NJ: Prentice-Hall, 1983.

[72] B. F. Lo, "A survey of common control channel design in cognitive radio networks," *Elsevier Physical Communication,* vol. 1, no. 4, pp. 26-39, 2011.

[73] B. F. Lo, I.F. Akyildiz, and A.M. Al-Dhelaan, "Efficient Recovery Control Channel Design in Cognitive Radio Ad Hoc Networks, *IEEE Transactions on Vehicular Tech.,* vol. 59, no. 9, pp. 4513-4526, 2010.

[74] D. Logothetis, K. S. Trivedi, and A. Puliafito, "Markov regenerative models," in *Proc. Int. Computer Performance and Dependability Symp.,* Erlangen, Germany, pp. 134-143, 1995.

[75] C. G. Lopes, and A. H. Sayed, "Diffusion Least-Mean Squares Over Adaptive Networks: Formulation and Performance Analysis," *IEEE Transactions on Signal Processing,* vol. 56, no. 7, pp. 3122-3136, July 2008.

[76] C. Luo, F. R. Yu, H. Ji, and V. C. M. Leung, Cross-Layer Design for TCP Performance Improvement in Cognitive Radio Networks, *IEEE Transactions Vehicular Technology,* vol. 59, no. 5, pp. 2485-2495, Jun. 2010.

[77] S. Maleki, A. Pandharipande, and G. Leus, "Energy-Efficient Distributed Spectrum Sensing for Cognitive Sensor Networks," *IEEE Sensors Journal,* vol. 11, no. 3, pp. 565-573, 2011.

[78] J. M. Mendel, *Lessons in Estimation Theory for Signal Processing, Communications, and Control.* Englewood Cliffs, NJ: Prentice-Hall, 1995.

[79] R. Moghe, Yi Yang, F. Lambert, and D. Divan, "A scoping study of electric and magnetic field energy harvesting for wireless sensor networks in power system applications," in *Proc. IEEE ECCE 2009,* pp. 3550-3557, Sept. 2009.

[80] K. Moslehi, and R. Kumar, "A Reliability Perspective of the Smart Grid," *IEEE Transactions on Smart Grid,* vol. 1, no. 1, pp. 57-64, June 2010.

[81] N. Nowsheen, C. Benson, and M. Frater, "A High Data-Rate, Software-Defined Underwater Acoustic Modem," in *Proc. OCEANS 2010,* 20-23 Sept. 2010.

[82] R. Oflati-Saber, J. A. Fax, and R. M. Murray, "Consensus and Cooperation in Networked Multi-Agent Systems," *Proceedings of the IEEE,* vol. 95, no. 1, pp. 215-233 Jan. 2007.

[83] M. C. Oto, and O. B. Akan, "Energy-efficient Packet Size Optimization for Cognitive Radio Networks," *IEEE Transactions on Wireless Commun.,* vol. 11, no. 4, pp. 1544-1553, April 2012.

[84] Y. Sankarasubramaniam, I. F. Akyildiz, and S. W. McLaughlin, "Energy Efficiency Based Packet Size Optimization in Wireless Sensor Networks," in *Proc. IEEE SNPA 2003,* pp. 1-8, 2003.

[85] S. Sardellitti, S. Barbarossa, and A. Swami, "Optimal Topology Control and Power Allocation for Minimum Energy Consumption in Consensus Networks," *IEEE Transactions on Signal Processing,* vol. 60, no. 1, pp. 383-399, Jan. 2012.

[86] D. Sarkar, and H. Narayan Transport Layer Protocols for Cognitive Networks, in *Proc. INFOCOM 2010,* USA, Mar. 2010.

[87] Y. Shi, Y. T. Hou, and H. Zhou, Per-node-based optimal power control for multihop cognitive radio networks, IEEE Transactions Wireless Commun., vol. 8, no. 10, pp. 5290-5299, Oct. 2009.

[88] Y. Shi, Y. T. Hou, H. Zhou, and S. F. Midkiff, "Distributed Cross-Layer Optimization for Cognitive Radio Networks," *IEEE Transactions on Vehicular Technology,* vol. 59, no. 8, pp. 4058-4069, Oct. 2010.

[89] M. K. Simon, and M. S. Alouini, *Digital Communication over Fading Channels - A Unified Approach to Performance Analysis,* 1st Ed., Wiley, 2000.

[90] A. M. R. Slingerland, P. Pawelczak, R. V. Prasad, A. Lo, and R. Hekmat, "Performance of Transport Control Protocol Over Dynamic Spectrum Access Links," in *Proc. IEEE DySPAN 2007,* Dublin, Ireland, Apr. 2007.

[91] Y. Song, and J. Xie, "Performance Analysis of Spectrum Handoff for Cognitive Radio Ad Hoc Networks without Common Control Channel under Homogeneous Primary Traffic," in Proc. *IEEE INFOCOM 2011,* April 2011.

[92] K. Sriram and W. Whitt, "Characterizing Superposition Arrival Processes in Packet Multiplexers for Voice and Data," *IEEE JSAC,* vol. 4, no. 6, pp. 833-846, Sept. 1986.

[93] F. Stan and J. Heidemann, "RMST: Reliable Data Transport in Sensor Networks," in *Proc. IEEE SNPA 2003,* pp. 102-112, May 2003.

[94] M. Stojanovic, and J. Preisig, "Underwater Acoustic Communication Channels: Propagation Models and Statistical Characterization," *IEEE Communications Magazine,* vol. 47, no. 1, pp. 84-89, Jan. 2009.

[95] H. Su, X. Zhang, "Cross-layer Based Opportunistic MAC Protocols for QoS Provisionings Over Cognitive Radio Wireless Networks," *IEEE Journal on Selected Areas in Communications,* vol. 26, no. 1, pp. 118-129, Jan. 2008.

[96] H. Tan, W. K. G. Seah, and L. Doyle, "Exploring Cognitive Techniques for Bandwidth Management in Integrated Underwater Acoustic Systems," in *Proc. IEEE OCEANS 2008 - MTS/IEEE Kobe Techno-Ocean,* Apr. 2008.

[97] W. Tan, and A. Zakhor, "Real-Time Internet Video Using Error Resilient Scalable Compression and TCP-Friendly Transport Protocol," *IEEE Transactions Multimedia,* vol. 1, no. 2, pp. 172-86, Jun. 1999.

[98] D. Torres, Z. Charbiwala, J Friedman, and M. Srivastava, "Spectrum Signaling for Cognitive Underwater Acoustic Channel Allocation," in *Proc. IEEE INFOCOM Workshops 2010,* 15-19 Mar. 2010.

[99] V. K. Tumuluru, P. Wang, D. Niyato, and W. Song, "Performance Analysis of Cognitive Radio Spectrum Access with Prioritized Traffic," *IEEE Transactions on Vehicular Tech.,* vol. 61, no. 4, pp. 1895-1906, May 2012.

[100] M. C. Vuran, O. B. Akan, and I. F. Akyildiz, "Spatio-temporal Correlation: Theory and Applications for Wireless Sensor Networks," *Comput. Netw. J.,* vol. 45, no. 3, pp. 245-261, Jun. 2004.

[101] R. J. Urick, *Principles of Underwater Sound.* McGraw-Hill, 1983.

[102] U.S. Department of Energy, "The Smart Grid: An Introduction," Washington, DC, Sep. 2008.

[103] C. Y. Wan, A. T. Campbell, and L. Krishnamurthy, "PSFQ: A Reliable Transport Protocol for Wireless Sensor Networks," in *Proc. ACM WSNA 2002,* pp. 1-11, Sept. 2002.

[104] C. Wan, S. B. Eisenman, and A.T. Campbell, "CODA: Congestion Detection and Avoidance in Sensor Networks," in *Proc. ACM Sensys,* Los Angeles, USA, Nov. 2003.

[105] C. Wang, M. Daneshmand, B. Li and K. Sohraby, "A survey of Transport Protocols for Wireless Sensor Networks," *IEEE Network,* vol. 20, no. 3, pp. 34-40, 2006.

[106] C. Wang, B. Li, K. Sohraby, M. Daneshmand, and Y. Hu, "Upstream Congestion Control in Wireless Sensor Networks Through Cross-Layer Optimization," *IEEE Journl of Selected Areas in Communications,* vol. 25, no. 4, pp. 786-795, May 2007.

[107] C. Wang, L. Wang, and F. Adachi, "Modeling and Analysis for Reactive-decision Spectrum Handoff in Cognitive Radio Networks," in Proc. *IEEE Globecom 2010,* December 2010.

[108] L. Wang, C. Wang, and C. Chang, "Modeling and Analysis for Spectrum Handoffs in Cognitive Radio Networks," *IEEE Transactions on Mobile Computing,* to appear in 2012.

[109] L. Wang, C. Wang, and K. Feng, "A Queueing-theoretical Framework for QoS-enhanced Spectrum Management in Cognitive Radio Network," *IEEE Wireless Communications,* December 2011.

[110] A. M. Wyglinski, M. Nekovee, and Y. T. Hou, "Cognitive Radio Communications and Networks: Principles and Practice," Elsevier, Amsterdam, The Netherlands, 2010.

[111] Y. Yang, F. Lambert, and D. Divan, "A Survey on Technologies for Implementing Sensor Networks for Power Delivery Systems," in *Proc. IEEE Power Engineering Society General Meeting,* 2007.

[112] X. Yin, X. Zhou, R. Huang, Y. Fang, and S. Li, "A Fairness-Aware Congestion Control Scheme in Wireless Sensor Networks," *IEEE Transactions on Vehicular Tech.,* vol. 58, no. 9, pp. 5225-5234, Nov. 2009.

[113] L. Ying-Chang, Z. Yonghong, E. Peh, and H. T. Anh , "Sensing-Throughput Tradeoff for Cognitive Radio Networks," *IEEE ICC 2007*, pp.5330-5335, 24-28 June 2007.

[114] W. Yonggang, T. Jiansheng, P. Yue, and H. Li, "Underwater communication goes cognitive," in *Proc. IEEE/OES OCEANS 2008,* 15-18 Sept. 2008.

[115] M. Zawodniok, and S. Jagannathan, "Predictive Congestion Control Protocol for Wireless Sensor Networks," *IEEE Transactions on Wireless Communications,* vol. 58, no. 9, pp. 3955-3963, Nov. 2007.

[116] Y. Zhang, "Spectrum Handoff in Cognitive Radio Networks: Opportunistic and Negotiated Situations," in *Proc. IEEE ICC 2009,* June 2009.

[117] R. Zhang, and Y.-C. Liang, "Exploiting Multi-Antennas for Opportunistic Spectrum Sharing in Cognitive Radio Networks," *IEEE Journal of Selected Topics in Signal Processing,* vol. 2, no. 1, pp. 88- 102, Feb. 2008.

[118] L. Zhang, Y. Xin, and Y.-C. Liang, "Weighted Sum Rate Optimization for Cognitive Radio MIMO Broadcast Channels," *IEEE Transactions on Wireless Commun.,* vol. 8, no. 6, pp. 2950-2959, July 2009.

[119] H. Zhang, Z. Zhang, X. Chen, and R. Yin, "Energy Efficient Joint Source and Channel Sensing in Cognitive Radio Sensor Networks" in *Proc. IEEE ICC 2011,* 2011.

[120] H. Zhang, Z. Zhang, H. Dai, R. Yin, and X. Chen, "Distributed Spectrum-Aware Clustering in Cognitive Radio Sensor Networks" in *Proc. IEEE Globecom 2011,* December 2011.

[121] Q. Zhao, B. Sadler, "A Survey of Dynamic Spectrum Access," *IEEE Signal Processing Magazine,* vol. 24, no. 3, pp. 79-89, May 2007.

[122] Q. Zhao, L. Tong, A. Swami, and Y. Chen, "Decentralized Cognitive MAC for Opportunistic Spectrum Access in Ad Hoc Networks: A POMDP Framework, *IEEE Journal on Selected Areas in Communications,* vol. 25, no. 3, pp. 589-600, April 2007.

[123] M. Zuniga, B. Krishnamachari, "Analyzing the Transitional Region in Low Power Wireless Links," in *Proc. IEEE SECON,* pp. 517-526, 2004.

CURRICULUM VITAE

Ahmet Ozan Bicen was born on December 16, 1987. He received his B.Sc. degree in Electrical and Electronics Engineering from Middle East Technical University, Ankara, Turkey, in 2010. He received his M.Sc. degree under the supervision of Prof. Ozgur B. Akan in Electrical and Electronics Engineering from Koc University, Istanbul, Turkey in 2012. At the same time, he was a research assistant in the Next-generation and Wireless Communications Laboratory (NWCL), Koc University.